

Structural System Identification and Damage Detection
through Regularization Technique Using Frequency Response
Function

2004 2

Seoul National University
Civil Engineering Department
Tin Tin Win

주파수 응답함수를 이용한 구조물
손상 탐지 기법

Structural System Identification and Damage Detection through
Regularization Technique Using Frequency Response Function

지도교수 이 해 성

이 논문을 공학박사 학위논문으로 제출함.

2003 년 10 월

서울대학교 대학원
토목공학과 토목공학전공
Tin Tin Win

Tin Tin Win 의 공학박사 학위논문을 인준함.

2003 년 12 월

위원장 高鉉武 

부위원장 李海成 

위원 金在寬 

위원 申修奉 

위원 金南植 

학위논문 원문제공 서비스에 대한 동의서

본인은 본인의 연구결과인 학위논문이 앞으로 우리나라의 학문발전에 기여할 수 있도록, 서울대학교중앙도서관을 통한 “학위논문 원문제공 서비스”에서 다음과 같은 방법 및 조건하에 논문을 제공함에 동의합니다.

1. 인터넷을 통한 온라인 서비스와 보존을 위하여 저작물의 내용을 변경하지 않는 범위내에서의 복제를 허용함.
2. 저작물을 PDF로 구축하여 인터넷을 포함한 정보통신망에서 공개하여 논문 일부 또는 전부의 복제·배포 및 전송에 동의함.
3. 해당 저작물의 저작권을 타인에게 양도하거나 또는 출판허락을 하였을 경우 1개월 이내에 서울대학교 중앙도서관에 알림.
4. 배포, 전송된 학위논문은 이용자가 다시 복제 및 전송할 수 없으며 이용자가 연구목적이 아닌 상업적 용도로 사용하는 것을 금함에 동의함.

2004 년 2 월 2 일

서울대학교총장 귀하

논문제목 : 주파수 응답함수를 이용한 구조물 손상 탐지 기법

학위구분 : 석사 박사

학 과 : 토목공학과

학 번 : 99415-817

연 락 처 : 02-880-8740

저 작 자 : 톰 톰 원



This thesis is dedicated to all of my teachers

ABSTRACT

A new damage detection algorithm based on a system identification scheme with regularization technique is developed using a frequency response function (FRF) in the frequency domain. The algorithm is applicable to for a time invariant model of a structure with recorded earthquake response or measured acceleration data from a dynamic test. The error function is defined as the frequency integral of the least squared error between the measured and calculated FRF. The FRF is obtained by a non-smooth, complex-valued finite Fourier transform of acceleration.

In most pervious studies on frequency domain in SI modal stiffness and modal damping properties are used as system parameters. In this work, stiffness properties of a structure and the coefficient of Rayleigh damping are selected as system parameters. Since it is impossible to measure acceleration at all of the degrees of freedom in structural modal. Sparseness of the measurements occurred due to incomplete data. Furthermore, the measured response included noise. Due to sparseness and completeness in measurement, SI problems are usually illposed.

Tikhonov regularization technique is applied to overcome the ill-posedness of system identification problems. The regularization function is defined as on the L_2 norm of the difference between estimated system parameter vector and the baseline system parameters. The singular value decomposition is utilized to investigate the role of the regularization and the characteristic of the non-linear inverse problem. The first order sensitivity of a finite Fourier transform is obtained by direct differentiation to develop the mathematical model. For an optimal regularization factor, a geometric mean scheme (GMS) method was used.

This method was a geometric mean between the maximum singular value and the minimum singular value of the sensitivity matrix of the response transform. A recursive quadratic programming (RQP) was used to solve a constrained nonlinear optimization problem. The Gauss-Newton approximation of the Hessian was used for a simple computation. The validity of the proposed method was demonstrated by numerical examples on shear buildings.

Keywords: system identification (SI), regularization technique, damage assessment, ill-posedness, Frequency Response Function (FRF), geometric mean scheme (GMS), recursive quadratic programming (RQP)

Student Number: 99415-817

CHAPTER

I	Introduction.....	1
	1.1 Research overview.....	2
	1.2 Research outline.....	3
	1.2.1 Frequency Response Function of the frame structure.....	3
	1.2.2 System identification and parameter estimation.....	4
	1.2.3 Regularization technique and regularization factor.....	6
	1.2.4 Damage assessment.....	7
	1.3 Literature review.....	8
II	Frequency Response Function (FRF) of the Frame structure.....	11
	2.1 Model description and governing equation.....	12
	2.2 Governing equation in modal coordinates.....	14
	2.3 Fourier Transformation of Response Functions (continuous).....	17
	2.4 Transfer Function (continuous).....	20
	2.5 Transfer Function (discrete).....	22
	2.6 Transfer function for continuous and discrete types at ground motion.....	26
III	Parameters Estimation and Damage Detection based on SI in Frequency Domain.....	33
	3.1 Theory.....	33
	3.1.1 Ill-posedness of the Output Error Estimator of the FRF.....	36
	3.1.1a Non-Uniqueness of the solution.....	36
	3.1.1b Discontinuity of the Solution.....	37

3.1.2	Regularization Preserving Regularity of the Solution of SI.....	38
3.1.3	Numerical Remedies for Output Error Estimator.....	42
3.1.3a	Truncated Singular Value Decomposition.....	43
3.1.3b	Tikhonov Regularization.....	43
3.1.4	Determination of an Optimal Regularization Factor.....	45
3.1.4a	Geometric Mean Scheme (GMS).....	45
3.1.4b	The L-Curve Method (LCM).....	47
3.1.4c	Variable Regularization Factor Scheme (VRFS).....	49
3.1.4d	Generalized Cross Validation (GCV).....	49
3.1.5	Recursive Quadratic Programming.....	50
3.1.6	Sensitivity of the objective function.....	51
3.2	Formulation.....	51
3.2.1	Governing Equation (used priori estimated system parameters).....	52
3.2.2	Acceleration response function.....	54
3.2.3	Frequency response function (discrete type).....	56
3.2.4	Output error estimator for FRF.....	57
3.2.5	Minimization of least square output error estimate of FRF.....	58
3.2.6	SVD of the output error estimator.....	64
IV	Numerical Example	66
4.1	Numerical example1-damage detection for a 5 story shear building.....	68
4.2	Numerical example2-damage detection for a 10 story shear building.....	90
4.3	Numerical example3-damage detection for a 5story shear building.....	111

4.4 Experimental study for a 3 story shear building.....	118
V Conclusions.....	124
VI References.....	127

List of Figures

1.1	Definition of forward and inverse problem.....	5
2.1	Diagram of the transfer function for frequency domain	13
2.2	Frame structure and modeling.....	13
2.3	Process of the FRF.....	32
3.1	System property, acceleration field, forward and inverse mappings.....	39
3.2	Inverse mapping with regularization.....	40
3.3	Alleviation of the non-uniqueness of the solution by regularization.....	41
3.4	Alleviation of the discontinuity of the solution by regularization.....	41
3.5	Schematic drawing for an optimal regularization factor in the GMS.....	46
3.6	Basic concept of the L-curve method.....	48
3.7	Diagram of the parameter estimation.....	53
4.1	Five story shear building (a) Frame structure, (b) modeling.....	69
4.2	Five story shear building. (a) Mode shapes. (b) Natural frequencies. (c) Modal damping ratios.....	71
4.3	Model with 30% reduced stiffness damage at first story.....	72
4.4	Exact FRF3 by using the damaged stiffness value and measured FRF3...	73
4.5	Estimated stiffness for regularization and non regularization, using full frequency band in SI for damaged structure.....	74
4.6	Damping ratios using full frequency band in SI for damaged Structure...	75
4.7	FRF for measured at first floor 10%noise-60% dand 30% damage at first floor and third floor respectively.....	77
4.8	Estimated stiffness with various frequency bands in SI.....	77

4.9	Estimated stiffness using regularization non regularization at frequency band up to mode3 in SI.....	78
4.10	FRF1for full measuring points at various frequency bands.....	79
4.11	Estimated stiffness for full measuring points at various frequency bands..	79
4.12	Estimated stiffness for full measuring points at mode2 frequency band...	80
4.13	Model for multi-damaged structure.....	81
4.14	FRF1 for full band frequency for multi-damaged structure.....	82
4.15	Estimated stiffness for regularization and non regularization using full frequency band in SI for damaged structure.....	83
4.16	Measuring point combinations.....	83
4.17	Estimated stiffness for measuring points (123, 125, 234, 345).....	84
4.18	Estimated stiffness for measuring points (123, 125, 234, 345).....	84
4.19	Damping ratios for measuring points combination 125.....	85
4.20	FRF1 for frequency band up to mode3.....	87
4.21.	Estimated stiffness for various frequency bands.....	87
4.22	5% noise-multi damage 40%and 30% at element 1 and 4 respectively.....	88
4.23	Estimated stiffness for full measuring points.....	89
4.24	Estimated stiffness for full measuring at frequency band up to mode 2....	89
4.25	Damping ratios for full measuring at frequency band up to mode 2.....	90
4.26	Ten story shear building. (a) Frame geometry. (b) Model.....	91
4.27	Ten story shear building. (a) Mode shapes. (b) Natural frequencies.(c) Modal damping ratios.....	92
4.28	Ten story shear building. (a) Frame geometry. (b) Model.....	95
4.29	FRF1 at full band frequency for example2-case1.....	96

4.30	Regularization effect for the estimated stiffness at full band frequency....	96
4.31	Model of the 10 story shear building with four measuring points 1,2,5,10.....	97
4.32	Comparison of estimated stiffness with three and four measuring points..	98
4.33	FRF1 at 5 mode frequency band for example2-case1.....	98
4.34	Estimated stiffness for various frequency bands.....	99
4.35	Regularization effect for estimated stiffness at 5 mode frequency band...	99
4.36	FRF1 at full measuring point for example2-case1.....	100
4.37	Effect of the frequency range for the estimated stiffness in SI. (a) 1-8 mode. (b) 1-10 mode.....	101
4.38	Regularization effect for the estimated stiffness.....	101
4.39	Model for 40% -and- 30% reduced stiffness damage at first and fourth stories, respetively.....	102
4.40	Estimated stiffness at different noises 5% and 10%.....	104
4.41	Estimated stiffness at different regularization factors.....	104
4.42	Estimated Rayleigh damping ratios using GMS regularization factor.....	105
4.43	FRF1 for 4 mode frequency band.....	105
4.44	Estimated stiffness for 4mode frequency band.....	106
4.45	Regularization effect of estimated stiffness at 4 mode frequency band....	106
4.46	Estimated damping ratios at 4mode frequency band.....	107
4.47	FRF1 at full measuring point and mode2 frequency band.....	107
4.48	Effect of the frequency range for the estimated stiffness in SI. (a)1-8 mode. (b) 1-10 mode.	108
4.49	Regularization effect of estimated stiffness at 2 mode frequency band....	109

4.50	Estimated damping ratios at 2mode frequency band and full measuring...	109
4.51	Five story shear building (a) Frame structure. (b) Modeling.....	111
4.52	Mode shapes of the structure.....	114
4.53	Measured FRF1 and exact FRF1 with 5%noise and no damage case.....	115
4.54	Detail A for second and third modes which are very close two modes.....	115
4.55	FRF1 at measuring point at 1.....	116
4.56	FRF3 at frequency band in SI and measuring point at 3.....	116
4.57	FRF5 at frequency band in SI and measuring point at 5.....	117
4.58	Comparison of the regularized estimated stiffness and non regularized stiffness.....	117
4.59	Comparison of the regularized and non regularized estimated stiffness....	118
4.60	Experimental model 3-story shear.....	119
4.61	Frame structural model.....	120
4.62	Joint damage status.....	121
4.63	Measured FRF at 1 st , 2 nd and 3 rd floor (no damaged condition).....	121
4.64	Measured FRF at 1 st , 2 nd and 3 rd floor (damaged condition).....	122
4.65	Measured FRF1 at 1 st floor and estimated FRF1.....	122
4.66	Regularized and non regularized estimated stiffness.....	123
4.67	Ray leigh estimated damping ratios.....	123

Tables

4.1	Material properties for a five story shear building.....	69
4.2	Baseline properties for a five story shear building.....	70
4.3	Natural frequencies (hz) for no-damage case and with 30% damage case..	73
4.4	Comparison of the initial, exact and estimated stiffness (N/m) with regularization and non regularization technique.....	76
4.5	Comparison of the natural frequencies (hz) base line data with 60% damage at first story and 30% damage at third story.....	82
4.6	Estimated stiffness (N/m) for various combinations of three measuring points.....	86
4.7	Error % of estimated stiffness (N/m) with respect to exact stiffness for kinds of combinations of measuring three points.....	86
4.8	Mechanical properties for the ten story shear building.....	90
4.9	Baseline properties for the example structure.....	94
4.10	Comparison of the natural frequency (hz) base line data with multi-damaged data.....	103
4.11	Summary for example 1 and 2.....	110
4.12	Structural properties.....	112
4.13	Natural Frequency.....	112
4.14	Stiffness.....	112
4.15	Damping ratios.....	113
4.16	Material properties of columns.....	119
4.17	Stiffness and mass of frame structure.....	120

1.4 Notations

The symbols used in this study are defined where they first appear in the text and whenever clarification is necessary. The most frequently used symbols are listed below.

O_i	spectra of output motion vector
H_{ij}	frequency response function matrix
I_j	linear spectra of input forces vector
mp	number of input points
np	number of output points or measuring points
ω	frequency
t	time
\mathbf{u}	displacement vector
\mathbf{v}	velocity vector
\mathbf{a}	acceleration vector
\mathbf{M}	mass matrix
\mathbf{K}	stiffness matrix
\mathbf{C}	damping matrix
\mathbf{F}	forced vector
n	number of degree of freedom
\mathbf{y}	modal displacement
Φ	modal matrix
ω_n	natural frequency

m_r	modal mass matrix
k_r	modal stiffness matrix
c_r	modal damping matrix
\hat{u}_{pr}	modal displacement for r^{th} mode at point p
\hat{v}_{pr}	modal velocity for r^{th} mode at point p
\hat{a}_{pr}	modal acceleration for r^{th} mode at point p
s	Laplace operator
Φ_r	eigen vector for r^{th} mode
\mathfrak{R}	transform forced vector
X_{pr}	transformed displacement response for r^{th} mode at point p due to forced vibration condition
d_{pr}	value of the modal displacement different between initial and final time
v_{pr}	value of the modal velocity different between initial and final time
$\mathfrak{I}[\hat{u}_{pr}]$	transformed modal displacement
$\mathfrak{I}[\hat{v}_{pr}]$	transformed modal velocity
$\mathfrak{I}[\hat{a}_{pr}]$	transformed modal acceleration
A_{pr}	transformed acceleration response for r^{th} mode at point p for zero initial conditions
Ac_{pr}	transformed acceleration response for r^{th} mode at point p

h_{pr}	FRF for r^{th} mode at point p for continuous type
H_p	FRF for total modes at point p for continuous type
\tilde{h}_{prj}	FRF for r^{th} mode at point p for discrete type
\tilde{H}_p	FRF for total modes at point p for discrete type
Hg_{pr}	FRF for total modes of structural system for ground acceleration at point p for continuous type
Xg_{pr}	transformed displacement response for r^{th} mode at point p due to ground motion condition
\hat{h}_{pr}	FRF for r^{th} mode at point p for discrete type
T	total sampling time
Δt	time increase
N	number of sampling point
F_{max}	maximum frequency
Δf	sampling rate
Γ_r	participation factor vector
$\ddot{\mathbf{z}}$	ground acceleration due to earthquake
Z	transformed ground acceleration due to earthquake in frequency domain
Ag_{pr}	transformed acceleration response for r^{th} mode at point p for zero initial conditions due to ground acceleration
$\bar{\mathbf{M}}$	initial mass matrix
$\bar{\mathbf{K}}$	initial stiffness matrix

$\bar{\mathbf{C}}$	initial damping matrix
$\bar{\mathbf{m}}_r$	modal mass matrix
$\bar{\mathbf{k}}_r$	modal stiffness matrix
$\bar{\mathbf{c}}_r$	modal damping matrix
H_p^c	calculated FRF for total modes at point p for discrete type
H_p^m	measured FRF for total modes at point p for discrete type
$\hat{h}_{g_{pr}}$	FRF for r^{th} mode at point p for discrete type
E_p	output errors estimator function at point p for discrete type
γ_p	normalization of the least square error
π_p	least square error function
Π_E	normalized total least square error
Π_R	Tikhonov regularization function
Π_{ER}	normalized total least square error with Tikhonov regularization function
λ	Tikhonov regularization factor
h_{pj}^m	measured FRF for r^{th} mode at point p for zero initial conditions due to ground acceleration
\bar{h}_{pj}^m	conjugate of the measured FRF for r^{th} mode at point p for zero initial conditions due to ground acceleration
h_{pj}^c	calculated FRF for r^{th} mode at point p for zero initial conditions due to ground acceleration

\bar{h}_{pj}^c	conjugate of the calculated FRF for r^{th} mode at point p for zero initial conditions due to ground acceleration
ζ_r	damping ratio for each mode
κ_1	mass proportional coefficient of Rayleigh damping
κ_2	stiffness proportional coefficient of Rayleigh damping
$\frac{\partial \phi_r}{\partial x_l}$	differentiation of the mode shape vector with respect to system parameter

Chapter 1

Introduction

Structural systems have to endure various events during their lifetime that may not be considered in their original design. In particular, civil structures experience unexpected severe loads such as earthquakes, blasts, gusts, fires and floods that may lead to damage. In transportation infrastructures, roads and bridges suffer from gradually increasing superimposed loads. Large damages due to unexpected loads may result into catastrophic failures of the structures. To prevent these serious events and damages during a given structure's lifetime, regular inspections are necessary.

The methods used for structural inspection can be categorized as destructive and non-destructive methods. Non-destructive methods include global and local inspections. Visual inspections, X-rays, ultrasonic tests, acoustic emissions, magnetic flux leakage techniques, radiographic techniques, penetrant techniques, and eddy current techniques are local non-destructive methods. These methods are used to inspect of local parts of complex structures [Par01].

Structural health monitoring, which is defined as the science of inferring the health and safety of an engineered system by monitoring its status [Par02, Akt00, Doe96], has been used in civil engineering structures during the last few decades. This is a global non-destructive method of system identification (S.I.). A mathematical model and measured responses are utilized in this method. Measured data can be obtained using sensors and computer simulations. Measured data with a high precision and a large amount of numerical calculations are involved in the implementation of the system identification

(S.I.) method.

Several approaches base on various concepts have been proposed for system identification in the time domain and frequency domain. However, previous approaches in frequency domain estimating the system parameters used modal stiffness and modal damping as system parameters while the regularization is not considered in system identification. This study focuses on obtaining the stable parameter estimation using the regularization technique in the frequency domain. A complex value finite Fourier transform of the measured acceleration and a corresponding transform calculated from the response of the mathematical model are used in the least squared error function, is defined as a frequency integral which a frequency band can be specified to obtain more reasonable results.

Tikhonov regularization technique can alleviate the ill-posedness of the inverse problem. Damage detection is determined by change in the dynamic properties of the structure. The basic concept is that modal parameters (frequencies, mode shapes, and modal damping) are functions of the physical properties of the structure (mass, damping, and stiffness). Therefore changes in physical properties will cause changes in modal properties and transfer functions are also changed.

1.1 Research overview

The layout of this thesis is as follows. Chapter 2 provides a frequency response function of a mechanical structure due to forced vibration, free vibration, and ground excitation. Included is an explanation of the fundamental frequency response function and formulation of the acceleration response from forced excitation and free vibration.

Afterwards we compute the transfer function, and relations of the structural vibration response as output and forced excitation as input. In chapter 3, system identification and damage detection of the structure is presented. First, the output error estimator for the transfer functions is computed using measured data and analysis techniques. Least squared error minimization with regularization techniques are performed with respect to system parameters, which include stiffness and damping properties. Verifications of the numerical examples on shear buildings are presented in chapter 4. In the numerical example, we investigate the regularization effect through a numerical simulation. Chapter 5 provides a conclusion and future research directions on damage detection and structural health monitoring.

1.2 Research outline

1.2.1 Frequency Response Function of the frame structures

The Fourier transform of the input and the output are related through a complex valued transfer function, which are called a Frequency Response Function. The initial conditions for this function are zero for and their complete histories are used in the calculations. The differential dynamic equation is used as the governing equation. The structure is modeled with classical normal modes, which are modal mass, modal stiffness and modal damping, modal displacement, modal velocity, and modal acceleration. Using the First Fourier Transform, the equation of motion is transferred from time domain to frequency domain. This process requires proper treatments to avoid erroneous results such as aliasing leakage, windowing, zooming, and averaging.

The modal velocity and modal acceleration and modal displacement in terms of

displacement and input ground acceleration or forced vibration are also transformed into the frequency domain. Then we compute the displacement response and acceleration response using the input ground acceleration or forced vibrations and free vibration, known system parameters such as mass, stiffness, modal damping, and initial conditions. We also calculate the theoretical transfer function with given initial conditions. Using the measured response as output data we can compute the transfer function by using the measured response and input ground acceleration according to the definition of the frequency response function, which is called the measured FRF. Moreover, the responses can be calculated with the known system parameters and initial condition for free vibration, which is called the initial FRF.

1.2.2 System identification and parameter estimation

In the last four decades, system identification and parameter estimation have become important in the structural engineering research field. If a structure is modeled as an analytical model with parameters and is passed through physical testing, there are differences between the test data and model data. Therefore, system identification and parameter estimation are used to reduce this gap.

Applications of inverse problems to engineering areas began in the 1970s for aerospace engineering [Ali75, Bec84, Bec85]. The application area of inverse problems include shape identification [Sch92, Lee99, Lee00], estimation of material properties [Nor89, Hon94, Mah96, Par01], reconstruction of traction boundaries [Man89, Sch90], tomography [Bui94], and defect identification [Tan89, Mei95].

System identification is an inverse problem in which the unknown model is obtained

from known inputs and outputs, while the unknown output is obtained by using the known input and model in forward problems (see fig.1.1).

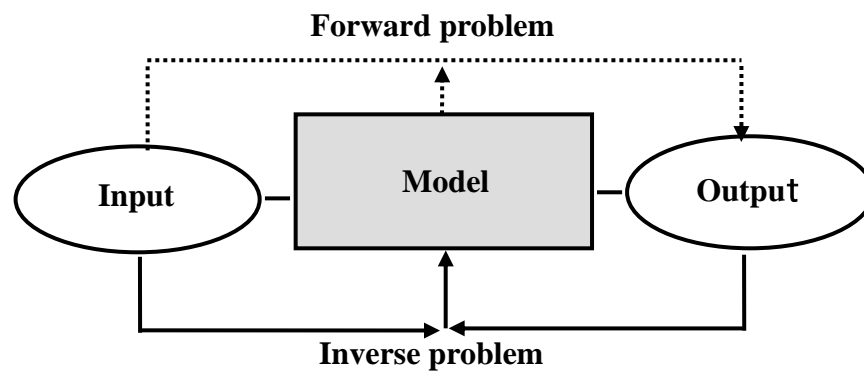


Fig.1.1. Definition of forward and inverse problem

Zadeh (1962) defined system identification as “the determination on the basis of input and output of a system within a specified class of systems, to which the system under test is equivalent”. Parameter estimation can be defined as the determination of values of the parameters that govern the behavior of the model. (Eykhoff 1974); this minimizes the error between the structure and the model. Maximum-likelihood, Bayesian, and cross-entropy estimators are mostly used in the field of system identification. The least square estimator belongs to the Maximum-likelihood estimator, and does not require probability density of measures or the parameter.

Basic approaches for parameter estimation are off-line or batch method and the on-line or recursive method. In the batch method, processing of the measurements continuously updates the estimation of parameters while working serially through the measurements. The recursive approach generates an updated estimation when it receives new information.

Although the batch method is computationally more efficient and robust, recursive methods are popular in the fields of control and automation because the methods do not require the storage of raw data.

The parameter estimation algorithm utilizes calculated responses and measured responses. The calculated responses are computed by a numerical modal of structure numerical integration methods. Unknown constitutive parameters are estimated by solving a constrained nonlinear optimization problem. The recursive quadratic programming method (RPQ) is to solve the estimation problem.

The minimization algorithm requires the gradient of the objective function with respect to the unknown variables. The modal stiffness and modal damping used as system parameters in the frequency domain approach have also been reported [Gra80]. If elemental stiffness and modal damping are used as system parameters in the frequency domain, the sensitivity of the mode shape vector is also required.

The recursive quadratic programming algorithm requires an estimate of the Hessian of the objection function. An exact Hessian and Gauss-Newton approximation may be used. The Gauss-Newton approximation of the Hessian is a part of the Hessian involving only the computed first derivative terms. The exact Hessian takes the second derivative terms of the objective function. The Gauss-Newton approximation of the Hessian needs less computation and storage than the exact Hessian.

1.2.3 Regularization technique and regularization factor

The forward problems are usually well-posed problems while inverse problems are typical ill-posed problems. The system identifications are inverse problems. Ill-posed

problems suffer from severe numerical instabilities, such as non-existence, non-uniqueness, and discontinuity of solution. Regularization techniques can overcome these instabilities.

Two different methods, truncated singular value decomposition (TSVD) [Gol96, Han 98] and Tikhonov regularization [Tik77, Gro84, Bui 94, Han 98], can be employed regularization technique. The regularization techniques improve the convergence and continuity of the solutions.

A regularization function is constructed by the L_2 -norm of the system property. The regularization factor controls the regularization effect through parameter estimation to obtain a physically meaningful and numerically stable solution of an inverse problem with the regularization technique. An optimal regularization factor can be determined by a well-defined method such as the L-curve method (LCM), generalized cross validation (GVC) method, geometric mean scheme (GMS), and the variable regularization factor (VRFS), proposed by Hansen [Han92a], Golub *et al.* [Gol78], Park *et al.*[Par02] and Lee *et al.*, respectively.

In this research, the GMS method is used to find the optimal regularization factor for the nonlinear inverse problem. An optimal regularization factor can be defined as the geometric average between the maximum and minimum singular values of the sensitivity matrix.

1.2.4 Damage assessment

Parameter estimation methods can determine the parameters for each member and damage can be detected and assessed directly at the elemental level. Damage is defined as a reduction in estimated parameters or physical properties of a structure between two-time

separated references assuming the base line values of the parameters of a presumably undamaged structure. The stiffness of a member cannot increase from a previous investigation of the baseline properties. The present work deals with a damage assessment based on system identification of a structure in the frequency domain by using the measured response.

1.3 Literature review

Various kinds of damage detection and assessment algorithms have been developed in engineering fields, and some algorithms are reviewed in this section. Graeme and Mcverry developed a method that identified the modal structural data such as modal stiffness, modal damping, and effective participation factor based on the system identification method using earthquake records as input data. A mathematical model in the frequency domain was used without regularization technique to obtain the finite Fourier transform of the measured acceleration response and calculated transform [Gra80]. Park Hyun Woo developed regularization techniques in system identification for damage assessment of a structure. He proposed regularization techniques and a regularization factor, which is a geometric mean scheme (GMS)], to alleviate ill-posedness of inverse problems. Shin *et. al*, proposed structural damage detection using modal data with a regularization technique [Par02,Shi94]. The authors used Tikhonove regularization function as a Frobenius norm for the change of stiffness of a structure and a regularization factor is determined by the VRFS. The sensitivity of the normalized mode shape vector by an arbitrary matrix was proposed. Lee *et al* [Lee02] reported similar model with the addition of a regularization function. The stiffness properties of the structure and Rayleigh damping were used as system parameters.

[Lee00] reported a structural damage detection algorithm for measured acceleration data by dynamic tests. [Lee00] developed a method for the damage assessment of bridged structures using measured acceleration data by a system identification scheme in the time domain. Fritzen and Zhu [91] used measured transfer functions to update the design parameters by exciting mechanical models with an impact hammer. The FEM models of a real structure were updated using the frequency domain. Yeo, I.H. developed a damage assessment algorithm using a parameter grouping technique to localize the damage members and to overcome sparseness of measured data. Statistical distributions of system parameters with a set of noise-polluted measurement data obtained from the data perturbation method [Yeo00]. Recently, Ge and Soong presented a solution procedure for damage identification using a cost function. This cost function is based on the regulation method for the inverse problem [Ge98a]. H.Y. Hwang developed an identification method for stiffness parameters and damping coefficient parameters of connections using test data. FRF was used as a response model to find the connection properties [Hwa98]. Ata Mogan presented a frequency domain analysis of time integration algorithms for semi-discrete finite element equations. An integral equation was obtained where the equation has to be satisfied by discrete-time transfer functions of time integration [Ata01]. Kan, J.S reported damage detection in structures based on mode shape change and operational mode shapes [Kan99]. A generalization of these methods to the whole frequency range of measurements was proposed. T.C.Lim and J.Li developed a theoretical and computational study of the FRF based on a sub-structuring technique by applying enhanced least square and TSVD approaches [Lim00]. H.Y. Kim proposed vibration based on damage identification using reconstructed FRF in composite structures. The FRF responses were obtained by vibration

testing of fatigue-damaged laminated composites [Kim03]. U.Lee and J.Shin developed a frequency domain method for structural damage identification derived from the dynamic stiffness equation of motion. The report describes a dynamic stiffness matrix for the intact state that appears in the final form of the damage identification algorithm [Lee02]

Chapter 2

Frequency Response Function (FRF) of the frame structure

The Frequency Response Function (FRF) is one of the dynamic properties of a mechanical structure. It describes the relation between the input and output as a function of frequency. An FRF is a complex valued function of frequency. It can be expressed as follows

$$O_i = H_{ij} I_j \quad (2.1)$$

Where, I_j is the linear spectra of input forces (mp vector), O_i is the linear spectra of output motion (np vector) and H_{ij} is the FRF matrix ($np \times mp$). mp is the number of inputs and np is the number of outputs in the frequency domain. If a system has mp inputs and np resultant outputs, then the system has $np \times mp$ transfer functions. The FRF matrix's columns and rows correspond to inputs and outputs, respectively. When the input is fixed and FRFs are measured for multiple outputs, this corresponds to measuring elements from a single column of the FRF matrix. This is used in a typical shaker test. Alternatively, when the output is fixed and FRFs are measured for multiple inputs, this corresponds to measuring element from a single row for the FRF matrix. This is a typical roving hammer impact test.

Depending on whether a motion is measured as a displacement, velocity, or acceleration, the FRF and its inverse can be described by a variety of terms. FRF such as

compliance, mobility and inertance are displacement per force, velocity per force, and acceleration per force, respectively. Dynamic stiffness, impedance and dynamic mass are inverse of compliance, inverse of mobility and inverse of inertance respectively. Fig 2.1 diagrams the relation of input, output, and transfer function.

2.1 Model description and governing equation

A structural dynamic analysis is an important part of the design process for any mechanical system. Structures deemed above or below optimum design and reliability are not desirable because of economic and environmental considerations. Customer demand for a structure include low cost, longer use, economical operation, the capacity to carry greater load, less run noise, less vibration, and less frequent failure. At present, many industries emphasize advanced structural dynamics testing and signal processing technology to support these demands.

Experimental structural dynamics have been tested widely in different industries. These techniques were first used in the aerospace field for predicting the dynamic performance of combat planes. Measurements of the dynamic properties of a structure and its components are essential to understand the dynamic behavior of a vibrating structure. In most cases, finite element model results are necessary to verify experimental results for the dynamic properties of certain components. Fig 2.2 shows a model of a frame structure.

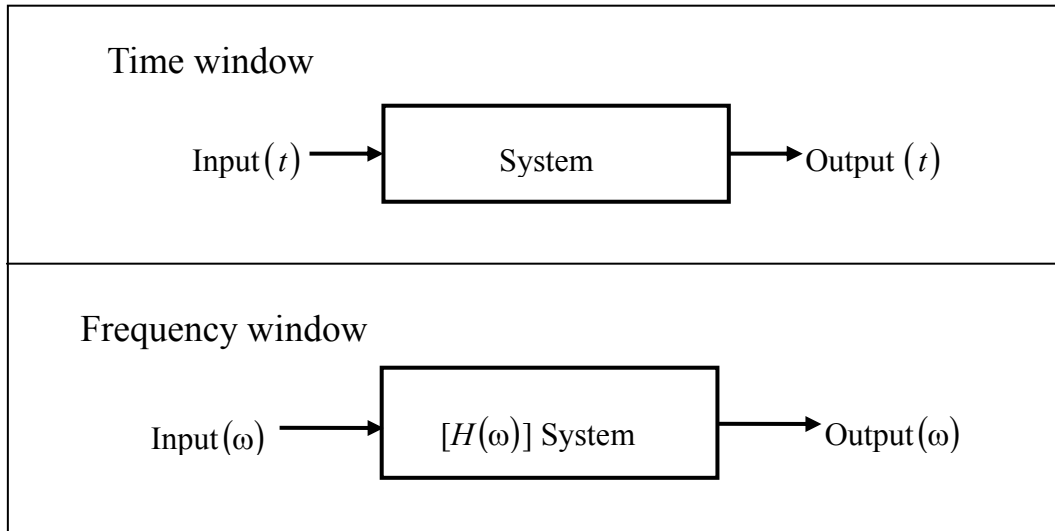


Fig. 2.1 Diagram of the transfer function for the frequency domain

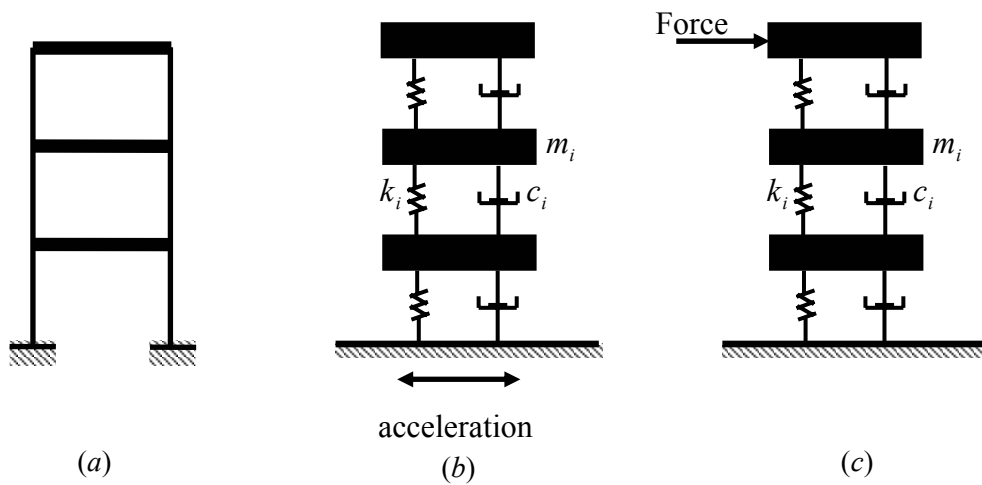


Fig. 2.2 Frame structure and modeling. (a) Frame Geometry. (b) Model (ground exciting). (c) Model (forcing).

The linear differential equation of motion for the relative displacement of a structure

subject to external excitations and its initial conditions are given expressed in Eq.(2.2).

$$\mathbf{M}\mathbf{a} + \mathbf{C}(\mathbf{x})\mathbf{v} + \mathbf{K}(\mathbf{x})\mathbf{u} = \mathbf{f}(t) \quad (2.2a)$$

$$\mathbf{v}(0) = 0 ; \mathbf{u}(0) = 0 \quad (2.2b)$$

where \mathbf{u} , \mathbf{v} , \mathbf{a} are displacement vector, velocity vector, and acceleration vector, respectively. \mathbf{M} , \mathbf{K} , \mathbf{C} , \mathbf{F} are mass matrix stiffness matrix, damping matrix, and force vector, respectively.

In this model, all of the necessary mass, stiffness and damping coefficients are included in the mass, stiffness, and damping matrices to obtain the correct time response due to any arbitrary applied forced. Eq.(2.2a) represents the time domain behavior of a complex dynamic system. Although Eq.(2.2a) can be used effectively in time domain, considerable frequency domain data is not obtainable in many cases. For example, natural frequency is an important characteristic of a mechanical system, and this can be more clearly identified by a frequency domain representation of the data. The choice of a domain is clearly a function of what information is desired. The present work observes the system parameters and acceleration response in the frequency domain approach.

2.2 Governing equation in modal coordinates

In the frequency domain, natural frequencies and eigenvectors are required. Eigenvalues and eigenvectors can be found using a diagonalization method in Eq.(2.2a). A

new coordinate system can be transformed from the equation of motion. This is called generalized coordinates, and is written as diagonal or coupled form coordinates. The transformation relating the generalized coordinates to the actual degrees of freedom of the structure is a matrix, the columns of which are the eigenvector of the system.

$$\mathbf{u} = \Phi \mathbf{y} \quad (2.3a)$$

In Eq.(2.3a), Φ is modal matrix and \mathbf{y} is modal displacement.

$$\Phi = [\phi_{jr}] = \begin{bmatrix} \varphi_{11} & \varphi_{12} & \cdots & \varphi_{1r} \\ \varphi_{21} & \varphi_{22} & \cdots & \varphi_{2r} \\ \vdots & \vdots & \ddots & \vdots \\ \varphi_{j1} & \varphi_{j2} & \cdots & \varphi_{jr} \end{bmatrix} \quad (2.3b)$$

where, j indicates the degree of freedom (DOFs), r is the number of modes, and ϕ_{jr} is the scalar value for the j^{th} element of the r^{th} natural vibration mode. Eq.(2.3b) is an expression of the modal matrix. Eigenvalue problem can be solved using Eqs.(2.4a), (2.4b) and (2.4c) [Ani 95]. Here the damping matrix is not a diagonal matrix if the damping in the system is non-classic.

$$\mathbf{K} \phi_n = \omega^2 \mathbf{M} \phi_n \quad (2.4a)$$

$$[\mathbf{K} - \omega^2 \mathbf{M}] \phi_n = 0 \quad (2.4b)$$

$$\det [\mathbf{K} - \omega^2 \mathbf{M}] = 0 \quad (2.4c)$$

where, ω_n is natural frequency and ω_n^2 is engine value. mass matrix \mathbf{M} and stiffness matrix \mathbf{K} are known and Eq.(2.3b) can be interpreted as a set of N homogeneous algebraic equations for N elements, ϕ_{jn} ($j=1,2,\dots,N$). Therefore natural frequencies can be known by Eq.(2.4c), the characteristic equation or frequency equation. When the natural frequencies are known, Eq.(2.4b) can be solved for the corresponding vector ϕ_n . The following Eqs.(2.5a) and (2.5b) are the modal coordinate system of the equation of motion.

$$\Phi^T \mathbf{M} \Phi \ddot{y} + \Phi^T \mathbf{C} \Phi \dot{y} + \Phi^T \mathbf{K} \Phi y = \Phi^T \mathbf{f} \quad (2.5a)$$

$$m_r \ddot{y}_r + c_r \dot{y}_r + k_r y_r = \mathbf{f}_r \quad (2.5b)$$

where, m_r, k_r, c_r are the modal mass matrix, modal stiffness matrix, and modal damping matrix, respectively.

$$m_r = \Phi^T \mathbf{M} \Phi \quad (2.5c)$$

$$k_r = \Phi^T \mathbf{K} \Phi \quad (2.5d)$$

$$c_r = \Phi^T \mathbf{C} \Phi \quad (2.5e)$$

multiplied by both sides of Eq.(2.5b) with ϕ_{pr}

$$m_r \phi_{pr} \ddot{y}_r + c_r \phi_{pr} \dot{y}_r + k_r \phi_{pr} y_r = \phi_{pr} \mathbf{f}_r \quad (2.6a)$$

$$m_r \hat{a}_{pr} + c_r \hat{v}_{pr} + k_r \hat{u}_{pr} = \phi_{pr} \mathbf{f}_r \quad (2.6b)$$

$$\hat{u}_{pr} = \phi_{pr} y_r \quad (2.6c)$$

where, $\hat{a}_{pr}, \hat{v}_{pr}, \hat{u}_{pr}$ is r^{th} mode's relative acceleration, relative velocity, and relative displacement at point p at time t . Eq.(2.6b) is the governing equation in modal coordinates.

2.3 Fourier Transformation of Response Functions (continuous)

The Fourier transform yields a frequency spectrum of the time domain function. It is defined for continuous functions. Laplace transformation and Fourier transformation allow data to be transformed from one independent variable to another, such as for time, frequency, or the Laplace s -variable. The Laplace transformation of a function of time may be transformed into a function of the complex variable s by :

$$F(s) = \int_0^{\infty} f(t) e^{-st} dt \quad (2.7a)$$

where, s is a Laplace operator (complex variable). Time is always real, whereas the equivalent information in the s domain described by the complex function ' s ' is complex and has real and imaginary parts. The Fourier transform is obtained by merely substituting ' $i\omega$ ' for ' s '.

$$F(i\omega) = \int_0^{\infty} f(t) e^{-i\omega t} dt \quad (2.7b)$$

The transforms of the relative displacement, relative velocity, and relative accelerations for

the sampled frequencies can be expressed in terms of X_{pr} in Eq.(2.8a).

$$\mathfrak{S}[\hat{u}_{pr}] = \int_0^T \hat{u}_{pr} e^{-i\omega t} dt \equiv X_{pr} \quad (2.8a)$$

$$\mathfrak{S}[\hat{v}_{pr}] = \int_0^T \hat{v}_{pr} e^{-i\omega t} dt = \underbrace{\hat{u}_{pr}(T) - \hat{u}_{pr}(0)}_{d_{pr}} + i\omega X_{pr} = d_{pr} + i\omega X_{pr} \quad (2.8b)$$

$$\begin{aligned} \mathfrak{S}[\hat{a}_{pr}] &= \int_0^T \hat{a}_{pr} e^{-i\omega t} dt = \underbrace{\hat{v}_{pr}(T) - \hat{v}_{pr}(0)}_{v_{pr}} + i\omega [\hat{u}_{pr}(T) - \hat{u}_{pr}(0)] - \omega^2 X_{pr} \\ &= v_{pr} + i\omega d_{pr} - \omega^2 X_{pr} \end{aligned} \quad (2.8c)$$

where, X_{pr} is the transformed modal displacement, d_{pr} is the value of different modal displacements at the initial and final time, and v_{pr} is the value of the different modal velocities at the initial and final time. d_{pr} and v_{pr} can be expressed as Eq.(2.8d) and Eq.(2.8e). Eqs.(2.8a-2.8c) are transformed modal displacement $\mathfrak{S}[\hat{u}_{pr}]$, transformed modal velocity $\mathfrak{S}[\hat{v}_{pr}]$, and transformed modal acceleration $\mathfrak{S}[\hat{a}_{pr}]$ [Gra80], respectively.

$$v_{pr} = \hat{v}_{pr}(T) - \hat{v}_{pr}(0) \quad (2.8d)$$

$$d_{pr} = \hat{u}_{pr}(T) - \hat{u}_{pr}(0) \quad (2.8e)$$

To obtain the modal displacement and modal velocity $\hat{u}_{pr}(T)$, $\hat{v}_{pr}(T)$ at time T by using the initial conditions, we use Eq.(2.8f) and Eq.(2.8g).

$$\hat{v}_{pr}(T) = e^{-\frac{1}{2}c_r T} \left\{ \hat{v}_{pr}(0) \text{Cos} \left(\sqrt{\left(k_r - \frac{1}{4}c_r^2\right)} T \right) - \frac{\frac{1}{2}c_r \hat{v}_{pr}(0) + k_r \hat{u}_{pr}(0)}{\sqrt{\left(k_r - \frac{1}{4}c_r^2\right)}} \text{Sin} \left(\sqrt{\left(k_r - \frac{1}{4}c_r^2\right)} T \right) \right\} \quad (2.8f)$$

$$\hat{u}_{pr}(T) = e^{-\frac{1}{2}c_r T} \left\{ \hat{u}_{pr}(0) \text{Cos} \left(\sqrt{\left(k_r - \frac{1}{4}c_r^2\right)} T \right) + \frac{\hat{v}_{pr}(0) + \frac{1}{2}c_r \hat{u}_{pr}(0)}{\sqrt{\left(k_r - \frac{1}{4}c_r^2\right)}} \text{Sin} \left(\sqrt{\left(k_r - \frac{1}{4}c_r^2\right)} T \right) \right\} \quad (2.8g)$$

Eq.(2.6b) becomes Fourier transformed equation using the Eqs.(2.8a-2.8g)

$$m_r \mathfrak{S}[\hat{a}_{pr}] + c_r \mathfrak{S}[\hat{v}_{pr}] + k_r \mathfrak{S}[\hat{u}_{pr}] = \phi_{pr} \phi_r^T \mathfrak{R} \quad (2.8h)$$

In the Eq.(2.8h) ϕ_{pr} is the scalar value of eigenvalue for r^{th} mode at point p , ϕ_r is the eigenvector for r^{th} mode and \mathfrak{R} is the transformed forced vector.

$$m_r (v_{pr} + i\omega d_{pr} - \omega^2 X_{pr}) + c_r (d_{pr} + i\omega X_{pr}) + k_r X_{pr} = \phi_{pr} \phi_r^T \mathfrak{R} \quad (2.9)$$

Eq.(2.9) can be calculated as displacement responses equation as below:

$$X_{pr} = \frac{\phi_{pr} \phi_r^T \mathfrak{R}}{(-m_r \omega^2 + k_r + i \omega c_r)} - \frac{m_r}{(-m_r \omega^2 + k_r + i \omega c_r)} v_{pr} - \frac{i \omega m_r + c_r}{(-m_r \omega^2 + k_r + i \omega c_r)} d_{pr} \quad (2.10)$$

There are three terms in Eq.(2.10) for the displacement response. The first term occurs by force and the structural system. The second and third terms occur due to the initial conditions of the structural system. Modification of Eq.(2.10) by multiplying the $(-\omega^2)$ give an acceleration response;

$$Ac_{pr} = -\omega^2 X_{pr} = -\frac{\phi_{pr} \phi_r^T \mathfrak{R} \omega^2}{(-m_r \omega^2 + k_r + i \omega c_r)} + \frac{m_r \omega^2}{(-m_r \omega^2 + k_r + i \omega c_r)} v_{pr} + \frac{(i \omega m_r + c_r) \omega^2}{(-m_r \omega^2 + k_r + i \omega c_r)} d_{pr} \quad (2.11)$$

where, Ac_{pr} is the acceleration response for the r^{th} mode at point p . The initial displacement and initial velocity are zeros, and Eq.(2.11) can be rewritten as Eq.(2.12):

$$A_{pr} = -\frac{\phi_{pr} \phi_r^T \mathfrak{R} \omega^2}{(-m_r \omega^2 + k_r + i \omega c_r)} \quad (2.12)$$

2.4 Transfer Function (continuous)

According to the transfer function definition, The transformed function h_{pr} can be

obtained from transformed output A_{pr} and transformed input \mathfrak{R} as Eq.(2.13a). This transfer function is for the r^{th} mode at point p for a given structural model.

$$h_{pr}(\omega) = -\frac{\phi_{pr} \phi_r^T \omega^2}{(-m_r \omega^2 + k_r + i \omega c_r)} \quad (2.13a)$$

The denominator of Eq.(2.13a), $(-m_r \omega^2 + k_r + i \omega c_r)$ is then assigned as ψ_r and some portion of the nominator of Eq.(2.13a) $-\phi_{pr} \phi_r^T$ as ξ_{pr} , as follows.

$$\psi_r = (-m_r \omega^2 + k_r + i \omega c_r) \quad (2.13b)$$

$$\xi_{pr} = -\phi_{pr} \phi_r^T \quad (2.13c)$$

Rewriting Eq.(2.13a) by using the Eq.(2.13b) and Eq.(2.13c) gives the following Eq.(2.13d)

$$h_{pr}(\omega) = \frac{\omega^2}{\psi_r} \xi_{pr} \quad (2.13d)$$

The Fourier transform of the forced response is obtained from a summation of the transforms of all of the excitation forces times the column of the FRF corresponding to the excitation DOFs.

$$H_p(\omega) = \sum_{r=1}^{mp} h_{pr}(\omega) \quad (2.13e)$$

where, H_p and mp are the transfer function measured at point p and number of modes, respectively.

2.5 Transfer Function (discrete)

One of the most important concepts used in digital signal processing is the ability to transform data between time and frequency via the Fast Fourier Transform (FFT) and the inverse FFT. The Fourier transform is defined for continuous functions but it is a discrete version of the frequency spectrum a sample time signal. This discretion, a finite length spectrum, is called a Discrete Fourier Transform (DFT). It is also a mathematical tool, which is easily implemented in a digital processor.

In the previous section, the Fourier transform is developed for continuous functions in Eqs.(2.13a-2.13e). Here we express a Discrete Fourier Transform as Eqs.(2.14a-2.14e) for the frequency response function (FRF).

$$\tilde{h}_{prj}(\omega) = -\frac{\phi_{pr}^T \tilde{\omega}_j^2}{(-m_r \tilde{\omega}_j^2 + k_r + i \tilde{\omega}_j c_r)} \quad (2.14a)$$

$$\psi_r = (-m_r \tilde{\omega}_j^2 + k_r + i \tilde{\omega}_j c_r) \quad (2.14b)$$

$$\tilde{h}_{prj}(\omega) = \frac{\tilde{\omega}_j^2}{\tilde{\psi}_{rj}} \xi_{pr} \quad (2.14c)$$

$$\hat{h}_{pr}(\omega) = \sum_{j=1}^{\omega \max} \frac{\tilde{\omega}_j^2}{\tilde{\psi}_{rj}} \xi_{pr} \quad (2.14d)$$

$$\tilde{H}_p(\omega) = \sum_{r=1}^{mp} \sum_{j=1}^{\omega \max} \tilde{h}_{prj}(\omega) \quad (2.14e)$$

where, (\sim) sign represents the discrete type. Eq.(2.14e) is the discretized form of the transfer function.

There are some rules for digital measurement. Although the Fourier transform is defined for continuous signals, DFT is defined for discrete signals and a finite number of samples of the time domain. First, time commences at $t = 0$ and ends at $t = T$. The time period of the sampling or the sample window is:

$$T = \Delta t N \quad (2.15a)$$

where, Δt is an increment of time in seconds between samples, N is the sampling numbers, and T is the time period. Second, DFT transforms N samples of real valued time domain data into $\left(\frac{N}{2}\right)$ samples of complex valued frequency data with frequency resolution Δf between samples. The frequency spectrum is defined for the frequency range $f = 0$ and $f = F_{\max}$. This can be described by the following equation.

$$F_{\max} = \Delta f \frac{N}{2} \quad (2.15b)$$

The third rule is Nyquist Sampling, which is a frequency spectrum containing unique frequencies in a range from $f = 0$ up to a maximum frequency $f = F_{\max}$ equal to one half of the sampling rate of the time domain signal. Therefore:

$$F_{\max} = \frac{1}{2} \frac{1}{\Delta t} \quad (2.15c)$$

$$\Delta f = \frac{1}{T} \quad (2.15d)$$

Sampling window length in time domain T is an influent digital spectrum. If samples are taken over a longer time period, we can obtain better frequency resolution [H. Mar 99].

The rules above are basically all that are required to make digital measurements. However, there are two remaining difficulties associated with the use of the FFT. These are aliasing and leakage.

Aliasing of a signal occurs when the signal is sampled at less than twice the highest frequency of the spectrum of the signal. When aliasing occurs, the part of the signal at frequencies above the sampling frequency adds to the part at lower frequencies, thus giving an incorrect spectrum. To prevent aliasing, the frequency content of the time domain signals must be bounded to satisfy the Nyquist criterion. That is, the maximum frequency in the analog signals cannot exceed one half of the sampling frequency used to digitize them.

If a signal is non-periodic in its sampling window, it will have leakage in its spectrum. Leakage distorts the spectrum and makes it inaccurate. In this case, leakage can never be eliminated but it can be minimized. To minimize the effects of leakage, specially shaped windows are applied to the time waveform after they are sampled, but before they are transformed using the FFT.

A Zoom transform is an essential digital filtering operation that takes place after the time waveform has been sampled. It involves re-sampling, frequency shifting, and low pass filtering of the sampled data to yield a DFT with increased frequency resolution, but over a smaller frequency band. The Zoom transform is very useful for obtaining better frequency resolution without performing an FFT on a very large number of samples. From a practical standpoint, the Zoom transform is much faster than using a base band FFT (starting at zero frequency) with more samples to greater frequency resolution.

Structural dynamic measurements are made by excitation provided with one or more shakers attached to the structure. Common types of shakers are electro-dynamic and hydraulic shakers. The sine wave excitation is useful for characteristic non-linearities in the structures. The sine wave excitation is the best signal-to-noise and random signal (RMS)-to-peak ratios of any signal controlled in terms of amplitude and bandwidth, with long histories of use. In this testing, care should be taken not to avoid over excitation, which may result in distortion. Broad band frequency means zero to nearly half of the sampling frequency. A variety of new broad band excitation signals have been developed for making

shaker measurements with FFT analyzers. These signals are transient, true random, pseudo random, periodic random, burst random, fast sine sweep (chip), and burst chirp. Although, a broad band excitation signal is faster than the sine wave excitation, it is still useful in some applications. In current research, sine wave excitation testing is used in the shaker measurements.

2.6 Transfer function for ground motion (continuous and discrete)

The response of structures to ground shaking caused by an earthquake is an important component of a structural dynamic analysis. Earthquakes can cause damage to many structures. There are two categories of mechanical systems, linearly elastic and inelastic systems. Time variation of ground acceleration is the most useful way of defining the shaking of the ground during an earthquake. The dynamic properties of many structures are markedly more different during their response to strong ground motion than in small amplitude ambient and forced vibration tests. Strong motion earthquake records provide one of the few sources of information on the response of large structures to potentially damaging excitations.

In this study, the transfer function is calculated using ground motion data. This transfer function approach in the frequency domain can be determined through the time variation of the system properties by a moving window Fourier analysis, considering the records segment by segment.

The modulus of the transfer function has been determined and the parameters of the lower mode are estimated from the theoretical form of the modulus of the transfer function. These estimates involve the use a few of the values of the modulus of the transfer function. Points near the maxima of the modulus of the transfer are used to determine the modal frequencies, and the amplitude of the peaks and bandwidth at the half-power points are used to estimate participation factors and modal dampings. The recorded ground motion at a site in EL Centro, California during the Imperial Valley California earthquake and the Kobe earthquake ground motion data are used as exciting forced. The ground acceleration is defined by numerical values at distant time instants. These time instants should be closely spaced to accurately describe the highly irregular variation of acceleration with time. Typically, the time interval is chosen to be 1/100 to 1/50 of a second, requiring 1500 to 3000 ordinates to describe the ground motion. The ground exciting EL Centro ground acceleration with time is used. The peak factor of ground acceleration is 0.319 in EL Centro and 0.831 in Kobe ground acceleration.

A generalization of the preceding derivations is useful if all the DOFs of the system are not in the direction of the ground motion or if the earthquake excitation is not identical at all of the structural supports. In this general approach the total displacement of each mass is expressed as its displacement due to static application of the ground motion plus the dynamic relative to the quasi-static displacement:

$$u_j^t(t) = u_j(t) + u_j^s(t) \quad (2.16)$$

The quasi-static displacements can be expressed as $\mathbf{u}^s(t) = \ell u_g(t)$, where the influence vector ℓ represent the displacements of the mass resulting from static application of a unit ground displacement. The governing equation for ground motion can be written as

$$\mathbf{M}\mathbf{a} + \mathbf{C}\mathbf{v} + \mathbf{K}\mathbf{u} = -\mathbf{M}\mathbf{1}\ddot{\mathbf{z}} \quad (2.17a)$$

$$\mathbf{v}(0) = 0 ; \mathbf{u}(0) = 0 \quad (2.17b)$$

where, $\ddot{\mathbf{z}}$ is acceleration and the governing equations for ground motion in modal coordinate are:

$$m_r \hat{a}_{pr} + c_r \hat{v}_{pr} + k_r \hat{u}_{pr} = -\phi_{pr} \phi_r^T \mathbf{M}\mathbf{1}\ddot{\mathbf{z}} \quad (2.18a)$$

$$\Gamma_r = \phi_r^T \mathbf{M}\mathbf{1} \quad (2.18b)$$

$$\hat{u}_{pr} = \phi_{pr} y_r \quad (2.18c)$$

These Eqs.(2.18a~2.18c) are similar to the Eqs.(2.6a~2.6c), except the right side of equations that forces term due to ground motion. where Γ_r is the participation vector. First, the Fourier transform is written as a continuous function of Eq.(2.19)

$$m_r (v_{pr} + i\omega d_{pr} - \omega^2 Xg_{pr}) + c_r (d_{pr} + i\omega Xg_{pr}) + k_r Xg_{pr} = -\phi_{pr} \Gamma_r Z(\omega) \quad (2.19)$$

$Z(\omega)$ is transformed ground acceleration due to an earthquake in the frequency domain and Xg_{pr} is a transformed displacement response for r^{th} mode at point p due to ground

motion conditions.

The displacement response is the structure displacement from the original position. The ground displacement that is not total displacement is not included. Inclusion of the initial condition effect can be achieved as follows.

$$Xg_{pr} = -\frac{\phi_{pr} \Gamma_r}{(-m_r \omega^2 + k_r + i\omega c_r)} Z(\omega) - \frac{m_r}{(-m_r \omega^2 + k_r + i\omega c_r)} v_{pr} - \frac{i\omega m_r + c_r}{(-m_r \omega^2 + k_r + i\omega c_r)} d_{pr} \quad (2.20)$$

The total acceleration response for ground excitation is computed from the above equation with initial conditions.

$$Ag_{pr} = -\omega^2 Xg_{pr} = Z(\omega) + \frac{\phi_{pr} \Gamma_r \omega^2}{(-m_r \omega^2 + k_r + i\omega c_r)} Z(\omega) + \frac{m_r \omega^2}{(-m_r \omega^2 + k_r + i\omega c_r)} v_{pr} + \frac{(i\omega m_r + c_r) \omega^2}{(-m_r \omega^2 + k_r + i\omega c_r)} d_{pr} \quad (2.21)$$

If the initial conditions are zero, the response acceleration can be written as

$$Ag_{pr} = Z(\omega) + \frac{\phi_{pr} \Gamma_r \omega^2}{(-m_r \omega^2 + k_r + i\omega c_r)} Z(\omega) \quad (2.22)$$

where, Ag_{pr} is the transformed acceleration response for r^{th} mode at point p . A transfer

or FRF function at zero initial conditions and ground acceleration and continuous type can be formulated as Eqs.(2.23a-2.23e)

Eq.(2.23a) is a frequency response function due to acceleration response in ground motion, and hg_{pr} is the transformed function for r^{th} mode at point p for zero initial conditions due to ground acceleration.

$$hg_{pr}(\omega) = \frac{\phi_{pr}\Gamma_r\omega^2}{(-m_r\omega^2 + k_r + i\omega c_r)} \quad (2.23a)$$

Eq.(2.22b-2.22d) are made the simplification of the Eq.(2.22a).

$$hg_{pr}(\omega) = \frac{\omega^2}{\psi_r} \zeta_{pr} \quad (2.23b)$$

$$\psi_r = (-m_r\omega^2 + k_r + i\omega c_r) \quad (2.23c)$$

$$\zeta_{pr} = -\phi_{pr}\Gamma_r \quad (2.23d)$$

Eq.(2.23e) is the FRF for total modes of the structure, summation of the each FRF for each mode of structure.

$$Hg_p(\omega) = \sum_{r=1}^{mp} hg_{pr}(\omega) \quad (2.23e)$$

Secondly, there Eqs.(2.24a - 2.24e) are FRF for discrete type of the frequency range.

$$\tilde{h}g_{prj}(\omega) = \frac{\phi_{pr}\Gamma_r \omega_j^2}{(-\mathbf{M}_r\omega_j^2 + \mathbf{K}_r + i\omega_j\mathbf{C}_r)} \quad (2.24a)$$

$$\tilde{h}g_{prj}(\omega) = \frac{\omega_j^2}{\tilde{\psi}_{rj}} \zeta_{pr} \quad (2.24b)$$

$$\tilde{\psi}_{rj} = (-\mathbf{M}_r\omega_j^2 + \mathbf{K}_r + i\omega_j\mathbf{C}_r) \quad (2.24c)$$

$$\zeta_{pr} = \phi_{pr}\Gamma \quad (2.24d)$$

Frequency response function (discrete type) for each mode.

$$\hat{h}g_{pr}(\omega) = \sum_{j=1}^{\omega \max} \frac{\tilde{\omega}_j^2}{\tilde{\psi}_{rj}} \zeta_{pr} \quad (2.24e)$$

FRF for total modes at point p.

$$\tilde{H}g_p(\omega) = \sum_{r=1}^{\text{mode}} \sum_{j=1}^{\omega \max} \tilde{h}_{prj}(\omega) \quad (2.24f)$$

In this chapter, if we know the system parameters (stiffness and damping) of a structure, we can calculate the displacement response, acceleration response, and frequency response function (FRF) in forced vibration including ground motion at zero initial conditions and known initial conditions.

The process of FRF is as Following fig. (2.3)

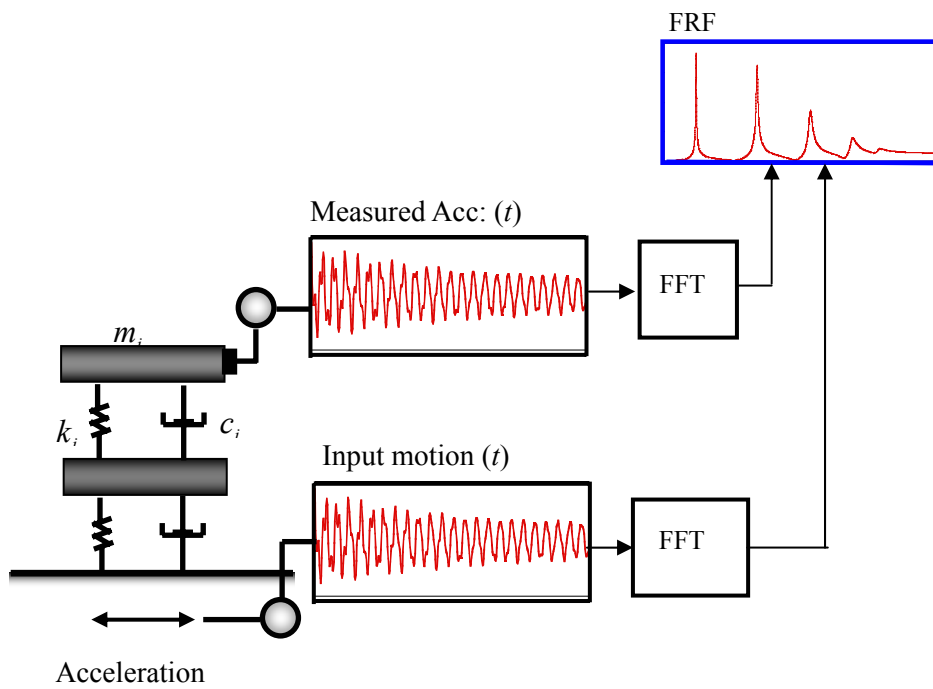


Fig. 2.3 Process of the FRF

Chapter 3

Parameters Estimation and Damage Detection Based on SI in Frequency Domain

3.1 Theory

This chapter describes a parameter estimation and damage detection method based on system identification (SI) through a regularization technique in the frequency domain. Parameter estimation from dynamic response data has been developed in recent years. There are two types of domains in dynamic response. One is time domain and the other is frequency domain. During last two decades [Fri86], the governing equation and mathematical models have been generally defined in the time domain; however, these can also be transformed to the frequency domain using an integral transform.

Ljung and Glover (1981) compared the frequency domain method and time domain method, and found that these methods complement each other. Banan and Hjelmsatd (1993) later came to the following conclusions:

“In general, the choice between time domain and frequency domain is dictated by the prior knowledge of the system and the intended use of the model. When the system is governed by differential or difference equations, or when the model is intended to predict future response or to simulate the system, or when a stochastic control is desired, a time domain model will eventually be required. When the objective of the identification process is to determine resonances in the response of the system, to design a model for a frequency domain control system, or when the bandwidth and the frequency resolution are available as a prior information, then a frequency domain model must be employed.” [Hje96a]

Here we describe a parameter estimation and damage detection method based on frequency response function (FRF) and system identification (SI) through a regularization technique in the frequency domain. FRFs can be obtained and transformed from the measured response and calculated response by using a mathematical model. A mathematical model can be constructed using dynamic equilibrium, if the structure is assumed as a linear time invariant system and its geometry and the boundary conditions are also known. The history of dynamic loads and measured response in the time domain are transformed to the frequency domain using fast Fourier transform (FFT). We then proceed to calculate the transformation function using these transformed measured responses as output and dynamic load as input, which is referred to as a measured transfer function or measured FRF. The responses at different locations do not interact with each other. The calculated FRF can be obtained from the mathematical model. This model is constructed using the transformed governing equation in the frequency domain with unknown system parameters and transformed dynamic loads.

The basic concept is to detect the structural damage by the least square error method. This minimizes the frequency integral of the least square error, which is the difference between transformation from measured acceleration data and the corresponding transformation calculated acceleration by the mathematical model, which is in turn the difference between measured FRF and calculated FRF. This is also known as model updating or the optimization method. Stiffness properties of the structural and structural modal damping are used as system parameters. The structural modal dampings are modeled by the Rayleigh damping method.

Damage detection of the structure using the measured response by the modal analysis

approach has been widely used. This approach has some disadvantages; for example, when structural properties are changed, the modal data shows insensitiveness and damping properties cannot be estimated. Kim *et al.* developed a damage assessment of bridge structures using measured acceleration data by using system identification in the time domain and the aforementioned drawback was also addressed. In the present work, structural properties and modal damping are used as system parameters for system identification in the frequency domain in order to overcome these drawbacks.

When taking measured data from a structure, we cannot take the measured data for all the unknown system parameters of a structure. In practicality, it is difficult to measure all degree of freedoms for a structure and total cost is also expensive for all measuring instruments. At large structures are many structural elements, which are many degrees of freedoms for the model. Therefore it is impossible to handle all the measured data. If the ratio of the measured points and the unknown system parameters is small, the sparseness of measurement effect may be large. Measuring error is called noise, and this occurs in measurements as a result of the sensitivity limits of the measuring instruments and uncertainty in experimental environments. Therefore SI for structural systems has sparseness and noise problems [Shi94, Yeo00, Par02]. For example, bridges are complex structures, and hence sparseness and noise problems are serious. This is because the number of measurable responses is much smaller than that of the system parameters and uncertainty in experimental environments.

System identification is an inverse problem. SI suffers from ill-posedness due to sparseness and noise in measurements. Ill-posedness of SI based on the output error estimator is investigated in the context of the inverse problems. Yeo00 and Par02 attempted

to reduce the instabilities of the output error estimator by using a regularization technique in the time domain. In current research, a similar concept of the regularization technique is used in the frequency domain. Here, the bandwidth and the frequency resolution are available as prior information.

3.1.1 Ill-posedness of the Output Error Estimator of the FRF

Non-uniqueness of a solution and discontinuity of solutions are characteristics of the ill-posedness of the output error estimator [Han98, Yeo00, Par01]. Ill-posedness can be overcome by using the solution of the linearized form of the output error estimator. Because the output error estimator is a nonlinear optimization problem, it should be solved iteratively by linearizing with respect to the system parameters.

Non-uniqueness of the solution problem in the sensitivity matrix is due to sparseness of measurements [Han98, Par01]. Discontinuity and convergence difficulties of the solution can appear due to inclusion of the noise in measurements [Gro84, Han98, Par01]. It can be said that numerical instabilities of the output error estimator are caused by rank-deficiency of the sensitivity matrix and violation of discrete Picard, respectively.

Singular value decomposition (SVD) investigates numerical instabilities of the linearized output error estimator [Gol96]. Either rank-deficiency or violation of the Picard condition can be solved through the SVD. Therefore, SVD can investigate non-uniqueness and discontinuity of solution of the output error estimator, which are two important kinds of ill-posedness.

3.1.1a Non-Uniqueness of the solution

Sparseness in measured data occurs when the numbers of measured degree of

freedoms are few as compared with the unknown system parameters in a finite model of the structure. When the measured data are so sparse that the resulting equation in the minimization problem of the output error estimator becomes underdetermined, there is an infinite number of solutions. The sparseness of the measured response occurs very often in the area of SI for structural systems.

3.1.1b Discontinuity of the solution

Discontinuity of the solution is due to the noise included in the measurements. The degree of discontinuity increases as the number of system parameters increase when there is noise in the measurements.

Measurement errors and modeling errors are sources of noise when SI algorithm is applied. When we collect data during actual measurement, misreading of test equipment or sensitivity of sensors can cause noise. Then the discrepancy between a real structure and its mathematical model causes noise in the SI. Although measurement errors are probabilistic, modeling errors are systematic in nature. Modeling errors cannot be reduced in minimization with a predefined structural model. Modeling errors, which lead to errors in the stiffness matrix, result in noise in the computed responses such as displacements, velocity, acceleration; they do not include in measured responses.

The measured acceleration $\bar{\mathbf{A}}$ can be theoretically decomposed into the noise-free acceleration $\bar{\mathbf{A}}^f$ and the noise vector \mathbf{e} as follows.

$$\bar{\mathbf{A}} = \bar{\mathbf{A}}^f + \mathbf{e} \quad (3.1)$$

According to Eq.(3.1), the noise-free displacements can be defined as the best-fitting

response with measured ones obtainable by adjusting predefined system parameters in the mathematical model. This decomposition of response cannot be achieved explicitly, and is purely conceptual. A small change in noise may yield a totally different solution because small singular values amplify the change in measurements, which is a source of discontinuity characteristics in SI problems.

3.1.2 Regularization Preserving Regularity of the Solution of SI

There are several kinds of complex methodologies and techniques that can realize the regularization. However, the main concept of the regularization is to preserve the regularity of the solution that defines a proper function space where the solution must exist [Tik77, Joh87, Bui94]. Since a proper function space for the solution is usually provided in a forward problem either explicitly or implicitly, the regularity of the solution is guaranteed and the forward problem is well-posed.

To explain the regularity of the solution by an illustration, Fig. 3.1 shows the function spaces representing the system property and the acceleration response field, and mapping between the system property and acceleration response field. x , x^* , a , and a^* represent the system property, an *admissible* system property, the acceleration response field, and an *admissible* acceleration response field, respectively. In this study, the term '*admissible*' implies that a function space representing a physical property should be regular so that it has both physical and mathematical significance. Whether a function space is regular is judged by the regularity (integrability) of the function space [Joh83].

In general, the forward mapping represented by a frequency response function (FRF) equation is performed from an admissible system property onto an admissible acceleration

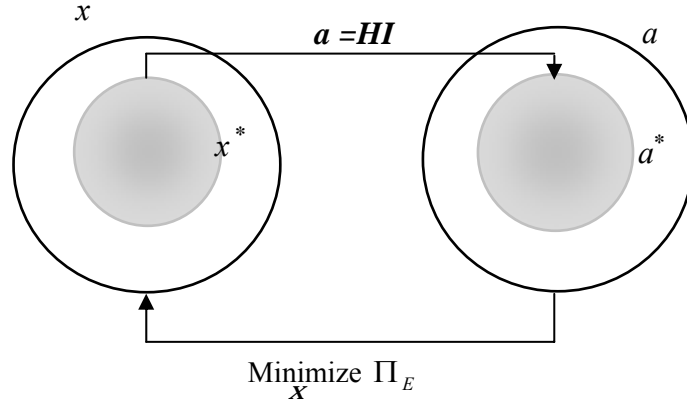


Fig.3.1 System property, acceleration response field, forward and inverse mappings

response field as shown in Fig. 3.1. Here, the FRF equation is derived from the dynamic differential equation and a First Fourier Transform. However, it is not guaranteed that the inverse mapping represented by the output error estimator between the measured and the calculated response is performed from the admissible. This is because a proper solution space of the system property is not defined by the output error estimator and the measurements inevitably contain random and modeling errors. In other words, ill-posedness of the inverse mapping represented only by the output error estimator occurs since there is no proper regularity condition of the system property. Therefore a proper regularity condition should be adopted to alleviate ill-posedness of the inverse mapping.

In general, a strong form of the regularity condition with respect to the model space is represented by the integrability of the model space [Joh87, Ode79].

$$\left(\int_V |x - x_0|^r dV \right)^{1/r} < \infty, \quad 1 \leq r \leq \infty \quad (3.2)$$

where, x_0 is the center of the function space given *a priori*. The system property satisfying Eq.(3.2) is an admissible system property, x^* in Fig. 3.1. The topology of the system property depends on r .

The weak form of the regularity is usually imposed in practice since it is impossible to employ the strong form of the regularity condition directly.

$$\int_V |x - x_0|^r dV < R_s^r \quad (3.3)$$

where, R_s denotes the size of the function space. r and R_s are determined properly by the regularization technique by considering the physical and the mathematical characteristics of the system property as known *a priori*. For example, standard Tikhonov regularization $r=2$, which means the original system property should be a square-integrable in the vicinity of x_0 . In other words, the system property defined by Tikhonov regularization is a subspace of the L_2 -space that consists of piecewise continuous functions [Joh87].

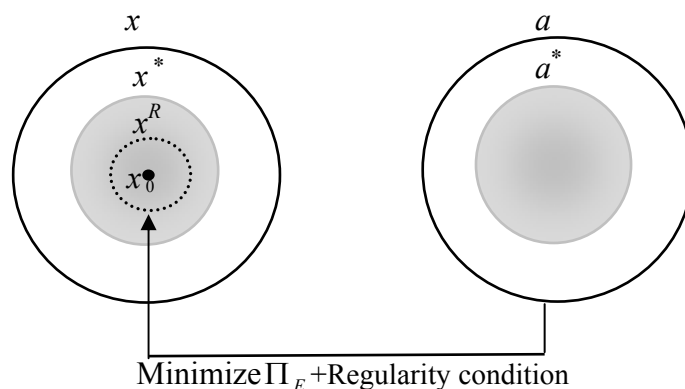


Fig. 3.2 Inverse mapping with regularization

$$\int_V |x - x_0|^2 dV < R_s^2 \quad (3.4)$$

A subspace of function space x^* satisfying Eq.(3.4) is also an admissible system property, x^R determined by the regularization technique in Fig. 3.2. Fig. 3.3 and Fig. 3.4 present the effect of the regularization that alleviate the typical ill-posedness, non-uniqueness, and the discontinuity of the solution. x_A , x_I , and a_A , denote elements that satisfy the following condition.

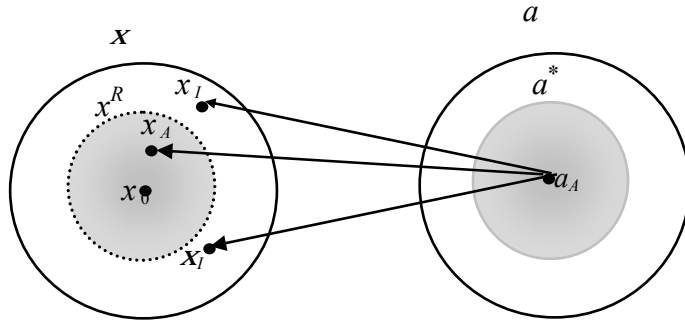


Fig. 3.3 Alleviation of the non-uniqueness of the solution by regularization

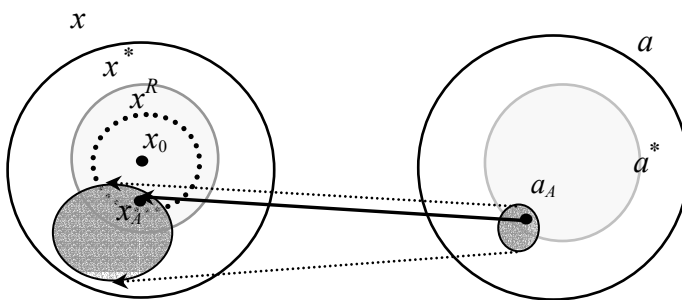


Fig. 3.4 Alleviation of the discontinuity of the solution by regularization

$$\begin{aligned}
x_A &\in x^R \\
x_I &\notin x^* \\
a_A &\in a^*
\end{aligned}
\tag{3.5}$$

Non-uniqueness of the solution may occur when the solution corresponding to the displacement a_A is not unique. Solutions obtained from the inverse mapping corresponding to a_A may include those in the admissible and inadmissible system property, as shown in Fig.3.3. If the regularity condition is enforced by the regularization technique, only the solution that belongs to an admissible system property can be obtained.

Discontinuity of the solution occurs when the inverse mapping from the acceleration response field in the vicinity of a_A to the system property yields large deviations, depicted as the darkly shadowed region in the vicinity of x_A . The darkly shadowed region includes solutions of admissible and inadmissible system properties. In general, most of the darkly shadowed region lies in the inadmissible system property, as shown in Fig. 3.4. Therefore, if the regularity condition is enforced by the regularization technique, solutions continuous with respect to the small perturbation of the output can be obtained, which lies in the admissible system property.

3.1.3 Numerical Remedies for Output Error Estimator

Ill-posedness of the inverse problems can be reduced by using the two major numerical remedies. These are truncated singular value decomposition (TSVD) [Gol96, Han98] and Tikhonov regularization technique [Tik77, Gro84, Bui94, Han98]. The TSVD can be used to resolve the non-uniqueness of the solution and then Tikhonov regularization enhances both convergence and continuity of the solution.

Both methods have balance power to convert the ill-posed problem into a well-posed problem by imposing the positive definiteness on the original ill-posed problems. The degree of smoothness is proportional to that of positive definiteness, which is determined by a truncation number of TSVD and a regularization factor in the regularization technique.

In these numerical remedies, the most important issue is to maintain a consistent regularization effect on the parameter estimation, which is controlled by the truncation number of TSVD [Vog86] and a regularization factor [Bui94, Han98, Par01] in the regularization technique. Therefore, it is crucial to determine a well-balanced truncation number and regularization factor in order to obtain a physically meaningful and numerically stable solution of an inverse problem. This section presents a detailed description of the TSVD and regularization technique

3.1.3a Truncated Singular Value Decomposition

There are an infinite number of solutions in the rank-deficient problem. Truncated singular value decomposition (TSVD) is motivated from the simple idea that feasible solutions are smooth rather than oscillatory among an infinite number of solutions if a priori estimation of the solution is smooth. The degree of the smoothness of the solution can be measured by the L_2 -norm of the solution vector. In TSVD, the solution with the least L_2 -norm is defined as the most feasible one [Gol96, Han98].

3.1.3b Tikhonov Regularization

In various types of inverse problems, the concept of the Tikhonov regularization has been successfully applied to overcome ill-posedness [Bec84, Sch92, Lee99, Lee00, Par02].

The regularization can be interpreted as a process of mixing a priori estimates of

system parameters and a posteriori solution [Bui94, Par01]. The baseline properties are selected as the a priori estimates of the system parameters in this work. The priori estimates are taken into account in the problem statement of inverse problems by adding a regularization function with the a priori estimates of the system parameters to the error function. The regularization function should be defined differently for different problems since each problem has a different regularity condition that defines the feasible solution space, as noted in section 3.1.2. It is square-integrable with respect to the system property since the physical distribution of the system property is piecewise continuous. [Tik77, Gro84, Mor93]. The regularization factor controls the degree of the regularity of the solution space [Tik77, Gro84, Mor93, Bui94, Par01].

$$\Pi_R = \frac{1}{2} \lambda^2 \int_V (x - x_0)^2 dV \quad (3.6)$$

where λ is the regularization factor that controls the degree of the regularity of the solution space [Tik77, Gro84, Mor93, Bui94, Par01]. Eq.(3.6) is the standard Tikhonov regularization function. Then Eq.(3.6) is converted into the discrete form, giving the following equation.

$$\Pi_R = \frac{1}{2} \lambda^2 \|\mathbf{x} - \mathbf{x}_0\|_2^2 \quad (3.7)$$

where \mathbf{x}_0 denotes the a priori estimates of system parameters.

The weighting factor α_j , which varies with the regularization factor from 0 to 1, adjusts the relative magnitude between a posteriori solution and a priori estimates in the

regularized solution. The weighing factor approaches zero as the regularization factor becomes smaller, and one as the regularization factor becomes larger. Therefore, the solution converges to a priori estimates for a large regularization factor while the solution converges to a posteriori solution for a small regularization factor. If the regularization factor is fixed, the weighting factors become larger for smaller singular values. This implies that the stronger effect of the a priori estimates is included in a solution component corresponding to the smaller singular value, and vice versa.

3.1.4 Determination of an Optimal Regularization Factor

An optimal regularization factor can be determined by several well-defined methods for linear inverse problems, including the L-curve method (LCM) proposed by Hansen [Han92a], the generalized cross validation (GCV) method proposed by Golub *et al.* [Gol78], and the geometric mean scheme (GMS) proposed by Park *et al.* Kaller and M. Bertrant utilized the GCV for medical image enhancing problems [Kal96]. Although (LCM) and (GCV) schemes have been proven to be effective in linear inverse problems, no rigorous schemes for nonlinear inverse analysis have thus far been proposed. These methods can determine the regularization factors of nonlinear inverse problems at each minimization iteration, where a linearized quadratic sub-problem is solved. The GCV is unable to effectively control the instabilities of the SI algorithms when regularization factor value is too small. (GMS) is utilized to overcome the drawbacks of the (LCM) and (GCV) schemes in the determination of the regularization factor for SI in elastic continua.

3.1.4a Geometric Mean Scheme (GMS)

One of the optimal regularization factors is the geometric mean scheme (GMS), proposed by Park *et al.*(2001). In this method, an optimal regularization factor is defined as the geometric average between the maximum and the minimum singular values of the sensitivity matrix. The regularization effect on each component of the solution depends on the magnitude of the corresponding singular value. Fig. 3.5 illustrates the variation of weighting factors for the maximum and the minimum singular values with the regularization factor. In the regularized solution, the maximum effect of a priori information and a posteriori solution occurs with the smallest singular value and the largest singular value, respectively. On the other hand, the minimum effect of a priori

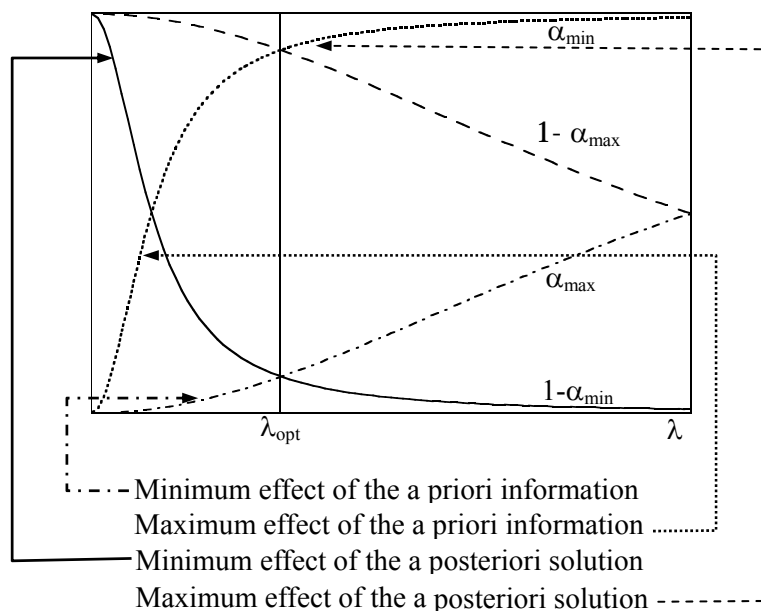


Fig. 3.5. Schematic drawing for an optimal regularization factor in the GMS

information and the a posteriori solution occurs for the largest singular value and the smallest singular value, respectively. Based on this observation, the optimal regularization factor is defined as the one that yields the same maximum and minimum effect of the a priori information and the a posteriori solution, which can be stated as

$$1 - \alpha_{\max} = \alpha_{\min}, \quad 1 - \alpha_{\min} = \alpha_{\max} \quad (3.8)$$

where, α_{\max} and α_{\min} are the weighting factors corresponding to the maximum singular value and the minimum singular value, respectively. The first and the second equation in Eq.(3.8) represent the balancing conditions on the maximum and the minimum effect, respectively, as shown in Fig. 3.5. An interesting point is that the two equations are identical and yield the geometric average between the smallest and the largest singular value for the optimal solution of Eq.(3.9)

$$\lambda_{opt} = \sqrt{\omega_{\max} \omega_{\min}} \quad (3.9)$$

If zero singular values exist, the smallest non-zero singular value may be used for ω_{\min} .

3.1.4b The L-Curve Method (LCM)

The L-curve is a log-log plot of the regularization function versus the error function for various regularization factors. Hansen showed for linear inverse problems that the plot always formed an ‘L’ shaped curve as shown in Fig. 3.6, and that the optimal regularization factor corresponds to the sharp edge of the curve where the curvature of the curve becomes maximal [Han92a]. For nonlinear inverse problems, the L-curve is defined at each iteration for the linearized error function.

The regularization function π_R and the linearized error function π_E^l are expressed in terms of the weighting factor, which is a function of the regularization factor as follows. The parametric form of the L-curve for the current iteration step is given by the following expression.

$$(\rho(\lambda), \eta(\lambda)) = (\log(\pi_E^l), \log(\pi_R)) \quad (3.10)$$

The curvature of the L-curve is given as

$$\kappa(\lambda) = \frac{\rho' \eta'' - \rho'' \eta'}{((\rho')^2 + (\eta')^2)^{1.5}} \quad (3.11)$$

where the superscript ' denotes the differentiation of a variable with respect to λ . Since ρ and η are continuous functions of λ and expressed explicitly for λ , the derivatives in Eq. (3.11) are obtained analytically. The optimal regularization factor that yields the maximum curvature of the L-curve is calculated precisely by a one-dimensional line search.

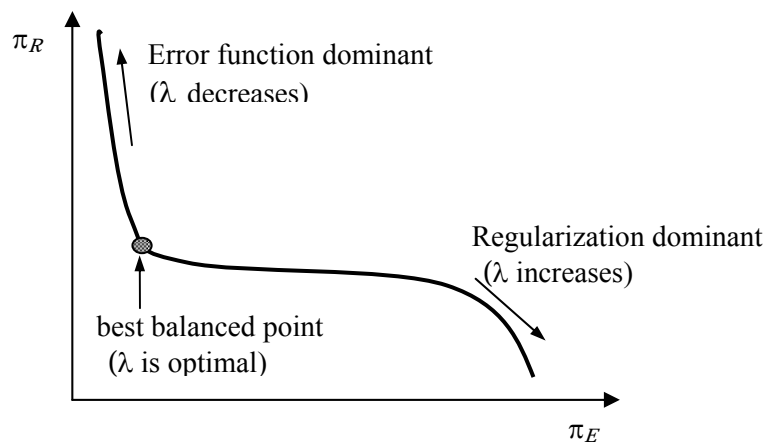


Fig. 3.6. Basic concept of the L-curve method

However, for some nonlinear inverse problems, the solutions by the LCM do not converge. The L-curve with a large regularization factor corresponds to a nonlinear problem affected by a solution error and the L-curve with a smaller regularization factor is affected by measurement noise.

3.1.4c Variable Regularization Factor Scheme (VRFS)

The variable regularization factor scheme (VRFS) is useful in nonlinear inverse problem. The regularization factor can be reduced by multiplying a prescribed reduction factor β ranging from 0 to 1 when the regularization function becomes larger than the error function by the solution of the current iteration. Lee *et al.* demonstrated that identification results are relatively insensitive to moderate values of the reduction factor around 0.1. For shape identification problems and damage detection in framed structures, VRFS with $\beta = 0.1$ has been successfully applied [Lee99, Lee00, Yeo00]. The VRFS method can be easily applied to any type of regularization functions, which is one of the strengths of the VRFS

3.1.4d Generalized Cross Validation (GCV)

A popular method to find the regularization factor is generalized cross validation (GCV). It can be used for determining the regularization factor and for estimating the noise amplitude of measurements [Gol78, Han98]. GCV is based on the statistical idea that an appropriate regularization factor should predict missing measurements. That is, if an arbitrary component of the measurement vector is left out, the corresponding regularization factor should predict this component of the measurement well. The minimization of the

GCV function with respect to the regularization factor can obtain the GCV optimal regularization factor [Gol78, Han98].

3.1.5 Recursive Quadratic Programming

The recursive quadratic programming (RQP) method can solve the constrained nonlinear optimization problem. The RQP algorithm can be applied directly to problems with inequality as well as equality constraints, it is globally convergent, and is amenable to large-scale computation. In a typical iteration of the recursive quadratic programming algorithm, the first step is selecting a feasible starting vector s_o . At the current estimate, the objective function is quadratified and the inequality constraints are linearized. The quadratic objective is minimized and the linearized constraints are satisfied, using an active set strategy. The search direction is then the solution to the quadratic subproblem. The length of the step in this direction is determined by minimizing a line search objective function and a penalty term that becomes positive whenever one or more of the constraints is violated. The line search producer ensures the global convergence of the RQP method. A general nonlinear optimization problem with both equality and inequality constraints can be written as follows:

Minimize $j(s)$

$$\begin{aligned} \text{Subject to } \quad & \mathbf{c}_i(s) = 0 \quad i = 1, \dots, m' \\ & \mathbf{c}_i(s) \leq 0 \quad i = m' + 1, \dots, m \end{aligned} \tag{3.12}$$

where, the object function j and/or some of the constraint c are nonlinear with respect to the unknown variables s . In this proposed parameter estimation problem, the loss function

is the squared error objective function. The vector of the unknown variable s may contain unknown parameters x (output error estimator) and the constraints simply bound the unknown parameters as shown below

$$x_1 \leq x \leq x_2 \quad (3.13)$$

3.1.6 Sensitivity of the objective function

The gradient of the objective function with respect to the unknown parameters: The recursive quadratic programming requires an estimate of the Hessian matrix of the objective function. The exact Hessian matrix and the Gauss-Newton approximation of the Hessian matrix can be used. In this study, the Gauss-Newton approximation of the Hessian matrix, where second derivatives are ignored, is adopted. If we use the Gauss-Newton approximation of the Hessian matrix, the equation becomes quite simple and we can obtain sufficient easily convergence.

3.2 Formulation

In the previous chapter, we computed the displacement response, acceleration response, and calculated frequency response function (calculated FRF.) using the ground acceleration and forced vibration, utilizing known system parameters such as mass, stiffness, and modal damping. Here, system parameter estimation and damage detection are based on system identification, which is an inverse problem. System parameters are priori estimated system parameters. Therefore, the governing equation and modal dynamic equation are used in the same manner as chapter 2. Here, continue to formulate for the output error estimator,

minimization of least square error. There is minimization of least square error with regularization functions by used Tikhonov regularization function. The next step is sensitivity and decomposition of the objective function. Finally, we can obtain a posteriori solution. Fig 3.7. shows the diagram of parameter estimation.

The frequency response function (FRF) is independent of the loading condition. It can be easily known that compare with continuous types of FRF the Eq.(2.13a) for forced vibration and the Eq.(2.23a) for ground motion (earthquake). Similarly, the discrete form of FRF expressed in Eq.(2.14a) and Eq.(2.24a), where the loading term has been omitted. In these equations the difference between two pairs difference is the forced acting points. For example, loading acts for all of the degrees of freedom in a shear building.

3.2.1 Governing Equation (used priori estimated system parameter)

The equation of motion is the same as Eq.(2.2a), for n-degrees of freedom subject to forced vibration for a structure can be written as:

$$\bar{\mathbf{M}} \mathbf{a} + \bar{\mathbf{C}} \mathbf{v} + \bar{\mathbf{K}} \mathbf{u} = \mathbf{f} \quad (3.14a)$$

$$\mathbf{v}(0) = 0 ; \mathbf{u}(0) = 0 \quad (3.14b)$$

where, \mathbf{u} , \mathbf{v} , \mathbf{a} are displacement vector, velocity vector and acceleration vector respectively. $\bar{\mathbf{M}}$, $\bar{\mathbf{K}}$, $\bar{\mathbf{C}}$, \mathbf{f} are priori estimated mass matrix, priori estimated stiffness matrix, priori estimated damping matrix, and force vector. System parameters are element stiffness of a structure and damping ratios or coefficients of Rayleigh damping.

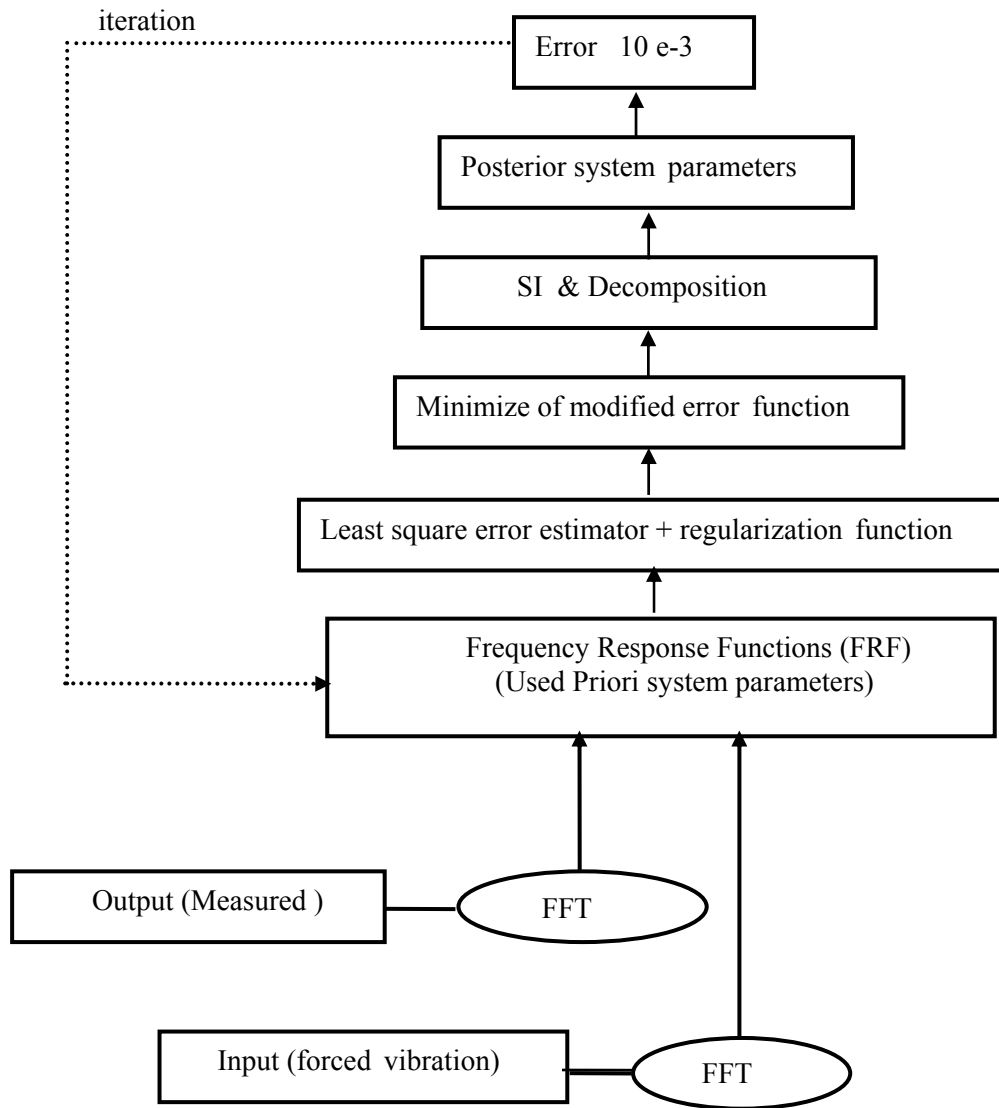


Fig. 3.7 Diagram of the parameter estimation

Eq.(3.14a) is changed to modal coordinate form as follows; it is also the same as

Eq.(2.6a).

$$\bar{m}_r \phi_{pr} \ddot{y}_r + \bar{c}_r \phi_{pr} \dot{y}_r + \bar{k}_r \phi_{pr} y_r = \phi_{pr} \phi_r^T \mathbf{f} \quad (3.15a)$$

$$\bar{m}_r \hat{a}_{pr} + \bar{c}_r \hat{v}_{pr} + \bar{k}_r \hat{u}_{pr} = \phi_{pr} \phi_r^T \quad (3.15b)$$

$$\hat{u}_{pr} = \phi_{pr} y_r \quad (3.15c)$$

where, \bar{m}_r , \bar{c}_r , \bar{k}_r are modal mass matrix, modal stiffness matrix, and modal damping matrix by using the priori estimated system parameters. Then \hat{a}_{pr} , \hat{v}_{pr} , \hat{u}_{pr} is r^{th} mode's relative acceleration, relative velocity, and relative displacement at point p at time t .

3.2.2 Acceleration Response Function

State here is an acceleration response function for forced vibration including initial conditions terms, where Ac_{pr} is the acceleration response for r^{th} mode at point p . \mathfrak{R} is the transformed forced vector.

$$Ac_{pr} = - \frac{\phi_{pr} \phi_r^T \mathfrak{R} \omega^2}{(-\bar{m}_r \omega^2 + \bar{k}_r + i\omega \bar{c}_r)} + \frac{\bar{m}_r \omega^2}{(-\bar{m}_r \omega^2 + \bar{k}_r + i\omega \bar{c}_r)} v_{pr} + \frac{(i\omega \bar{m}_r + \bar{c}_r) \omega^2}{(-\bar{m}_r \omega^2 + \bar{k}_r + i\omega \bar{c}_r)} d_{pr} \quad (3.16)$$

If the initial conditions are zero, the Eq.(3.16) becomes as follows:

$$Ac_{pr} = - \frac{\phi_{pr} \phi_r^T \mathfrak{R} \omega^2}{(-\bar{m}_r \omega^2 + \bar{k}_r + i\omega \bar{c}_r)} \quad (3.17)$$

We can then calculate the acceleration response for the ground motion, including the ground acceleration. In Eq.(3.18), Ag_{pr} is the transformed acceleration response for r^{th} mode at point p .

$$Ag_{pr} = Z(\omega) + \frac{\phi_{pr}\Gamma_r \omega^2}{(-\bar{m}_r\omega^2 + \bar{k}_r + i\omega\bar{c}_r)} Z(\omega) + \frac{\bar{m}_r \omega^2}{(-\bar{m}_r\omega^2 + \bar{k}_r + i\omega\bar{c}_r)} v_{pr} + \frac{(i\omega\bar{m}_r + \bar{c}_r)\omega^2}{(-\bar{m}_r\omega^2 + \bar{k}_r + i\omega\bar{c}_r)} d_{pr} \quad (3.18)$$

Γ_r is the participation vector, expressed as

$$\Gamma_r = \phi_r^T \bar{\mathbf{M}} \mathbf{1} \quad (3.18a)$$

If the initial conditions are zero, the response acceleration can be written as

$$Ag_{pr} = Z(\omega) + \frac{\phi_{pr}\Gamma_r \omega^2}{(-\bar{m}_r\omega^2 + \bar{k}_r + i\omega\bar{c}_r)} Z(\omega) \quad (3.19)$$

where, Ag_{pr} is the transformed acceleration response for r^{th} mode at point p . In Eq.(3.19), the acceleration response is an absolute value, while the input data uses absolute measured acceleration. We can use the measured acceleration response, since the calculated acceleration response is also a relative acceleration response, as in Eq.(3.20)

$$(rel)Ag_{pr} = \frac{\phi_{pr}\Gamma_r \omega^2}{(-\bar{m}_r\omega^2 + \bar{k}_r + i\omega\bar{c}_r)} Z(\omega) \quad (3.20)$$

3.2.3 Frequency response Function (discrete type)

Eq.(3.21a) to the frequency response function

$$\tilde{h}_{prj}(\omega) = -\frac{\phi_{pr}\phi_r^T \tilde{\omega}_j^2}{(-\bar{m}_r\omega^2 + \bar{k}_r + i\omega\bar{c}_r)} \quad (3.21a)$$

$$\psi_r = (-\bar{m}_r\omega^2 + \bar{k}_r + i\omega\bar{c}_r) \quad (3.21b)$$

$$\xi_{pr} = -\phi_{pr}^T \quad (3.21c)$$

Simplifying Eq.(3.21a) using Eq.(3.21b) and Eq.(3.21c) gives:

$$\tilde{h}_{prj}(\omega) = \frac{\tilde{\omega}_j^2}{\tilde{\psi}_{rj}} \xi_{pr} \quad (3.21d)$$

$$\hat{h}_{pr}(\omega) = \sum_{j=1}^{\omega \max} \frac{\tilde{\omega}_j^2}{\tilde{\psi}_{rj}} \xi_{pr} \quad (3.21e)$$

$$\tilde{H}_p(\omega) = \sum_{r=1}^{mp} \sum_{j=1}^{\omega \max} \tilde{h}_{prj}(\omega) \quad (3.21f)$$

hg_{pr} transforms function for r^{th} mode at point p for zero initial conditions due to ground acceleration. Eqs.(3.22a-3.22e) are FRF for discrete type of the frequency range.

$$\tilde{h}g_{prj}(\omega) = \frac{\phi_{pr}\Gamma_r \omega_j^2}{(-\bar{m}_r\omega^2 + \bar{k}_r + i\omega\bar{c}_r)} \quad (3.22a)$$

Modifying to simple a form of Eq.(3.22a) gives

$$h^c_{prj}(\omega) = \frac{\omega_j^2}{\tilde{\psi}_{rj}} \zeta_{pr} \quad (3.22b)$$

$$\tilde{\psi}_{rj} = (-\bar{m}_r\omega^2 + \bar{k}_r + i\omega\bar{c}_r) \quad (3.22c)$$

$$\zeta_{pr} = \phi_{pr}\Gamma_r \quad (3.22d)$$

$$\hat{h}g_{pr}(\omega) = \sum_{j=1}^{\omega \max} \frac{\tilde{\omega}_j^2}{\tilde{\psi}_{rj}} \zeta_{pr} \quad (3.22e)$$

FRF for total modes

$$H^c_p(\omega) = \sum_{r=1}^{mp} \sum_{j=1}^{\omega \max} h^c_{prj}(\omega) \quad (3.22e)$$

3.2.4 Output error estimator for FRF

Here we formulate the output error estimator function using Eq.(3.22b) and Eq.(3.22b) for ground motion. The output error function is different between the measured response function (measured FRF) and the corresponding calculated FRF by the mathematical model.

$$E_p = H_p^m - H_p^c \quad (3.23)$$

where E_p , H_p^m and H_p^c are the output errors estimator function of the total modes FRFs at measured point p , measured FRF (transformed form measured acceleration), and calculated FRF for total modes (transform by calculated acceleration) from the mathematical model

3.2.5 Minimization of least square output error estimator for FRF

The least square error of the output error estimator is expressed by the following Eq. (3.24a).

$$\pi_p = \int_0^{\omega} E_p \bar{E}_p d\omega \quad (3.24a)$$

where, π_p is the least square error for measured point, \bar{E}_p is the conjugate of E_p , and FRF are complex numbers. Here the Euclidean norm is used in Eq.(3.24a). Then, substituting the output error estimator function, we can obtain the following equation:

$$\pi_p = \int_0^{\omega} [H_p^m - H_p^c] [\bar{H}_p^m - \bar{H}_p^c] d\omega \quad (3.24b)$$

where, \bar{H}_p^m, \bar{H}_p^c are the conjugates of H_p^m, H_p^c , respectively.

$$\gamma_p = \int_0^{\omega} [H_p^c \bar{H}_p^c] d\omega \quad (3.24c)$$

where, γ_p is the normalization of the least square error by using the estimated system parameter.

$$\Pi_E = \sum_{p=1}^{npo\ int} \frac{\pi_p}{\gamma_p} = \sum_{p=1}^{npo\ int} \frac{\int_0^{\omega} [H_p^m - H_p^c][\bar{H}_p^m - \bar{H}_p^c] d\omega}{\int_0^{\omega} [H_p^c \bar{H}_p^c] d\omega} \quad (3.25a)$$

where, Π_E is the normalized total least square error or objective function. Eq.(3.25a) is expanded as Eq.(3.25b)

$$\Pi_E = \sum_{p=1}^{npo\ int} \frac{\pi_p}{\gamma_p} = \sum_{p=1}^{npo\ int} \frac{\int_0^{\omega} [H_p^m \bar{H}_p^m - H_p^m \bar{H}_p^c - \bar{H}_p^m H_p^c + H_p^c \bar{H}_p^c] d\omega}{\int_0^{\omega} [H_p^c \bar{H}_p^c] d\omega} \quad (3.25b)$$

Eqs.(3.24a) to (3.25b) are expressed as a continuous type for frequency integrity. Now we change the normalized total least square error function to a discrete type as follows:

$$\Pi_E = \frac{1}{2} \sum_{p=1}^{npo\ int} \frac{1}{\gamma_p} \sum_{p=1}^{n\omega} \left(\begin{array}{l} h_{pj}^m \bar{h}_{pj}^m - h_{pj}^m \sum_{r=1}^{n\ mode} \bar{h}_{prj}^c \\ - \bar{h}_{pj}^m \sum_{r=1}^{n\ mode} h_{prj}^c + \sum_{r=1}^{n\ mode} h_{prj}^c \sum_{r=1}^{n\ mode} \bar{h}_{prj}^c \end{array} \right) \quad (3.25c)$$

where, h_{pj}^m, \bar{h}_{pj}^m are measured FRF and conjugate of measured FRF for each mode and

$h_{prj}^c, \bar{h}_{prj}^c$ are calculated FRF and conjugate of the calculated FRF.

The normalized minimization problem can be written in the following form.

Minimize Π_E
 \mathbf{x}

$$\Rightarrow \frac{\partial}{\partial x_l} \left(\frac{1}{2} \sum_{p=1}^{n_{po\ int}} \frac{1}{\gamma_p} \sum_{p=1}^{n_{\omega}} \left(\begin{array}{l} h_{pj}^m \bar{h}_{pj}^m - h_{pj}^m \sum_{r=1}^{n_{\text{mode}}} \bar{h}_{prj}^c \\ - \bar{h}_{pj}^m \sum_{r=1}^{n_{\text{mode}}} h_{prj}^c + \sum_{r=1}^{n_{\text{mode}}} h_{prj}^c \sum_{r=1}^{n_{\text{mode}}} \bar{h}_{prj}^c \end{array} \right) \right) \leq 0 \quad (3.25d)$$

subject to $\mathbf{R}(\mathbf{x}) \leq 0$

Eqs.(3.24a-3.54d) are not included in the regularization function to overcome the ill-posedness. Here through the Tikhonov regularization function adds at least square error function. Π_R is the Tikhonov regularization function. Modified error functions has been expressed as Eq.(3.6)

$$\Pi_{ER} = \Pi_E + \Pi_R \quad (3.26a)$$

In Eq(3.25a), we obtain the new least square error function as follows:

$$\Pi_{ER} = \sum_{p=1}^{n_{po\ int}} \frac{\int_0^{\omega} [H_p^m - H_p^c][\bar{H}_p^m - \bar{H}_p^c] d\omega}{\int_0^{\omega} [H_p^c \bar{H}_p^c] d\omega} + \frac{1}{2} \lambda^2 \int_V (x - x_0)^2 dV \quad (3.26b)$$

where, x_0 is the center of the function space given *a priori*, λ is a regularization factor that controls the degree of the regularity of the solution space standard Tikhonov regularization function. Then Eq.(3.26b) is expanded and converted into discrete form.

$$\begin{aligned}
\Pi_{ER} &= \frac{1}{2} \sum_{p=1}^{n_{point}} \frac{1}{\gamma_p} \sum_{p=1}^{n_{\omega}} \left(\begin{aligned} &h_{pj}^m \bar{h}_{pj}^m - h_{pj}^m \sum_{r=1}^{n_{mode}} \bar{h}_{prj}^c \\ &-\bar{h}_{pj}^m \sum_{r=1}^{n_{mode}} h_{prj}^c + \sum_{r=1}^{n_{mode}} h_{prj}^c \sum_{r=1}^{n_{mode}} \bar{h}_{prj}^c \end{aligned} \right) + \frac{1}{2} \lambda^2 \|\mathbf{x} - \mathbf{x}_c\|^2 \\
&= \frac{1}{2} \frac{\partial}{\partial x_l} \left(\sum_{p=1}^{n_{point}} \frac{\pi_p}{\gamma_p} \right) + \lambda^2 \|\mathbf{x} - \mathbf{x}_0\| \leq 0
\end{aligned} \tag{3.26c}$$

subject to $\mathbf{R}(\mathbf{x}) \leq 0_2^2$

where, \mathbf{x} , \mathbf{x}_0 are system parameter vector and priori system parameter, respectively.

The least square error minimization is also changed. Therefore Eq.(3.25d) becomes Eq.(3.26d)

$$\begin{aligned}
\text{Minimize}_{\mathbf{x}} \Pi_{ER} &\Rightarrow \frac{\partial \Pi_{ER}}{\partial x_l} = \frac{\partial (\Pi_E + \Pi_R)}{\partial x_l} = \frac{\partial \Pi_E}{\partial x_l} + \frac{\partial \Pi_E}{\partial x_l} \\
&= \frac{1}{2} \frac{\partial}{\partial x_l} \left(\sum_{p=1}^{n_{point}} \frac{\pi_p}{\gamma_p} \right) + \lambda^2 \|\mathbf{x} - \mathbf{x}_0\| \leq 0 \\
&\text{subject to } \mathbf{R}(\mathbf{x}) \leq 0
\end{aligned} \tag{3.26d}$$

Here the gradient of the objective function differentiates with respect to system parameters.

The first term of Eq.(3.26d) is a little complex. Therefore it needs to be derived in more detail.

$$\begin{aligned}
\frac{\partial}{\partial x_l} \left(\sum_{p=1}^{npo \text{ int}} \frac{\pi_p}{\gamma_p} \right) &= \sum_{p=1}^{npo \text{ int}} \frac{1}{\gamma_p} \frac{\partial \pi_p}{\partial x_l} \\
&= \sum_{p=1}^{npo \text{ int}} \frac{1}{\gamma_p} \sum_{j=1}^{n\omega} \left[\begin{aligned} &\sum_{r=1}^{n \text{ mode}} \frac{\partial h_{prj}^c}{\partial x_l} \sum_{r=1}^{n \text{ mode}} \bar{h}_{prj}^c + \sum_{r=1}^{n \text{ mode}} h_{prj}^m \sum_{r=1}^{n \text{ mode}} \frac{\partial \bar{h}_{prj}^c}{\partial x_l} \\ &- h_{pj}^m \sum_{r=1}^{n \text{ mode}} \frac{\partial \bar{h}_{prj}^c}{\partial x_l} - \bar{h}_{pj}^m \sum_{r=1}^{n \text{ mode}} \frac{\partial h_{prj}^c}{\partial x_l} \end{aligned} \right] \\
&= \sum_{p=1}^{npo \text{ int}} \frac{1}{\gamma_p} \sum_{j=1}^{n\omega} \left[\begin{aligned} &\left(\sum_{r=1}^{n \text{ mode}} \bar{h}_{prj}^c - \bar{h}_{pj}^m \right) \sum_{r=1}^{n \text{ mode}} \frac{\partial h_{prj}^c}{\partial x_l} \\ &+ \left(\sum_{r=1}^{n \text{ mode}} h_{prj}^c - h_{pj}^m \right) \sum_{r=1}^{n \text{ mode}} \frac{\partial \bar{h}_{prj}^c}{\partial x_l} \end{aligned} \right] \tag{3.27a} \\
&= \sum_{p=1}^{npo \text{ int}} \frac{1}{\gamma_p} \sum_{j=1}^{n\omega} \left[\begin{aligned} &\left(\sum_{r=1}^{n \text{ mode}} \text{conjg}(h_{prj}^c) - \text{conjg}(h_{pj}^m) \right) \sum_{r=1}^{n \text{ mode}} \frac{\partial h_{prj}^c}{\partial x_l} \\ &+ \left(\sum_{r=1}^{n \text{ mode}} h_{prj}^c - h_{pj}^m \right) \sum_{r=1}^{n \text{ mode}} \text{conjg} \left(\frac{\partial h_{prj}^c}{\partial x_l} \right) \end{aligned} \right]
\end{aligned}$$

In the last sentence of Eq.(3.27a) , the calculated FRF must be differentiated with respect to the system parameters.

$$\frac{\partial h_{prj}^c}{\partial x_l} = \frac{\partial}{\partial x_l} \left(\frac{\omega_j^2}{\tilde{\psi}_{rj}} \zeta_{pr} \right) = \frac{\omega_j^2}{\tilde{\psi}_{rj}^2} \left(\tilde{\psi}_{rj} \frac{\partial \zeta_{pr}}{\partial x_l} - \frac{\partial \tilde{\psi}_{rj}}{\partial x_l} \zeta_{pr} \right) \tag{3.27b}$$

$$\frac{\partial \tilde{\psi}_{rj}}{\partial x_l} = -\frac{\partial \bar{m}_r}{\partial x_l} \omega_j^2 + \frac{\partial \bar{k}_r}{\partial x_l} + i\omega_j \frac{\partial \bar{c}_r}{\partial x_l}; \tag{3.27c}$$

$$\frac{\partial \zeta_{pr}}{\partial x_l} = \frac{\partial \phi_{pr}}{\partial x_l} \Gamma_r + \phi_{pr} \frac{\partial \Gamma_r}{\partial x_l} \tag{3.27d}$$

If the eigenvectors are mass-normalized, then $\bar{m}_r = \phi_r^T [\bar{\mathbf{M}}] \phi_r = 1$ for all modes

$$\bar{m}_r = \phi_r^T [\bar{\mathbf{M}}] \phi_r = 1 \quad (3.27e)$$

Gradient of the modal mass with respect to the system parameters is

$$\frac{\partial \bar{m}_r}{\partial x_l} = \frac{\partial}{\partial x_l} [\phi_r^T [\bar{\mathbf{M}}] \phi_r] = \frac{\partial}{\partial x_l} [1] = 0 \quad (3.27f)$$

Gradient of the modal stiffness w.r.t system parameters is

$$\frac{\partial \bar{k}_r}{\partial x_l} = \frac{\partial}{\partial x_l} [\phi_r^T \bar{\mathbf{K}} \phi_r] = \frac{\partial \phi_r^T}{\partial x_l} \bar{\mathbf{K}} \phi_r + \phi_r^T \frac{\partial \bar{\mathbf{K}}}{\partial x_l} \phi_r + \phi_r^T \bar{\mathbf{K}} \frac{\partial \phi_r}{\partial x_l} = 2 \frac{\partial \phi_r^T}{\partial x_l} \bar{\mathbf{K}} \phi_r + \phi_r^T \frac{\partial \bar{\mathbf{K}}}{\partial x_l} \phi_r \quad (3.27g)$$

Gradient of the modal damping w.r.t system parameters is

$$\frac{\partial \bar{c}_r}{\partial x_l} = \frac{\partial}{\partial x_l} [\zeta_r \bar{k}_r] = \frac{\partial \zeta_r}{\partial x_l} \bar{k}_r + \frac{\partial \bar{k}_r}{\partial x_l} \zeta_r \quad (3.27h)$$

where, ζ_r is the damping ratio for each mode. The modal damping ratios are used as the system parameters. If we substitute the coefficients of the Rayleigh damping in modal damping, the following is obtained

$$\zeta_r = \frac{\kappa_1}{2} \frac{1}{\sqrt{\frac{\bar{k}_r}{\bar{m}_r}}} + \frac{\kappa_2}{2} \sqrt{\frac{\bar{k}_r}{\bar{m}_r}} \quad (3.27i)$$

where, κ_1, κ_2 are coefficients of Rayleigh damping

Gradient of the participation w.r.t system parameters is

$$\frac{\partial \Gamma_r}{\partial x_l} = \frac{\partial}{\partial x_l} [\phi_r^T [\bar{\mathbf{M}}] \{1\}] = \frac{\partial \phi_r^T}{\partial x_l} [\bar{\mathbf{M}}] \{1\} + \phi_r^T \frac{\partial [\bar{\mathbf{M}}]}{\partial x_l} \{1\} \quad (3.27j)$$

$$\frac{\partial [\bar{\mathbf{M}}]}{\partial x_l} = 0 \quad (3.27k)$$

$$\frac{\partial \Gamma_r}{\partial x_l} = \frac{\partial \phi_r^T}{\partial x_l} [\bar{\mathbf{M}}] \{1\} \quad (3.27l)$$

Eq.(3.27g) and Eq.(3.27g) included the differentiation of the mode shape vector. They can be solved using the reference of [Kan02]

$$\frac{\partial \phi_r}{\partial x_l} = \sum_{\substack{s=1 \\ s \neq r}}^N \alpha_{rs} \phi_s \quad (3.27m)$$

$$\alpha_{rs} = -\frac{\phi_r^T \frac{\partial \bar{k}_r}{\partial x_l} \phi_r}{\bar{k}_s - \bar{k}_r} \quad (r \neq s) \quad (3.27n)$$

$$\frac{\partial \phi_r}{\partial x_l} = \sum_{\substack{r=1 \\ r \neq s}}^{n \text{ mode}} -\frac{\phi_r^T \frac{\partial \bar{k}_r}{\partial x_l} \phi_r}{\bar{k}_s - \bar{k}_r} \phi_s \quad (3.27o)$$

If r is equal to s , Eq.(3.27n) change to follow

$$\frac{\partial \phi_r}{\partial x_l} = 0 \quad , \quad (\alpha_{rr} = 0) \quad (3.27p)$$

3.2.6 SVD of the Output Error Estimator

The solution of the minimization problem Eq.(3.26d) is obtained by solving iteratively. The second order sensitivities of the objective function differentiate with respect to the system parameters. It is the Gauss-Newton Hessian matrix, can be expressed as follow

$$\begin{aligned}
hessian &= \frac{\partial^2 \Pi_{ER}}{\partial x_l \partial x_t} = \frac{\partial^2 (\Pi_E + \Pi_R)}{\partial x_l \partial x_t} = \frac{\partial^2 \Pi_E}{\partial x_l \partial x_t} + \frac{\partial^2 \Pi_E}{\partial x_l \partial x_t} \\
&= \frac{1}{2} \frac{\partial^2}{\partial x_l \partial x_t} \left(\sum_{p=1}^{npo \text{ int}} \frac{\pi_p}{\gamma_p} \right) + \lambda^2 \leq 0
\end{aligned} \tag{3.28a}$$

subject to $\mathbf{R}(\mathbf{x}) \leq 0$

Expanding the Eq.(3.28a)

$$\begin{aligned}
&\frac{\partial^2}{\partial x_l \partial x_t} \left(\sum_{p=1}^{npo \text{ int}} \frac{\pi_p}{\gamma_p} \right) \\
&= \sum_{p=1}^{npo \text{ int}} \frac{1}{\gamma_p} \frac{\partial^2 \pi_p}{\partial x_l \partial x_t} \\
&= \sum_{p=1}^{npo \text{ int}} \frac{1}{\gamma_p} \sum_{j=1}^{no} \left(\sum_{r=1}^{n \text{ mode}} \frac{\partial h_{prj}^c}{\partial x_l} \sum_{r=1}^{n \text{ mode}} \frac{\partial \bar{h}_{prj}^c}{\partial x_t} + \sum_{r=1}^{n \text{ mode}} \frac{\partial h_{prj}^c}{\partial x_t} \sum_{r=1}^{n \text{ mode}} \frac{\partial \bar{h}_{prj}^c}{\partial x_l} \right) \\
&= \sum_{p=1}^{npo \text{ int}} \frac{1}{\gamma_p} \sum_{j=1}^{no} \left(\sum_{r=1}^{n \text{ mode}} \frac{\partial h_{prj}^c}{\partial x_l} \sum_{r=1}^{n \text{ mode}} \text{conjg} \left(\frac{\partial h_{prj}^c}{\partial x_t} \right) + \sum_{r=1}^{n \text{ mode}} \frac{\partial h_{prj}^c}{\partial x_t} \sum_{r=1}^{n \text{ mode}} \text{conjg} \left(\frac{\partial h_{prj}^c}{\partial x_l} \right) \right)
\end{aligned} \tag{3.28b}$$

The next chapter is verification of these formulations and concept.

Chapter 4

Numerical Example

In this chapter, the effectiveness of the regularization of SI for shear building framed structures is investigated through numerical simulation studies. Noise caused by measurement error is simulated by adding random noise generated from a uniform probability function to acceleration calculated by a frame structure model [par02].

Here, existing damping models cannot exactly describe the actual damping characteristics of the real structure. Therefore, the damping properties are assumed as known properties, and only stiffness properties are identified. The damping has an important effect on the dynamic response of a structure. Although the damping properties are not known a priori, they should be included in the system parameters in the SI. The modal damping ratios are used as known damping properties when simulating the acceleration response. The coefficients of Rayleigh damping can be determined when any two modal damping ratios and the corresponding modal frequencies are specified. Rayleigh damping coefficients are taken as the system parameters. Because the modal damping is employed in the parameters, the number of system parameters associated with the damping is equal to that of the total number of DOFs, which increases the total number of unknowns in the optimization problem.

Both of Rayleigh damping and modal damping cannot exactly describe actual damping. The modal damping requires more unknown parameters than the Rayleigh damping in the system parameter estimation. Here, Rayleigh damping coefficients are used as system parameters to reduce the unknown system parameters. The approximate natural frequency

frame structure can be obtained from the UBC formula as follows

$$T = C_t (h_n)^{3/4} \quad (4.1)$$

where, C_t is equal to 0.0488 as a factor (MKS) and h_n is the total height of the building. 25% of the Kobe ground accelerations with a peak factor of 0.831 are used. Time interval of ground accelerations is 0.005 seconds. One of the every four data is picked up from the acceleration data in the time domain to change the acceleration response data in frequency domain. In the examples, the stiffness of each element and Rayleigh damping coefficients are taken as system parameters.

The convergent criterion, $\|\Delta\varepsilon\| / \|\varepsilon\| \leq 10^{-3}$, is used to terminate optimizations unless otherwise stated. The baseline properties are assumed for the stiffness of elements and Rayleigh damping coefficients. The initial values of the system parameters are taken to be the same as the baseline properties for the optimization. The upper and lower bounds of the stiffness system parameters are 0.01 times and 3 times the baseline stiffness, 0.01 times and 10 times for mass-proportional damping coefficient, and 0.01 times and 100000 times for the stiffness-proportional damping coefficient of the baseline Rayleigh damping coefficients. Recursive quadratic programming with an active set algorithm [Lue89] is utilized for optimization.

Damage detection based on SI algorithms has been proposed for frame structures in a global sense [San91, Doe96, Hje96, Yeo00, Par02]. All of these methods have respective advantages and limitations.

For a framed structure, the solution space of SI is properly defined by the L_2 -norm of the system property. To overcome difficulties caused by sparseness of measurements and measurement noise, an SI-based damage assessment algorithm is presented.

In modeling a framed structure (shear building), model is idealized by a line representing the story stiffness, which is a summation of column stiffness in each story. The material properties of a member are considered to calculate the column stiffness and total weight of each floor as a lump mass. Numerical examples are five story shear building and ten story shear building. And three story shear building is experimental example.

The solution space of the SI problems can be defined by the regularity condition that represents the integrability condition of the system property. For the solution of a square integrable function, the following regularity condition defined by the L_2 -norm around the baseline value is appropriate.

4.1. Numerical Example1 – Damage detection for a 5 story shear building

Numerical simulation studies are performed for two damage cases with the proposed method to determine the damage status of the five stories shear building. Fig. 4.1a is the frame structural geometry, support conditions, and Fig. 4.1b is the model of the structure. Each story's stiffness is summation of total columns' stiffness in each floor. Story's stiffness is used as the element stiffness as shown Fig. 4.1b. The material properties of the structure are as shown in Table 4.1.

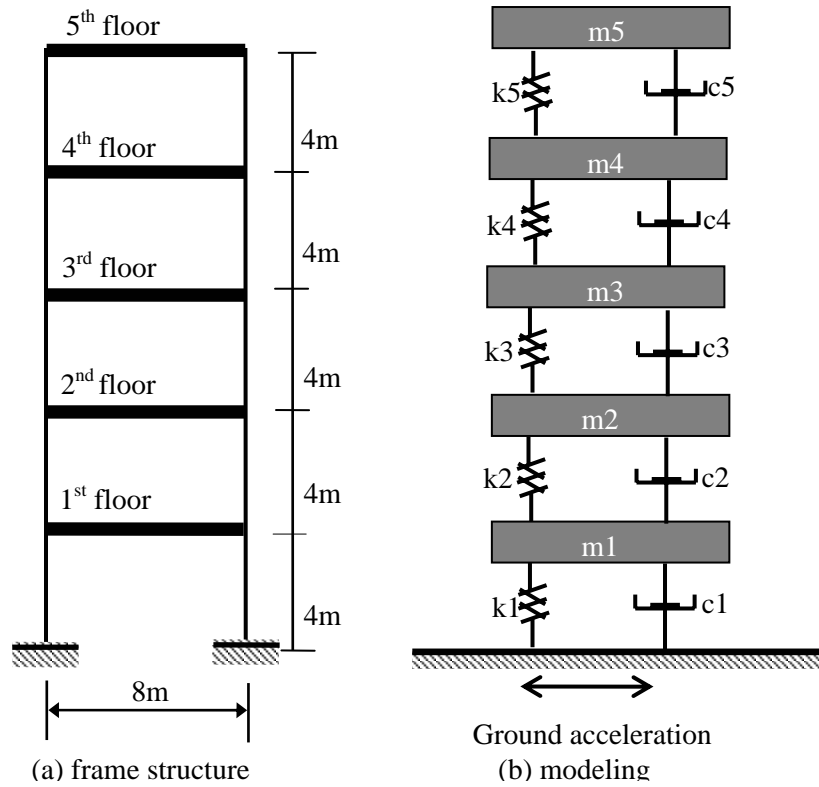


Fig. 4.1 Five story shear building (a) Frame structure, (b) modeling

Table 4.1 Material properties for a five story shear building

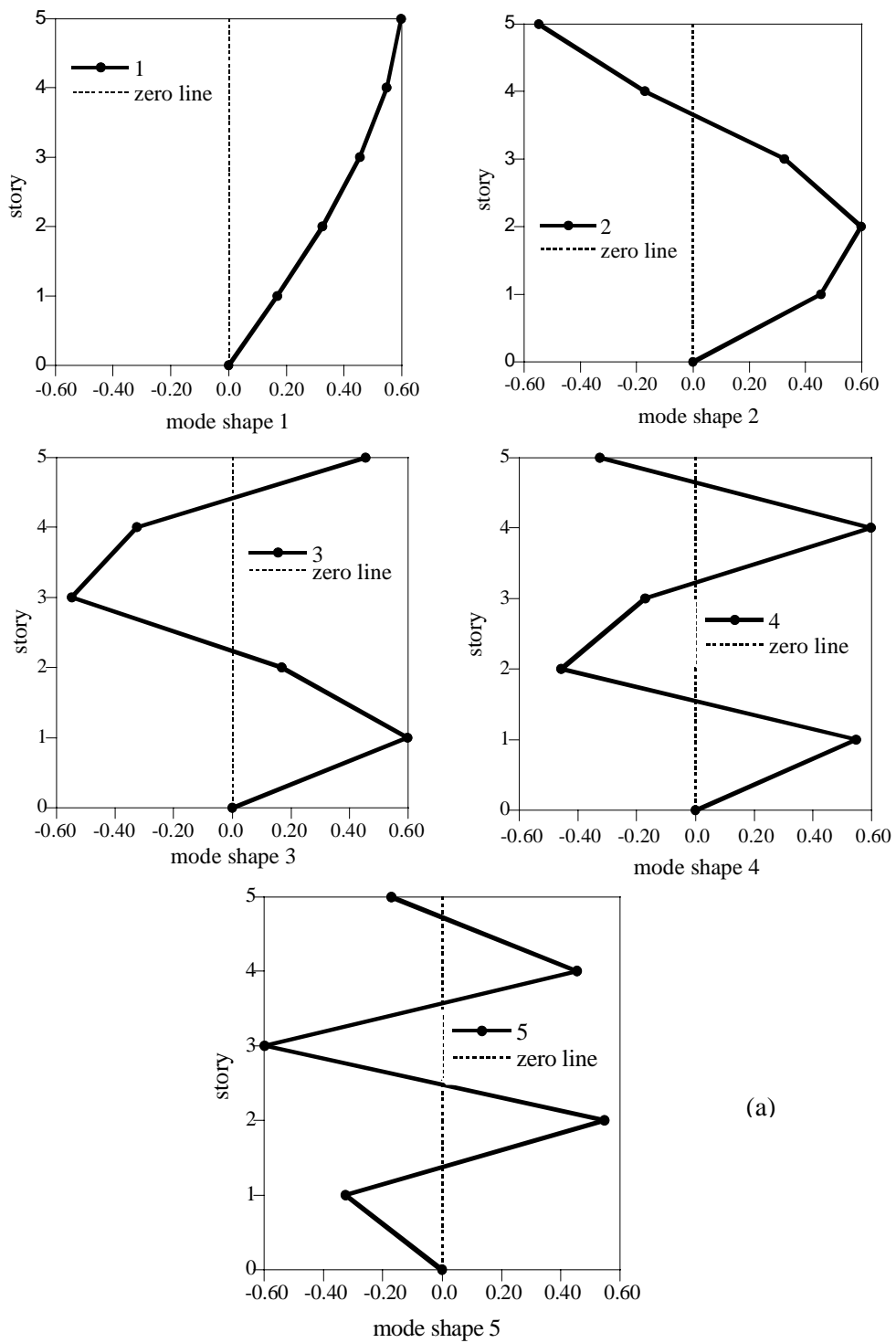
Type	Amount	Unit
Stiffness (For each story)	75,000,000.0	N/m
Mass	45,000.0	kg
Young's modulus	210.0	Gpa

Table 4.2 Baseline properties for a five story shear building

Mode no	Frequency (rad/sec)	Frequency(Hz)	Modal damping ratio
1	11.6200	1.8486	0.0100
2	33.9185	5.3961	0.0101
3	53.4693	8.5065	0.0134
4	68.6881	10.9276	0.0199
5	78.3423	12.4635	0.0296

The mode shapes and the natural frequencies are computed by using baseline properties and assumed modal damping ratios shapes as shown in Fig. 4.2a, Fig. 4.2b.and Fig. 4.2c, respectively. Fig. 4.2a shows the mode shapes of the no damage structure. These mode shapes are used in selecting the measured points. If one point is an inflection point which point can not use as a measuring point. In this structure, the point of inflection is not on the any node. Therefore every point can be used as a measuring point. But results have differences depend on selected measuring point or measuring point combinations. It can be seen in example case2. The values of the natural frequencies and modal damping ratios are given in Table 4.2.

This example has two damaged cases. Case 1 is single damaged case that is 30% reduced stiffness at the first story with 10% noise and two measuring points at the top floor and third floor. Case 2 is multi-damaged case. In case 2, damages are 60% reduced stiffness at the first floor and 30% reduced stiffness at the third floor. 10% noise includes as error and three measuring points are at the first floor, third floor and top floor, respectively. Comparison of the frequency response functions and system parameters are tested by various combinations of measured points, various frequency bands, and full measuring



(a)

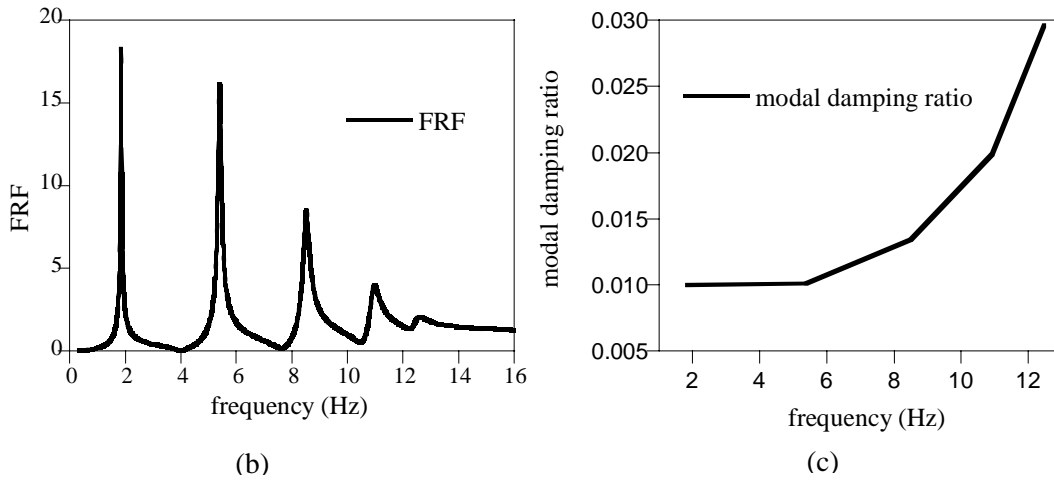


Fig. 4.2 Five story shear building. (a) Mode shapes. (b) Natural frequencies.
(c) Modal damping ratios.

points. Moreover, the estimated system parameters are compared with using regularization function in objection function and no using regularization function.

Case 1. *Two points measuring at 3rd and 5th floor, 10% noise–30% damage at element 1*

(a) Full frequency band used in SI

Damage is simulated with 30% reduction in the stiffness of the first story, as shown in Fig. 4.3. Proportional random noise generated by a uniform probability function between \pm noise amplitude is added to the acceleration response obtained by a mathematical model to simulate real measurements. Unless otherwise stated a noise amplitude of 10% is used in examples. There are five unknown system parameters of stiffness and two unknowns for the coefficients of Rayleigh damping. In this case, the measuring point is located at the top floor and 3rd floor. The natural frequencies for the damaged structure are shown in Table 4.3. The frequency response function at measured point 3 can be seen as

shown in Fig. 4.4. Also the estimated stiffness and damping ratios are shown in Fig. 4.5 and Fig. 4.6, respectively. At the damaged structure, reduced the stiffness and mass are not changed. Therefore, values of the damaged natural frequencies are smaller than the value of no damage can be seen easily in Table 4.3.

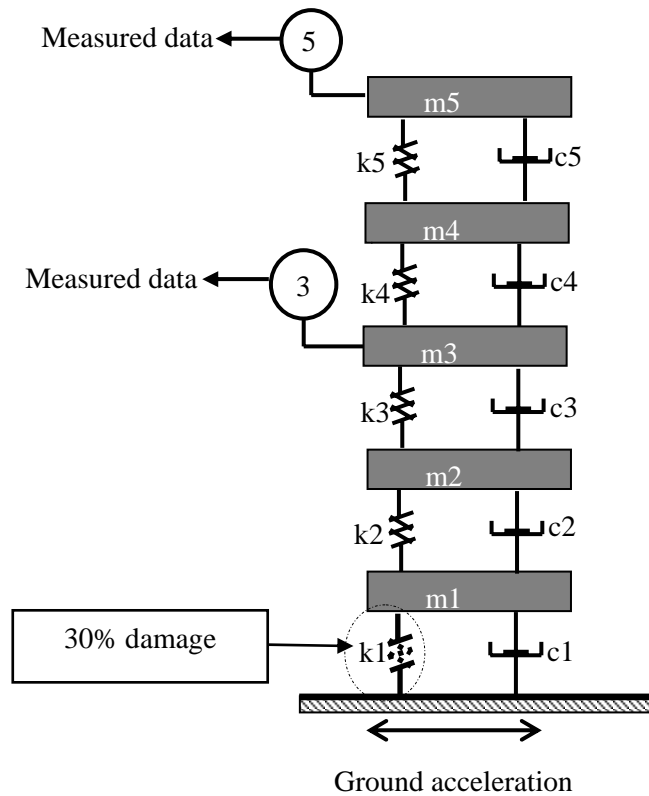


Fig 4.3 Model with 30% reduced stiffness damage at first story

Table 4.3 Natural frequencies (Hz) for no-damage case and with 30% damage case

Mode no	no damaged case	With 30% damaged case
1	1.8486	1.7196
2	5.3961	5.1077
3	8.5065	8.2329
4	10.9276	10.7685
5	12.4635	12.4180

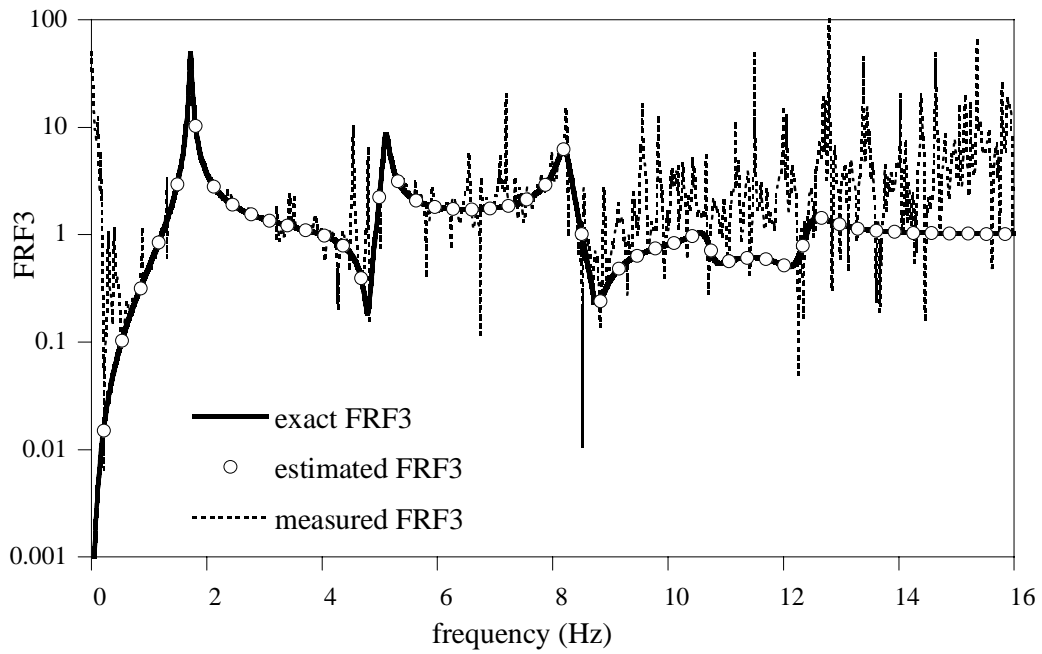


Fig. 4.4 Exact FRF3 by using the damaged stiffness value and measured FRF3

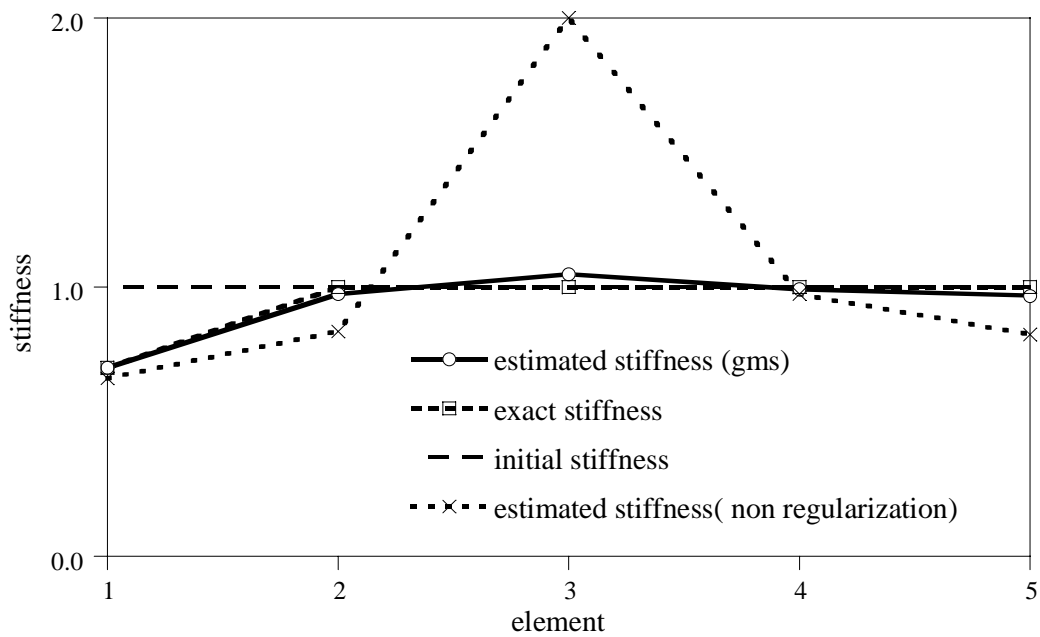


Fig 4.5 Estimated stiffness for regularization and non regularization, using full frequency band in SI for damaged structure

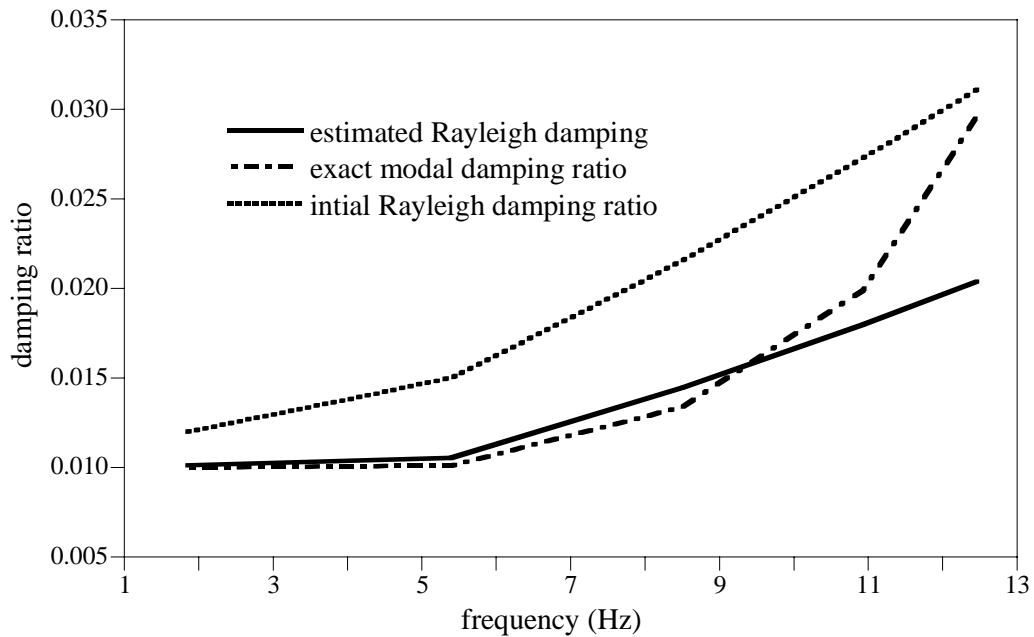


Fig. 4.6 Damping ratios using full frequency band in SI for damaged Structure

Fig. 4.4 shows the exact FRF3 by using damaged stiffness, measured FRF3 calculated from the mathematical model with 10% noise and estimated FRF3 from the author's proposed method. The FRF3 is the measured point at the third floor. The peak points' frequency values of FRF3 are the natural frequencies and the peak values are damping.

The regularization effect can be seen in Fig. 4.5, in which the results of estimated stiffness values of the structure show better accuracy than when the regularization technique is not used. Tikhonov Regularization method is used followed by the Geometric Mean Scheme (GMS) regularization factor. The baseline properties are used as the initial stiffness. Table 4.4 shows the value of estimated stiffness at using the regularization and not using the regularization. The regularized estimated stiffness is more similar to the exact value than no regularized estimated stiffness.

The estimated damping ratios are shown in Fig. 4.6. The damping ratios' results are reasonable. Initial damping is Rayleigh damping. It has just two unknowns which are mass proportional coefficient and stiffness proportional coefficient. But exact damping is assumed modal damping and it has five unknowns as the modal damping ratios. Therefore, the first and the second estimated damping ratios are nearly exact damping ratios and others are different from exact damping ratios.

Table 4.4 Comparison of the initial, exact and estimated stiffness (N/m) with regularization and non regularization technique

Story no.	Initial	Exact	Estimated with regularization	Estimated non regularization
1	75,000,000	52,500,000	52,506,818	49,93,907
2	75,000,000	75,000,000	73,073,452	62,735,391
3	75,000,000	75,000,000	78,631,133	150,040,046
4	75,000,000	75,000,000	74,475,631	73,121,757
5	75,000,000	75,000,000	72,491,802	61,695,421

(b) Various frequency bands used in SI

Frequency bands are used in system identification. This is one of the advantages of the SI in frequency domain. Mostly, frequency ranges are used within first and third mode frequency range in SI and do not use full frequency range because noise is dormant in full frequency band. Fig. 4.7 is mode3 frequency range FRF and full band frequency FRF. Here, noise is dormant in after mode3 frequency range. Both of the estimated FRFs are same shape with exact FRF. The frequency band needs to take just before noise dormant portion. In this example, the frequency band up to mode 2 is not enough to get the good result and

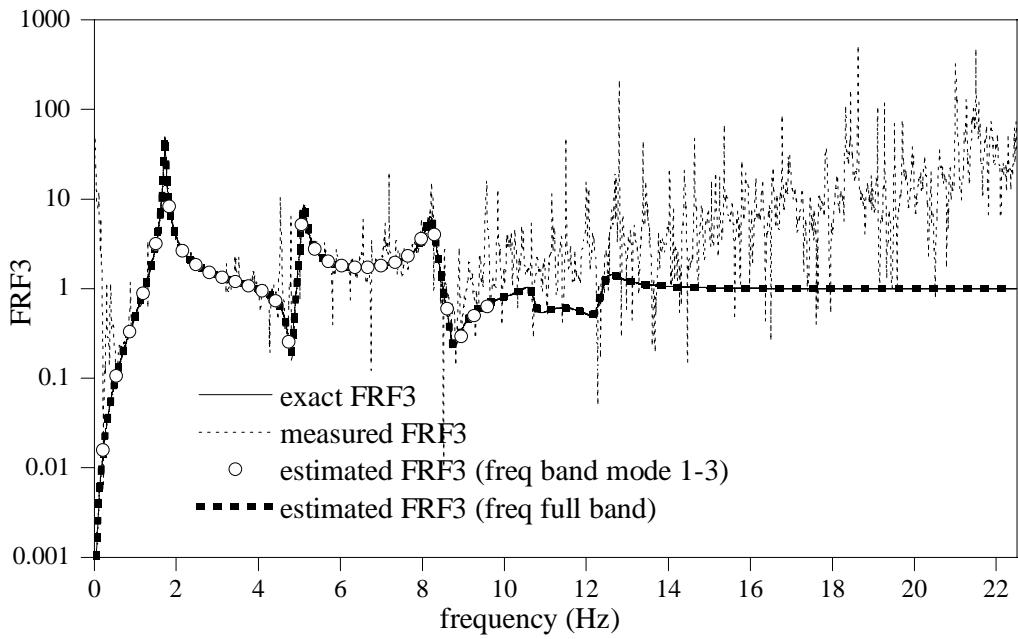


Fig. 4.7 FRF3 for full band frequency and FRF3 for frequency band up to mode3

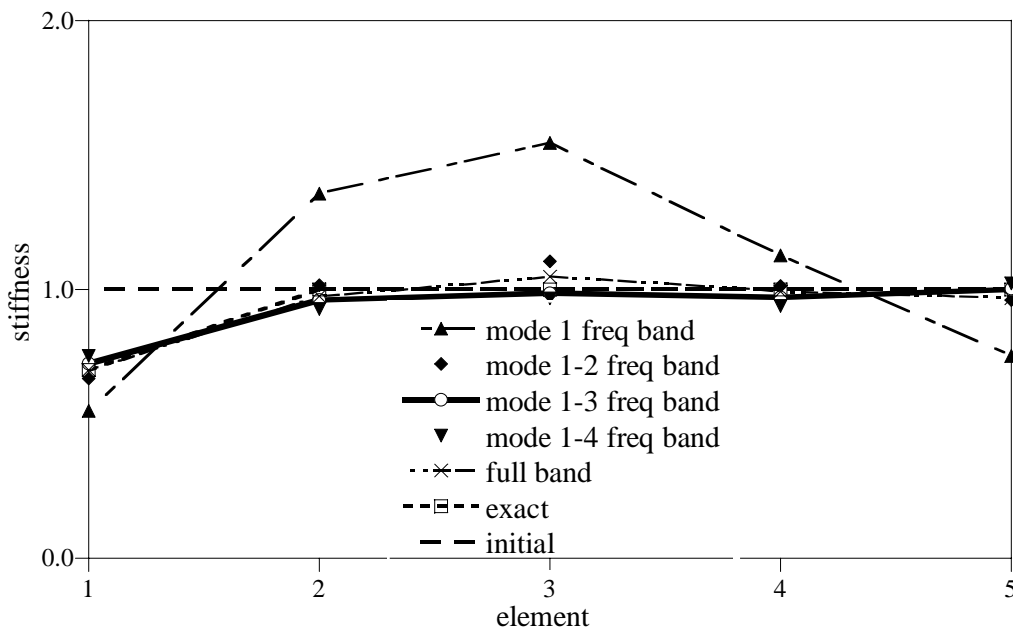


Fig. 4.8 Estimated stiffness with various frequency bands in SI

needs the frequency band up to mode 3. Fig. 4.8 shows the estimated stiffness that used the mode 3 frequency range in SI is the best among the estimated stiffness at mode1 frequency band, mode 2 frequency band and full band. The estimated stiffness which mode 3 frequency band and using regularization function in SI is more reasonable than the estimated stiffness without regularization as shown in Fig. 4.9.

(c) Full measuring points

In Fig. 4.10, FRF1s are using the full measuring data at full band frequency and mode 2 frequency band. The reasonable estimated stiffness results can be obtained at frequency band up to mode 2 and full measuring data. Although using the frequency band up to first

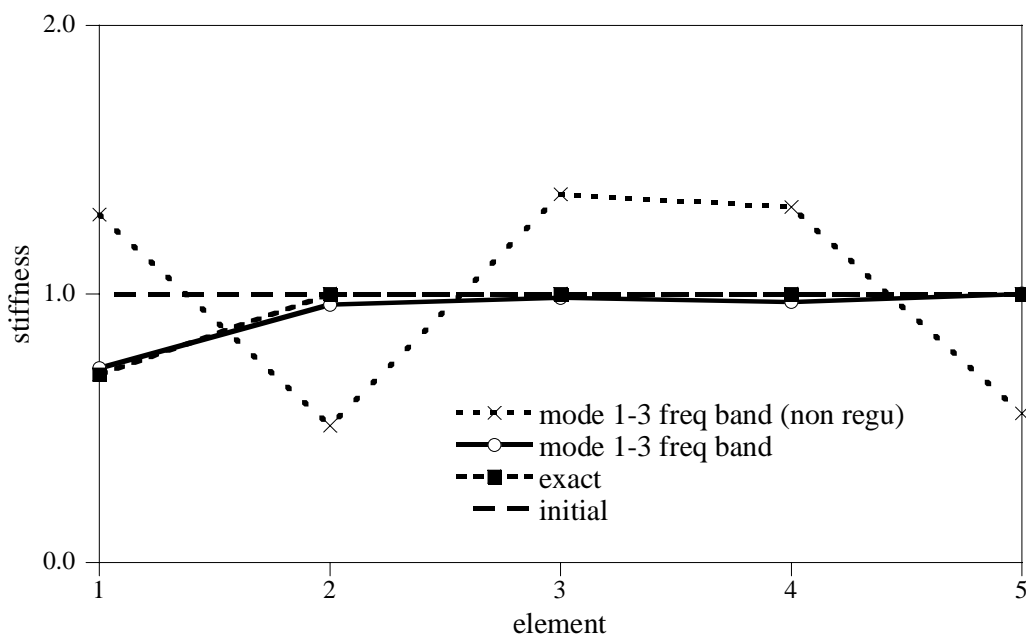


Fig. 4.9 Estimated stiffness using regularization and non regularization at frequency band up to mode 3 in SI).

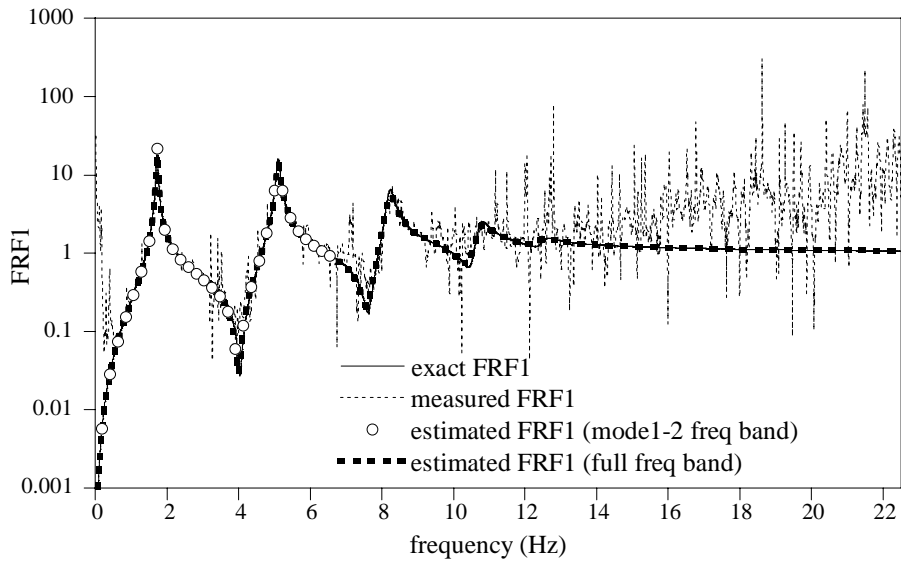


Fig. 4.10 FRF1 for full measuring points at various frequency bands

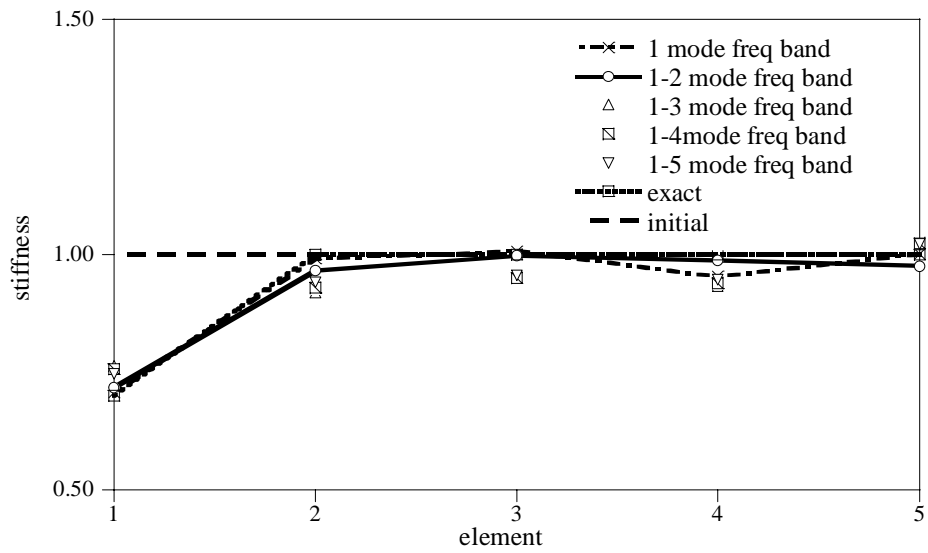


Fig. 4.11 Estimated stiffness for full measuring points at various frequency bands

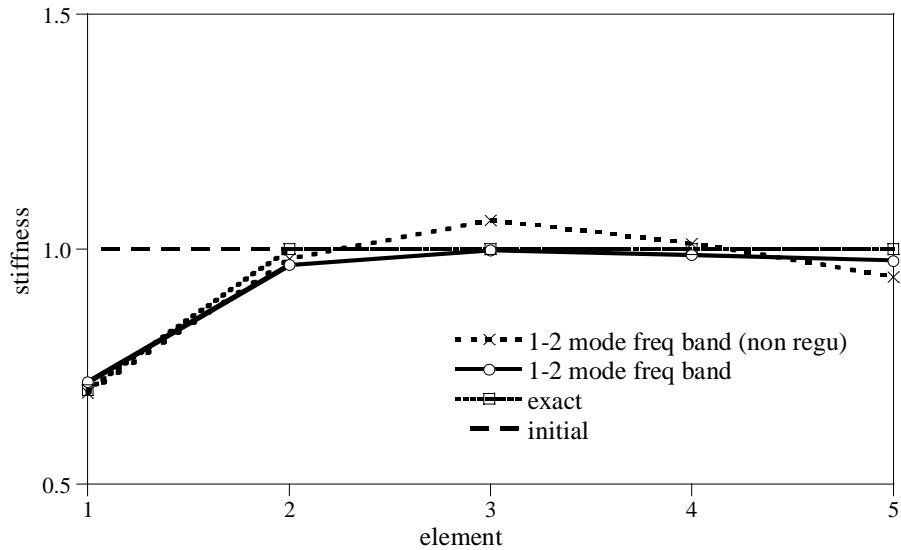


Fig. 4.12 Estimated stiffness for full measuring points at mode2 frequency band

mode and full measuring is also good result, the regularization factor is too small in SI.

Therefore, the regularization effect is not influent in parameter estimation and the estimated stiffness used regularization function and do not use the regularization are same. Fig. 4.11 shows the estimated stiffness for various frequency bands. Frequency band up to second mode is the best result. The result of regularized estimated stiffness which is better than without regularized estimated stiffness are shown in Fig. 4.12.

Case 2 10% noise , three measuring points are at first floor , third floor and fifth floor , 60% damage at element 1 and element 3

Fig. 4.13 shows a multi-damaged case. There are 60% damage at the first floor of the structure (element 1 of the model) and 30% damage at the third floor (element 3). The percentage of the generated noise is 10. The measuring points are at first, third and fifth

floors. The frequency response functions, estimated FRF, measured FRF, and exact FRF for point 1 are presented in Fig. 4.14. We can then obtain the natural frequency, which corresponds to the point of the peak values of FRF, where the peaks points are slightly different from the exact and estimated FRF at 3rd mode and 4th mode. The regularized estimated stiffness results are better than the not-regularized estimated stiffness.

(a) Full frequency band used in SI

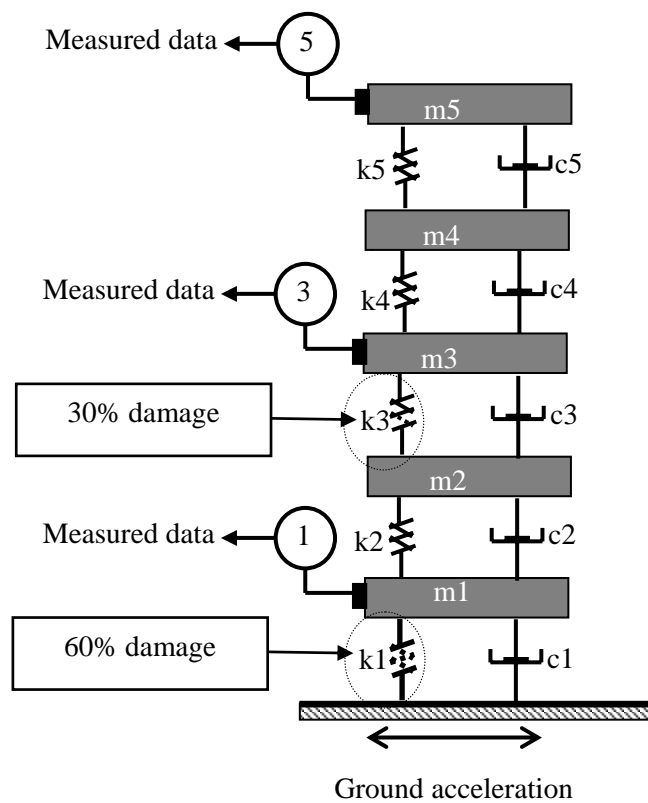


Fig. 4.13 Model for multi-damaged structure

Table 4.5 Comparison of the natural frequencies (Hz) base line data with 60% damage at first story and 30% damage at third story

Mode no	No damage	With damage
1	1.8486	1.4418
2	5.3961	4.5007
3	8.5065	7.6572
4	10.9276	10.4256
5	12.46350	11.8055

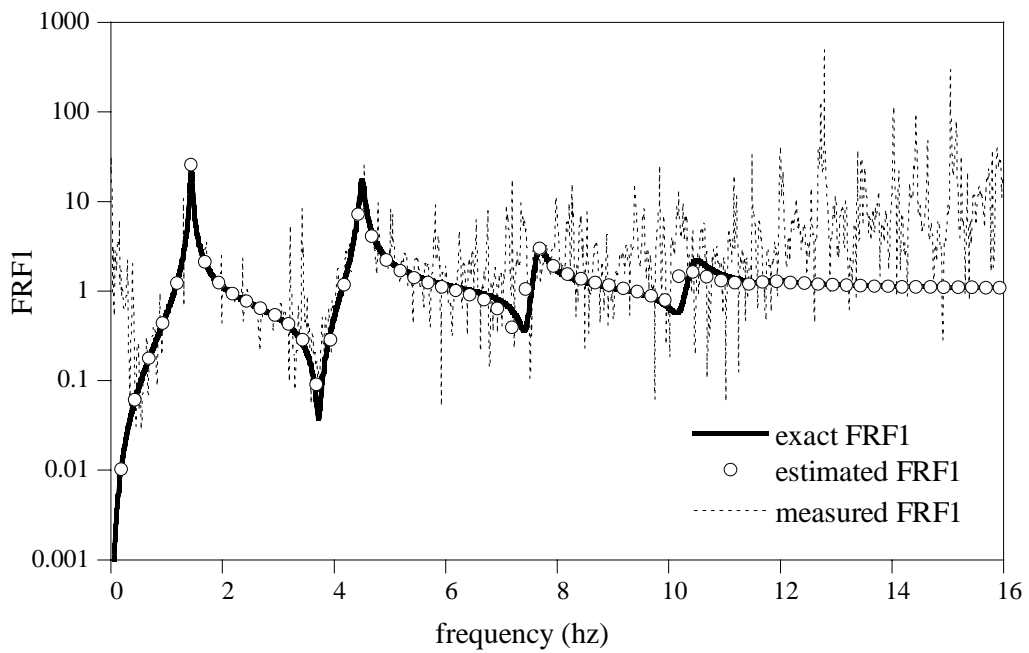


Fig. 4.14 FRF1 for full band frequency for multi-damaged structure

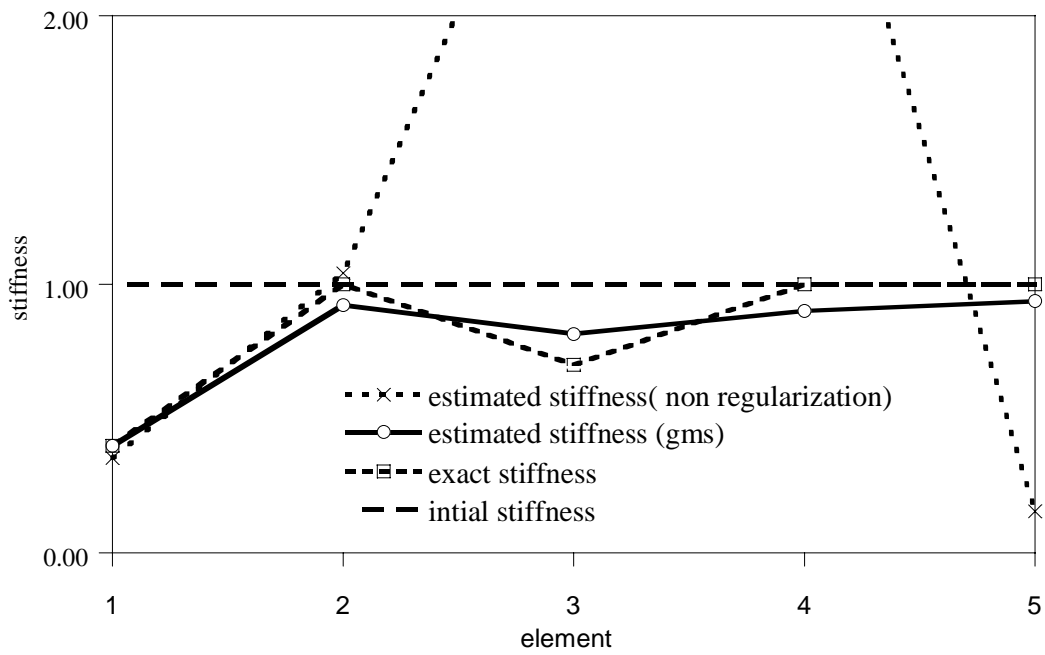


Fig. 4.15 Estimated stiffness for regularization and non regularization using full frequency band in SI for damaged structure

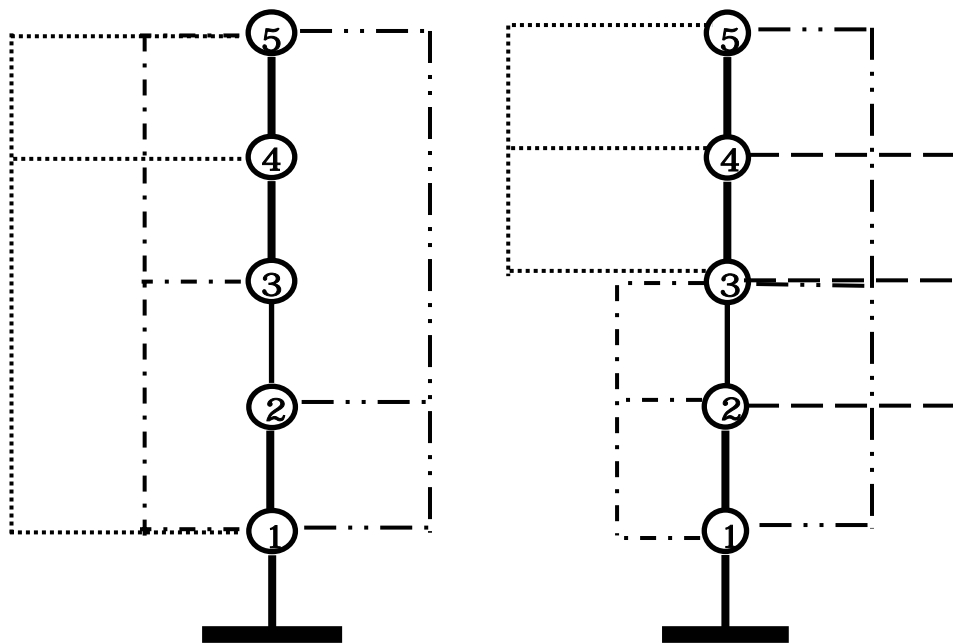


Fig. 4.16 Measuring point combinations. (a) 135, 145, 125. (b) 123, 345, 234, 135.

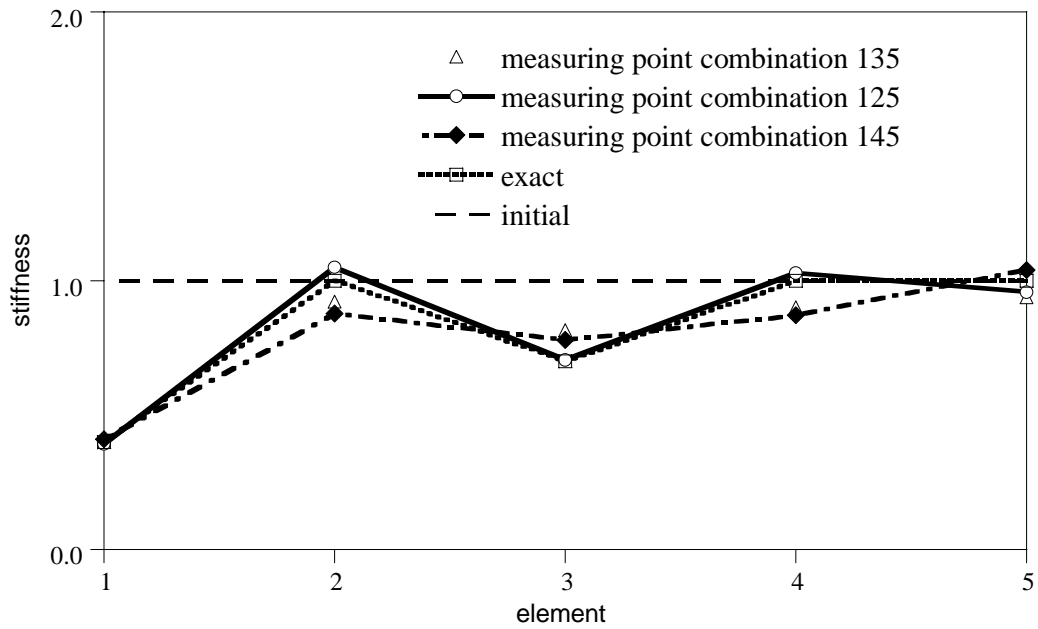


Fig. 4.17 Estimated stiffness for measuring points (123, 125, 234, 345)

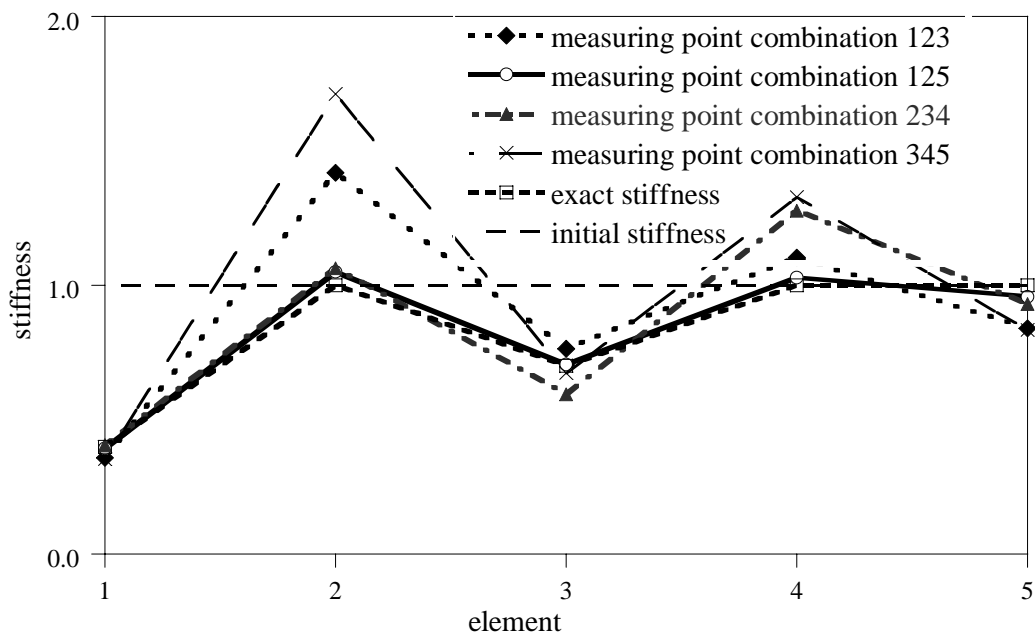


Fig. 4.18 Estimated stiffness for measuring points (123, 125, 234, 345)

there is a slight difference from the exact values (see Fig.4.15). Adjusting the measuring points gives more reasonable results. The measuring points are changed as the combinations of points 125 , 145, and 234. Among these combinations, the best results are the point 125 combinations, as shown in Fig 4.17 and Fig 4.18. Also we can see the numerical data in Table 4.6 and the error percentage of the estimated stiffness with respect to the exact stiffness for kinds of combinations of three measuring points which can be seen in Table 4.7. The 125 measuring point combination is the smallest error percentage of estimated stiffness among the all measuring point combinations. The results of the damping properties can be seen in Fig. 4.19.

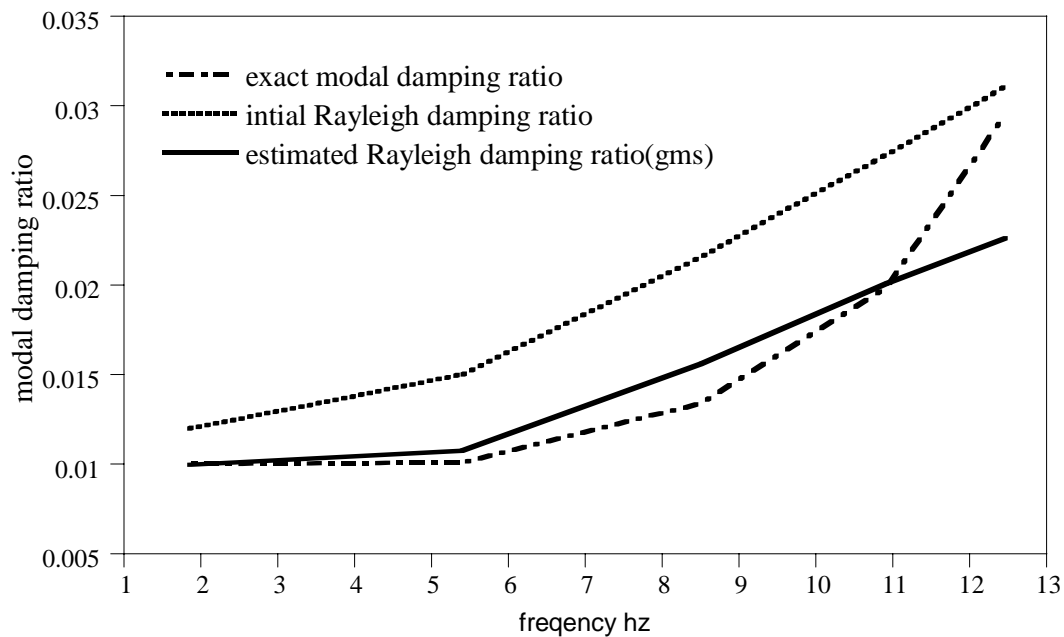


Fig. 4.19 Damping ratios for measuring points combination 125

Table 4.6 Estimated stiffness (N/m) for various combinations of three measuring points

story no	exact	135	125	245
1	30,000,000	29,895,578	29,469,070	34,570,551
2	75,000,000	69,297,444	78,712,602	50,012,544
3	52,500,000	61,212,729	52,828,121	64,359,905
4	75,000,000	67,600,742	77,096,990	58,896,987
5	75,000,000	70,421,493	71,714,473	68,443,300

Table 4.7 Error % of estimated stiffness (N/m) with respect to exact stiffness for kinds of combinations of measuring three points.

story no	135	125	245
1	0.35	1.77	15.24
2	7.60	4.96	33.32
3	16.60	0.63	22.59
4	9.87	2.80	21.47
5	6.10	4.38	8.74

Bolds numbers represent the smallest error percentage.

(b) Various frequency bands used in SI

The measuring point combination 125 is used in the testing for the various frequency bands in SI. According to measuring FRF1 in Fig. 4.20, noise is dormant nearly third mode. Therefore, the best result of the estimated stiffness can be obtained when using the frequency range is taken start to third mode as shown in Fig.21.

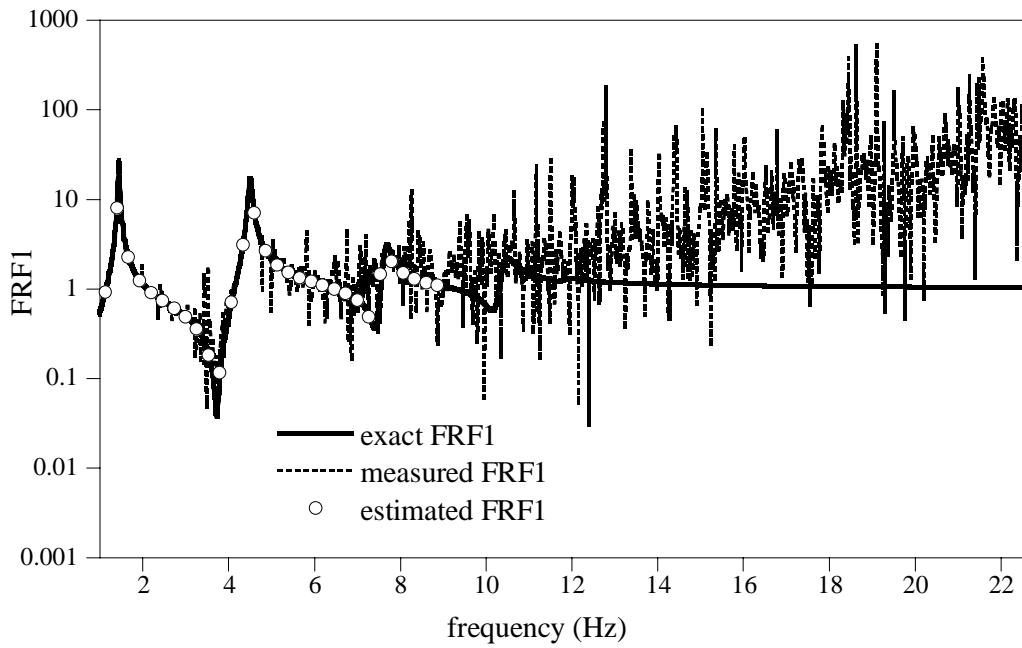


Fig. 4.20 FRF1 for frequency band up to mode3

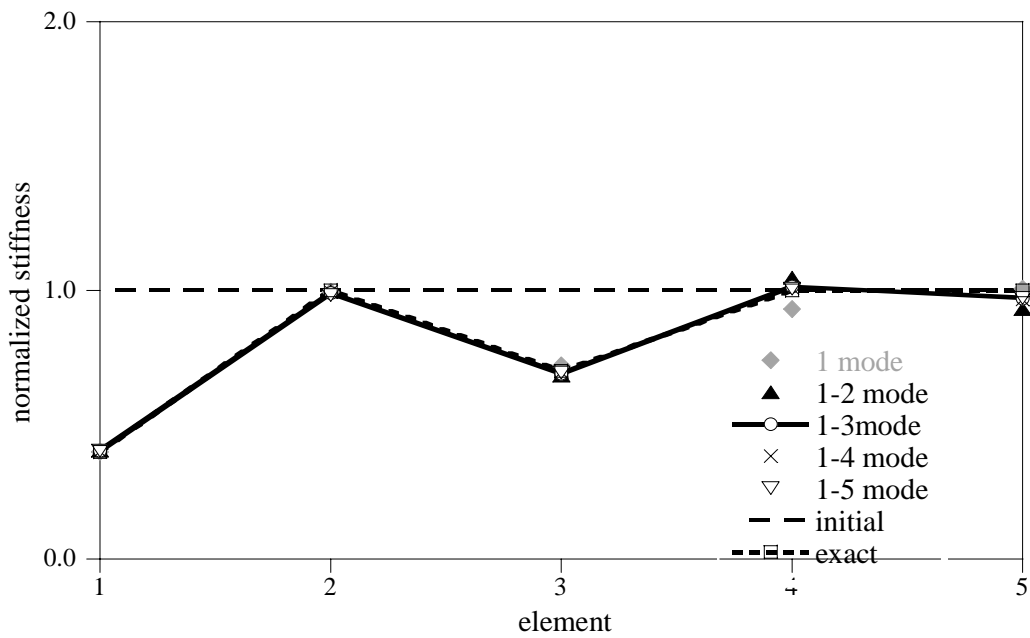


Fig. 4.21 Estimated stiffness for various frequency bands

(c) Full measuring points

The natures of the FRF and estimated stiffness of this example1-case 2 is similar to the example1-case 1. Fig. 4.22 shows the FRF1 for frequency band taking three modes at full measuring points and Fig. 4.23 is estimated stiffness for various frequency bands and Fig. 4.24 shows the estimated stiffness which using regularization function in SI and estimated stiffness do not use the regularization function. In the results of the estimated stiffness, effect of regularization function can be known. The estimated Rayleigh damping ratios are in Fig. 4.25.

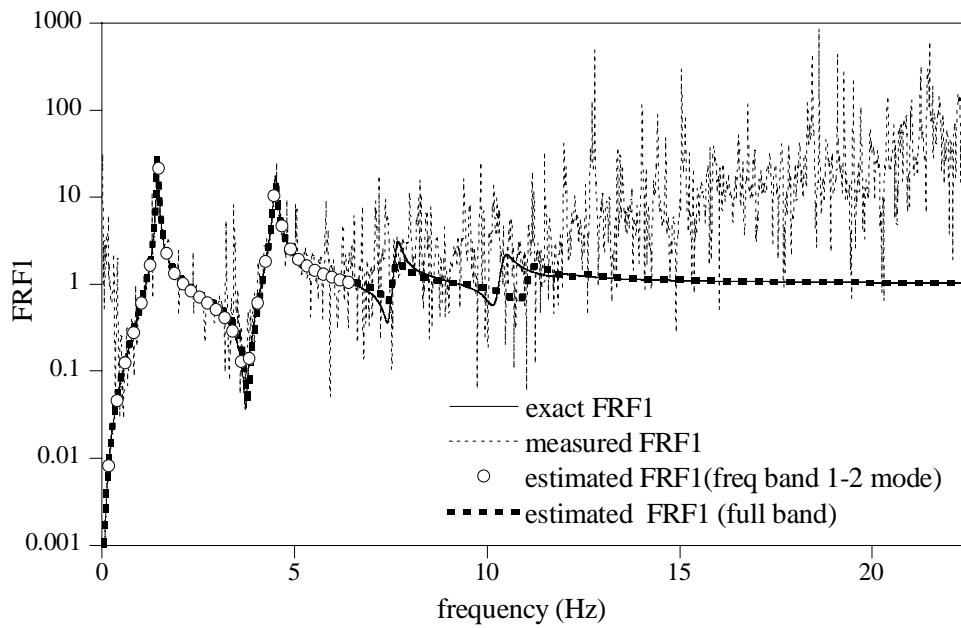


Fig. 4.22 FRF1 for full measuring points at frequency band up to mode2

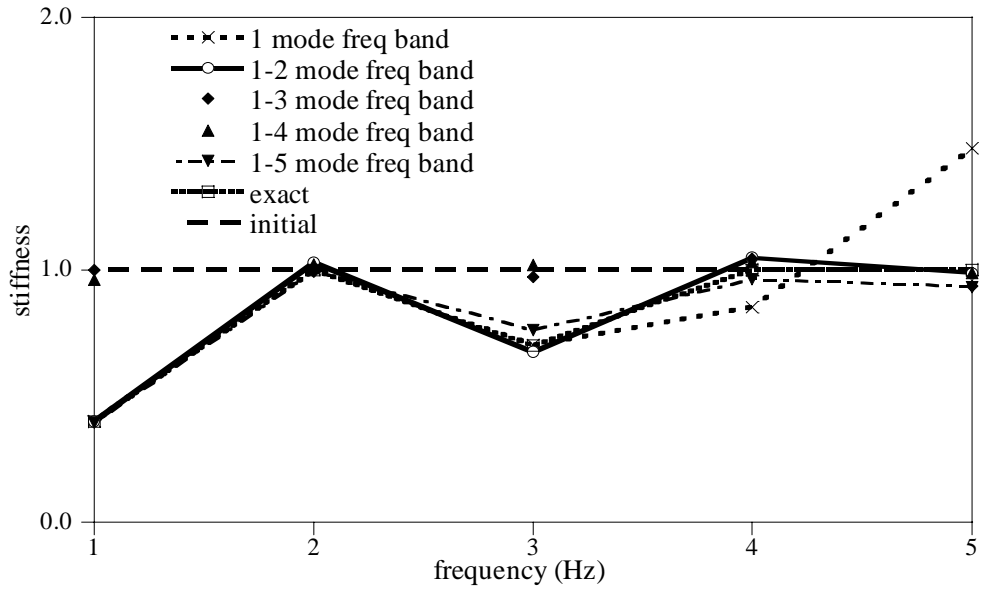


Fig. 4.23 Estimated stiffness for full measuring points

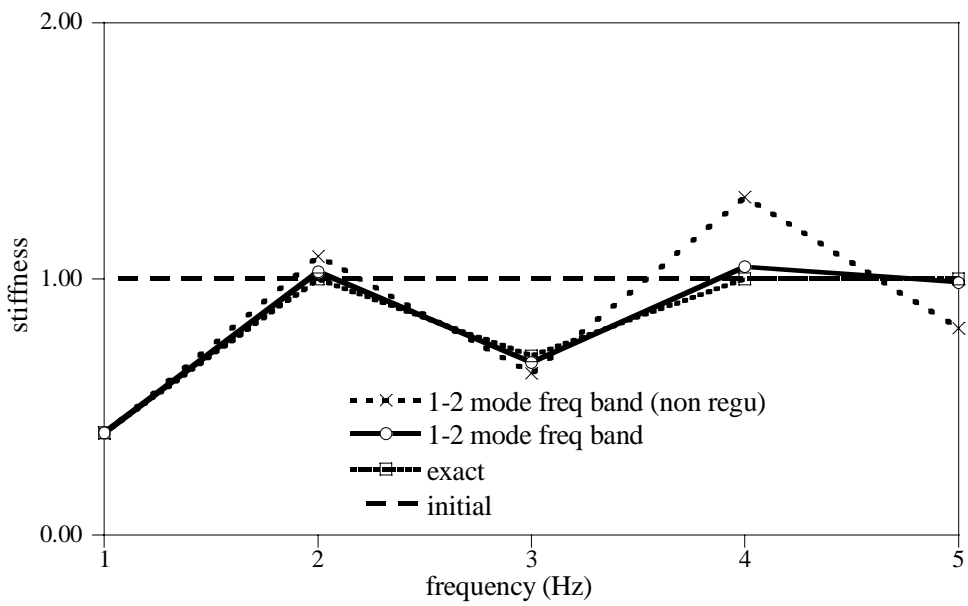


Fig. 4.24 Estimated stiffness for full measuring at frequency band up to mode 2

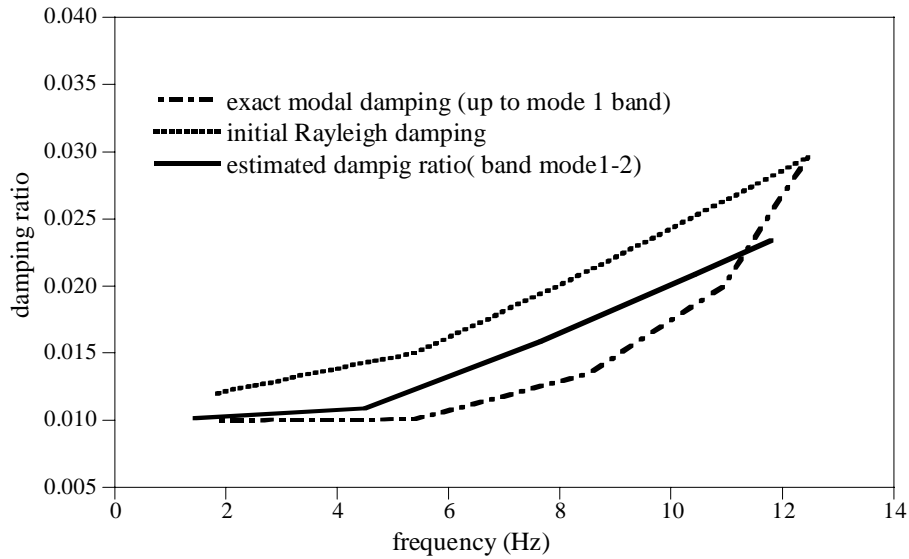


Fig. 4.25 Damping ratios for full measuring at frequency band up to mode 2

4.2. Numerical Example2 – Damage detection for a 10 story shear building

For a 10 story shear building, the mechanical properties are as listed in Table 4.8. Structural geometry and modeling are presented in Fig. 4.26a and Fig. 4.26b. Mode shape and baseline properties of the structure data such as stiffness and damping ratio are given in Table 4.9 and Fig. 4.27a, Fig. 4.27b and Fig. 4.27c. Inflection points are 3,6,7 and 9 at mode shapes are in the Fig. 4.27a. Therefore, these points 3,6,7 and 9 can not be used as measuring points. In this example 2, point 1, 2, 5 and 10 are used as measuring points.

Table 4.8 Mechanical properties for the ten story shear building

Type	Amount	Unit
Stiffness (For each story)	131,436,076.0	N/m
Mass	450,000.0	kg
Young's modulus	210.0	Gpa

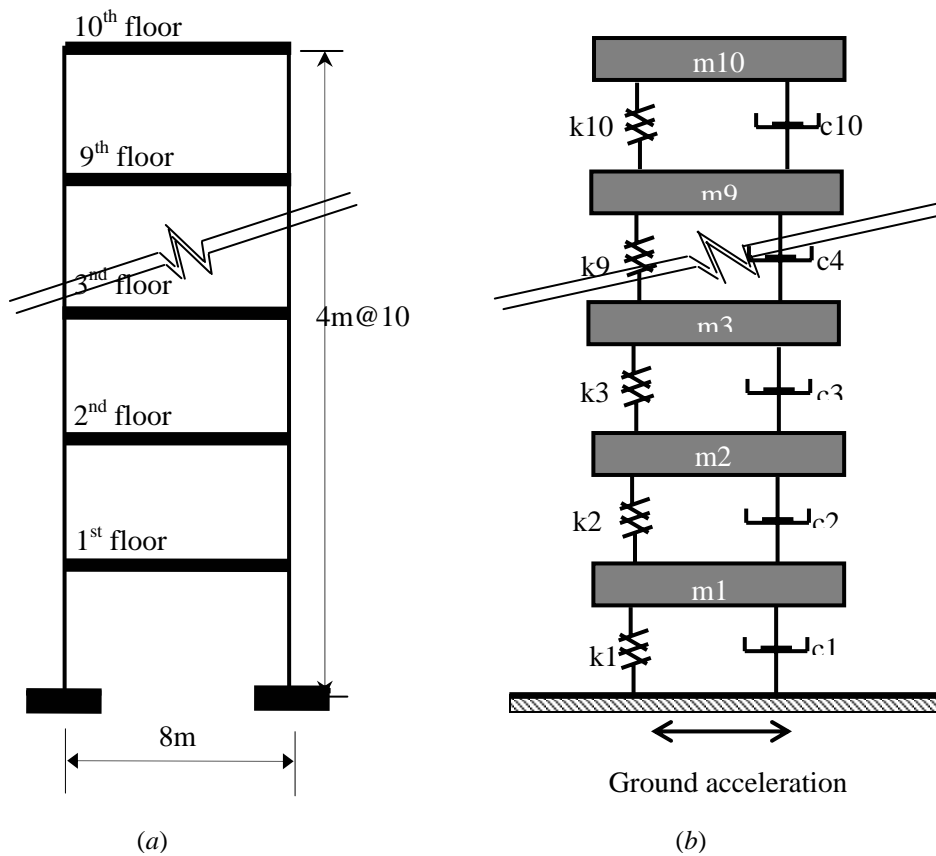
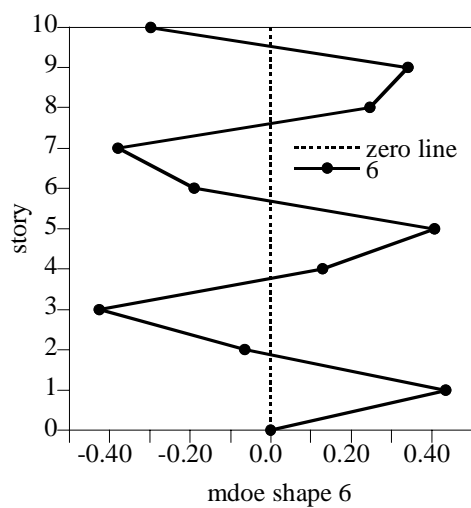
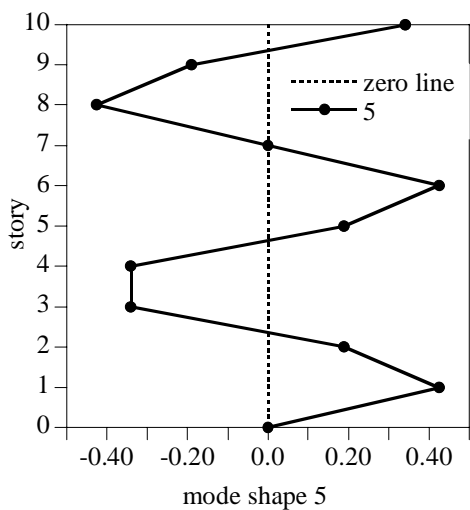
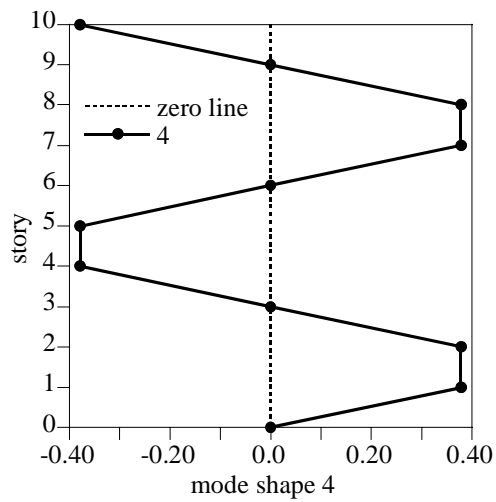
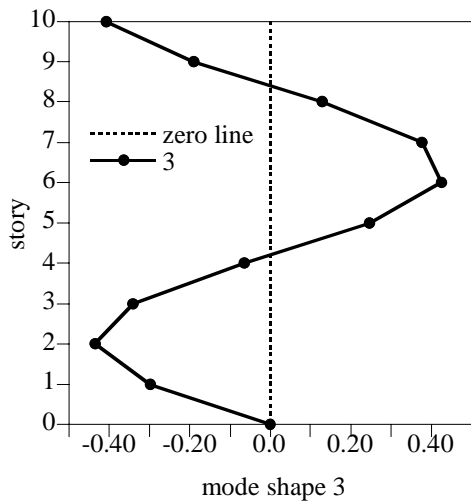
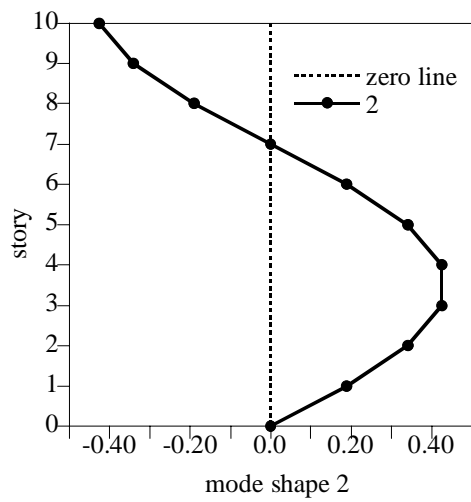
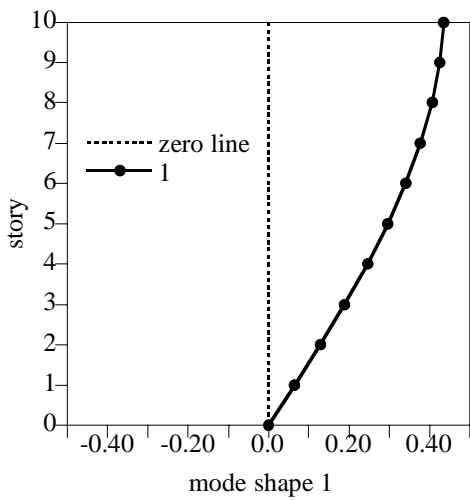


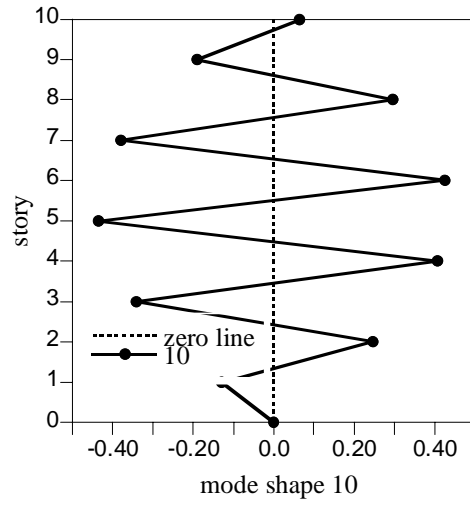
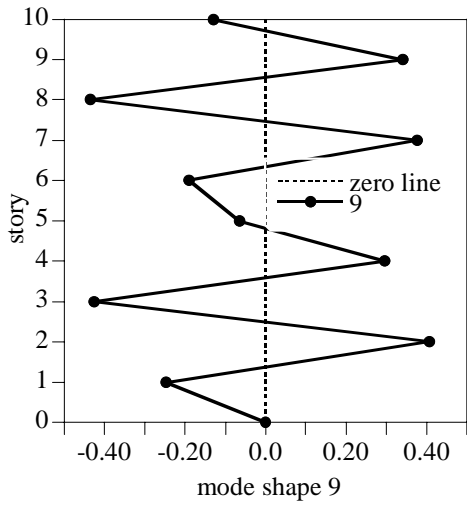
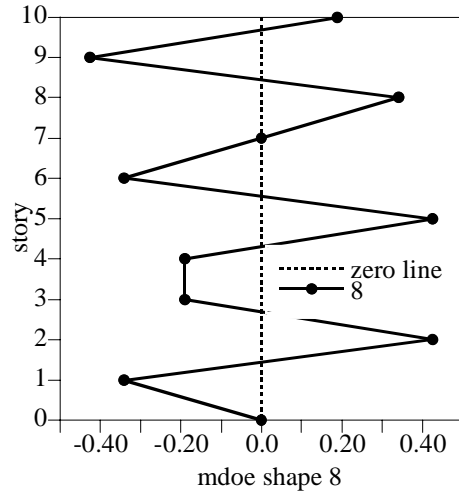
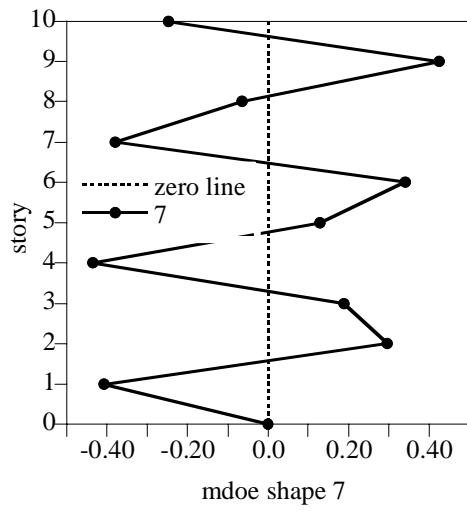
Fig. 4.26 Ten story shear building. (a) Frame geometry. (b) Model.

Case 1. Three points measuring at 1st, 5th and 10th floor--30% damage at element 1.

(a) Full frequency band

Damage is 30% reduction in the stiffness of the first story, as shown in Fig. 4.28 and Fig. 4.31. Three measuring points 1, 5, 10 and four measuring points 1, 2, 5, 10 are used in SI. The results are better than the three points measuring results, as shown in Fig.4.32. If there are more measuring points, the sparseness will be reduced and estimated system parameter results are better. At measuring points 1, 5, 10 and using the full band frequency in SI of the FRF1 and estimated stiffness are shown in Fig. 4.29 and Fig. 4.30., respectively.





(a)

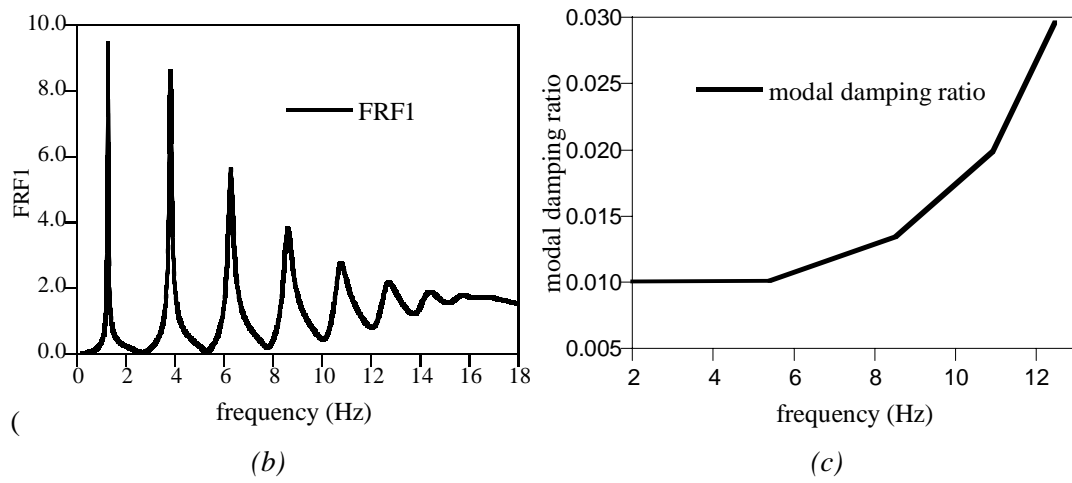


Fig. 4.27 Ten story shear building. (a) Mode shapes. (b) Natural frequencies. (c) Modal damping ratios.

Table 4.9 Baseline properties for the example structure

Mode no	Frequency (rad/sec)	Frequency (Hz)	Damping ratio
1	8.0775	1.2851	0.0100
2	24.0520	3.8265	0.0105
3	39.4893	6.2824	0.0122
4	54.0444	8.5980	0.0149
5	67.3923	10.7215	0.0188
6	79.2348	12.6055	0.0238
7	89.3072	14.2080	0.0299
8	97.3847	15.4930	0.0372
9	103.2868	16.4320	0.0455
10	106.8816	17.0039	0.0550

(b) Various Frequency bands used in SI

Fig. 4.33 and Fig. 4.34 show the FRF1 and estimated stiffness for frequency range are

taken up to mode4. Fig. 4.35 is comparison of estimated stiffness results with regularization and without regularization.

(c) Full measuring points

There is also same as example1. The best estimated stiffness results are at frequency range up to mode 2. It can be known in Fig. 4.36, Fig. 4.37a and Fig.4.37b. Fig. 4.38 shows the effect of regularization.

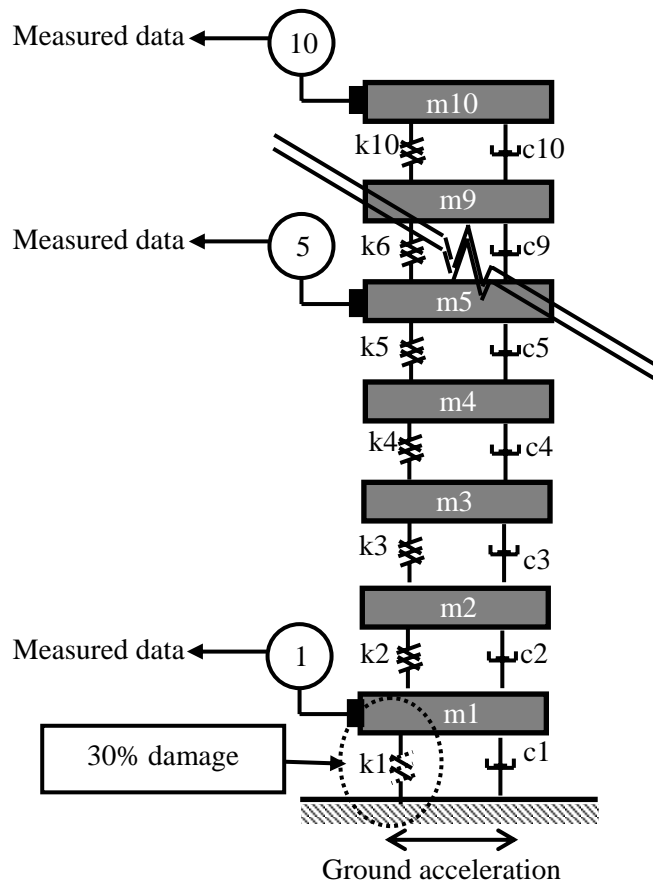


Fig. 4.28 Ten story shear building. (a) Frame geometry. (b) Model.

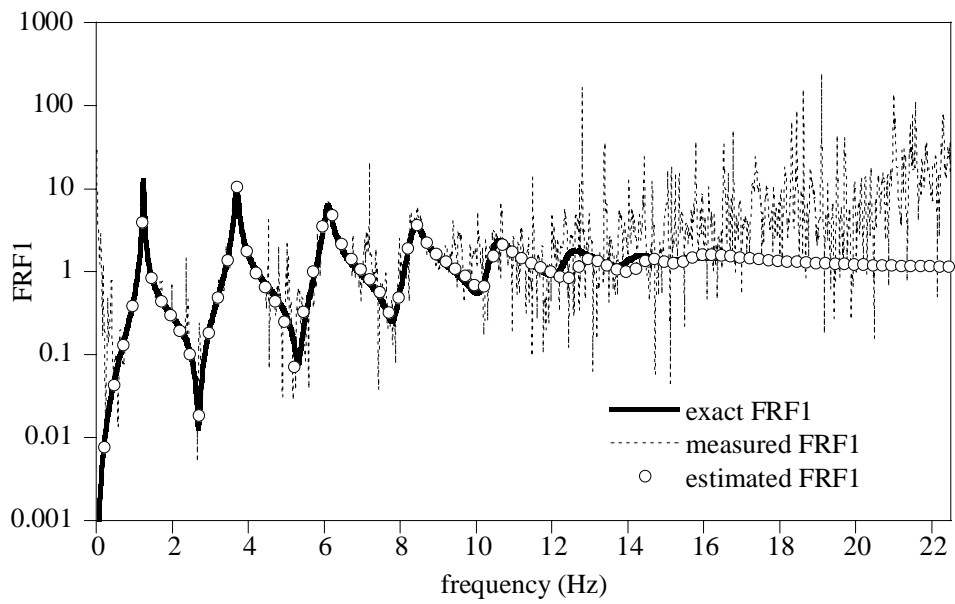


Fig. 4.29 FRF1 at full band frequency for example2-case1

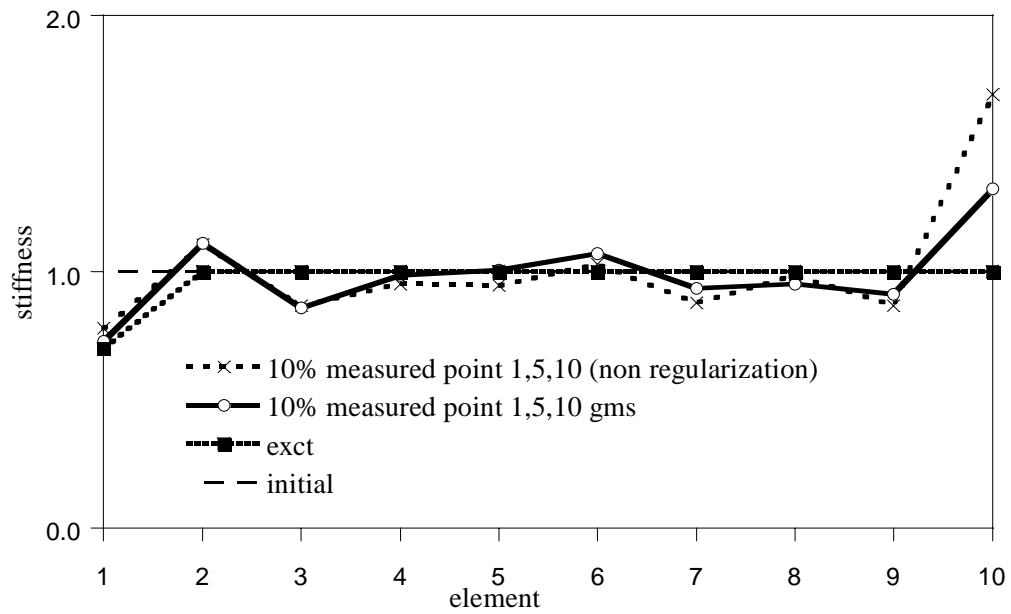


Fig. 4.30 Regularization effect for the estimated stiffness at full band frequency

Four points measuring at 1st, 2nd, 5th and 10th floor--30% damage at element 1.

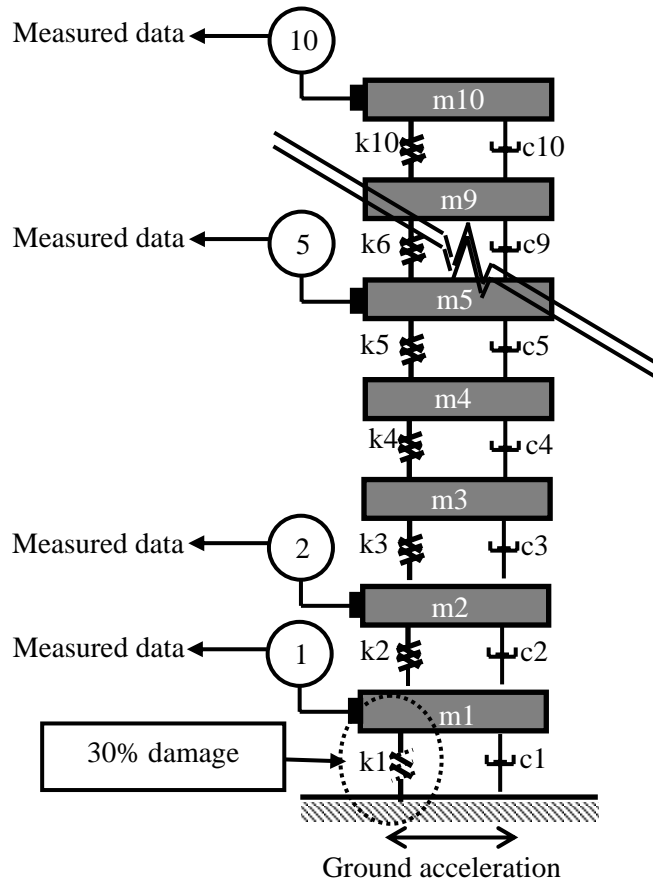


Fig. 4.31 Model of the 10 story shear building with four measuring points 1,2,5,10

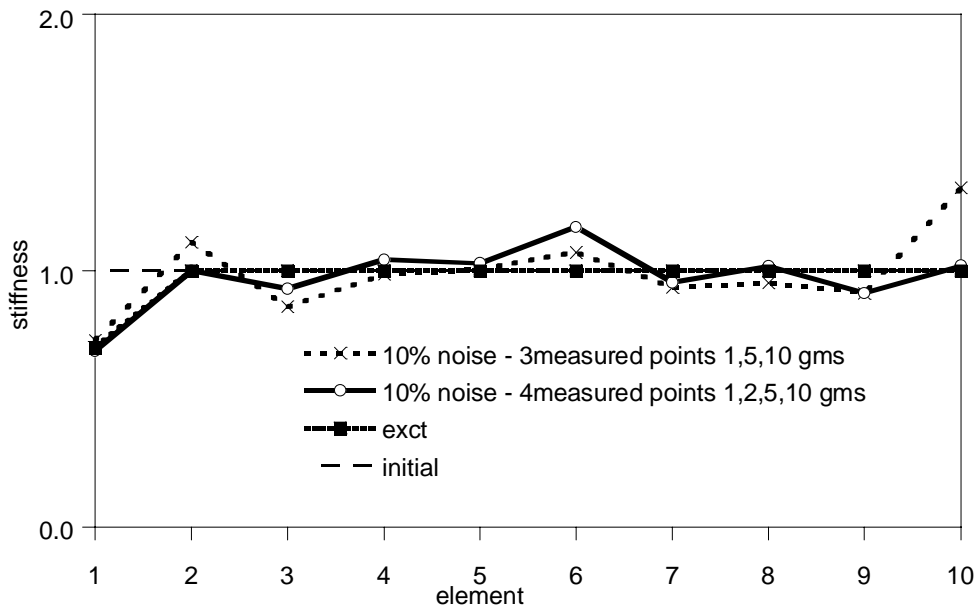


Fig. 4.32 Comparison of estimated stiffness with three and four measuring points

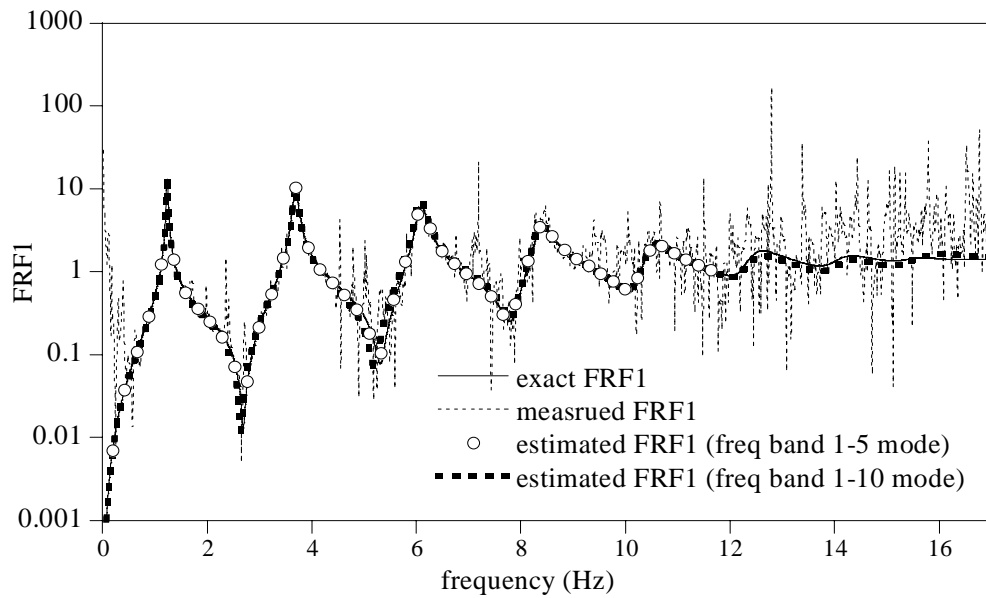


Fig. 4.33 FRF1 at 5 mode frequency band for example2-case1

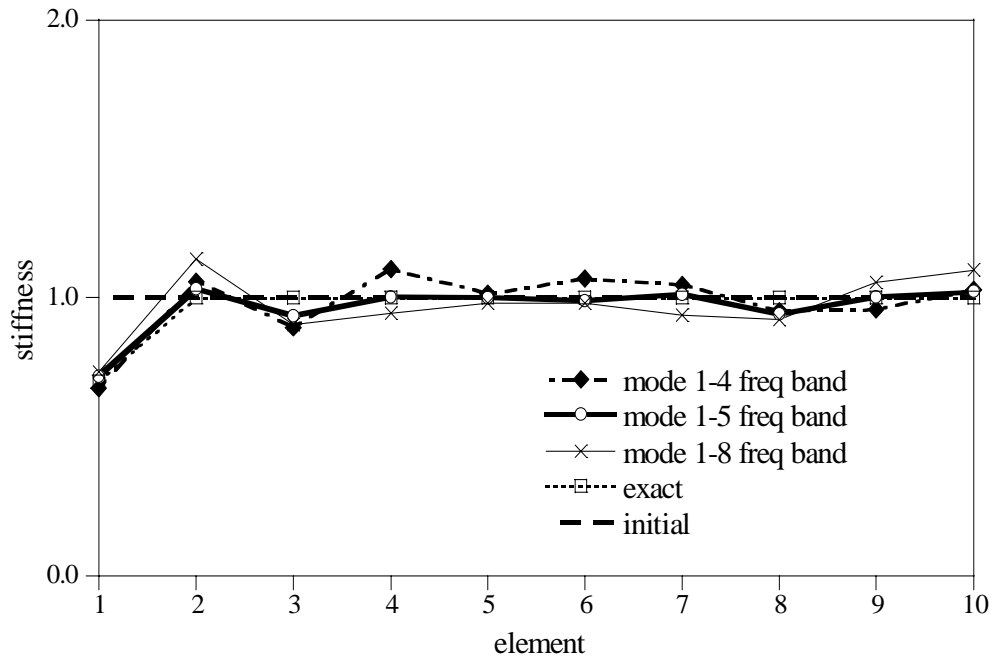


Fig. 4.34 Estimated stiffness for various frequency bands

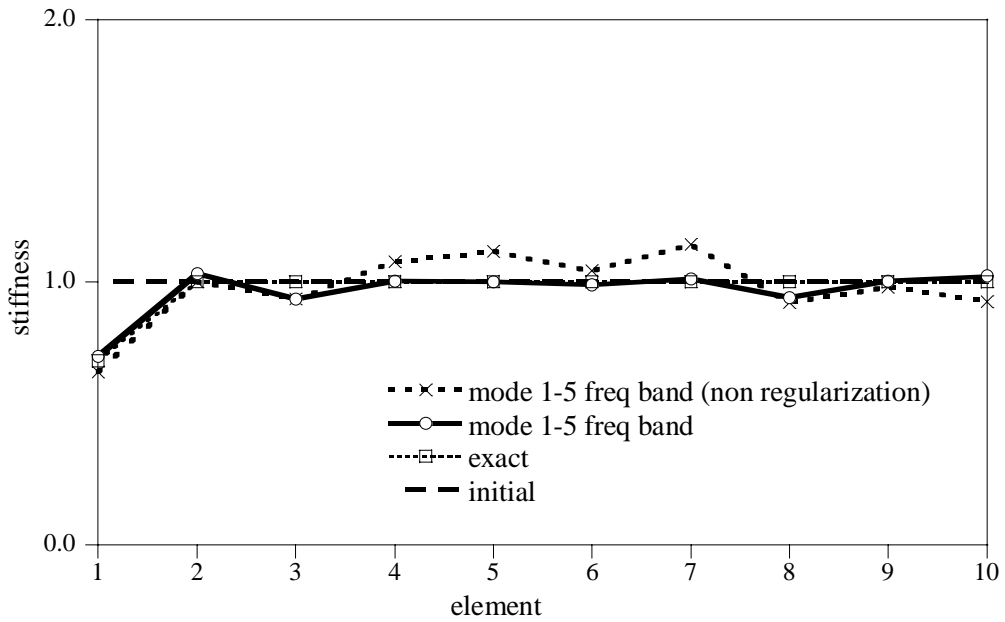


Fig. 4.35 Regularization effect for estimated stiffness at 5 mode frequency band

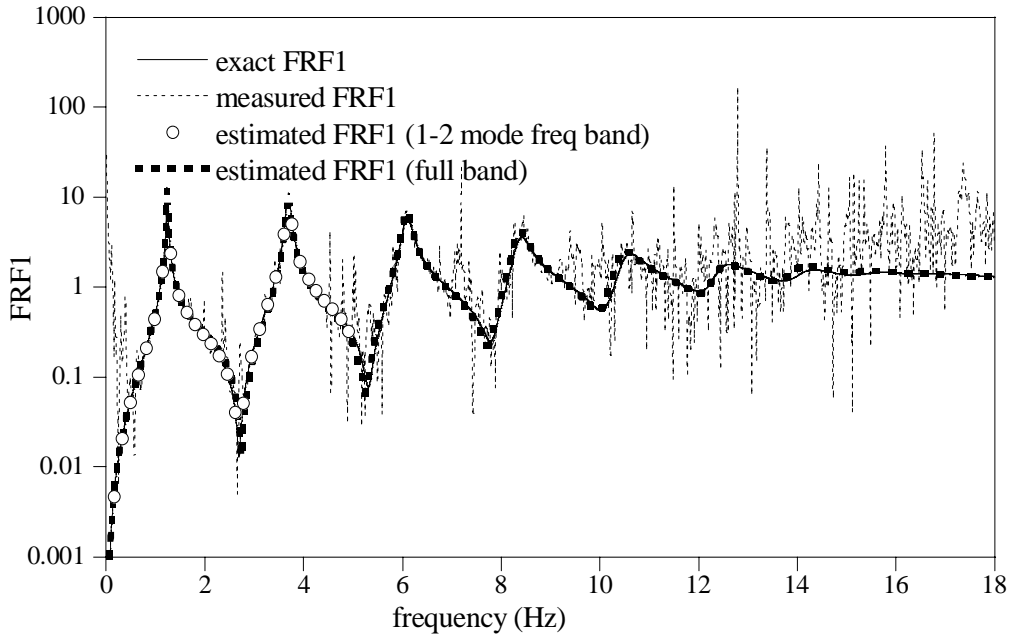
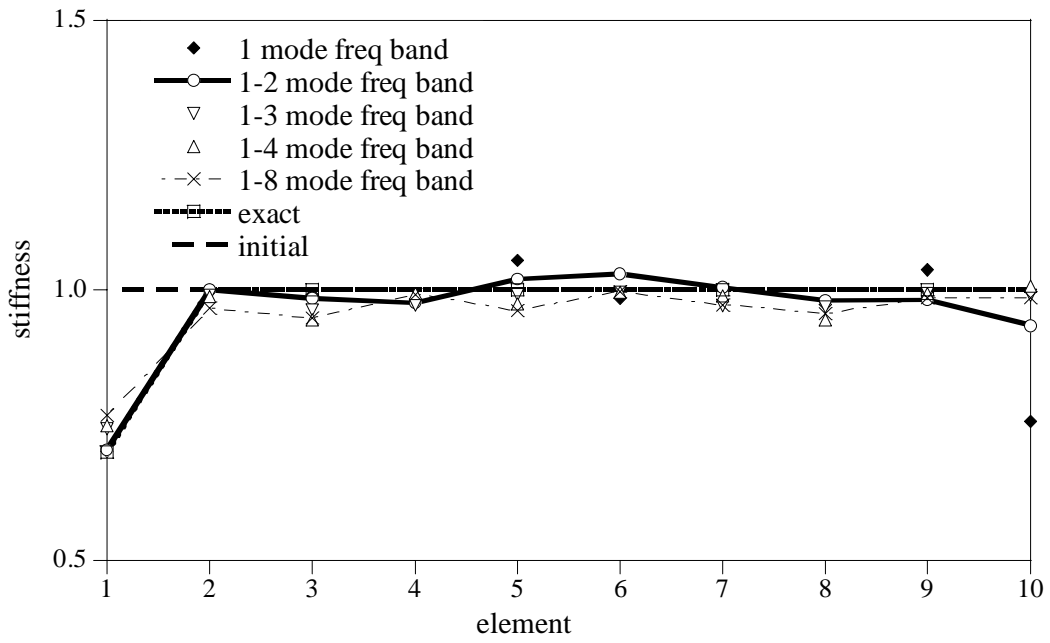


Fig. 4.36 FRF1 at full measuring point for example2-case1



(a)

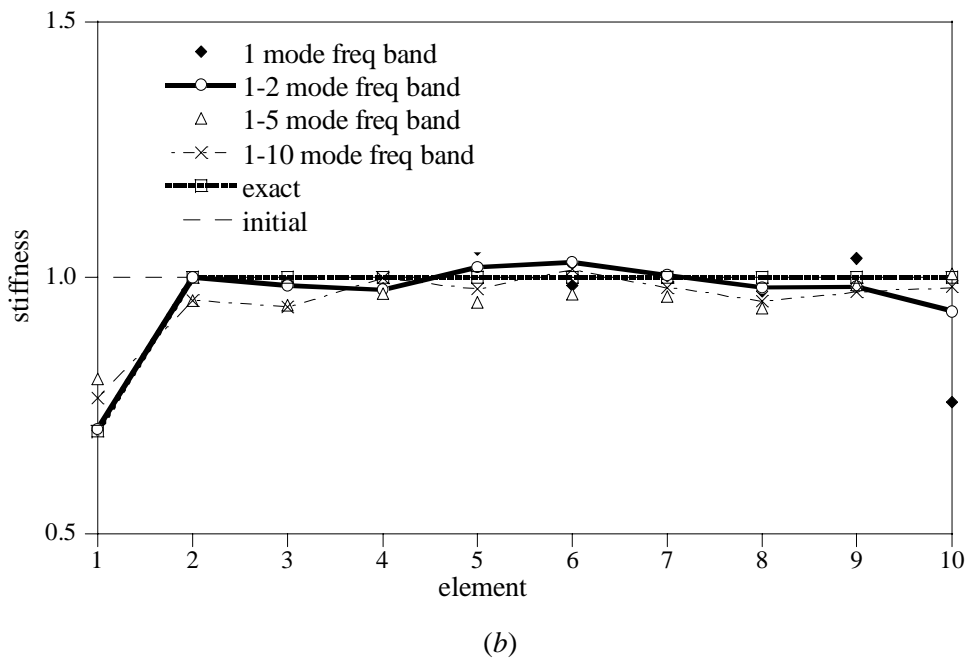


Fig. 4.37 Effect of the frequency range for the estimated stiffness in SI.
 (a) 1-8 mode. (b) 1-10 mode.

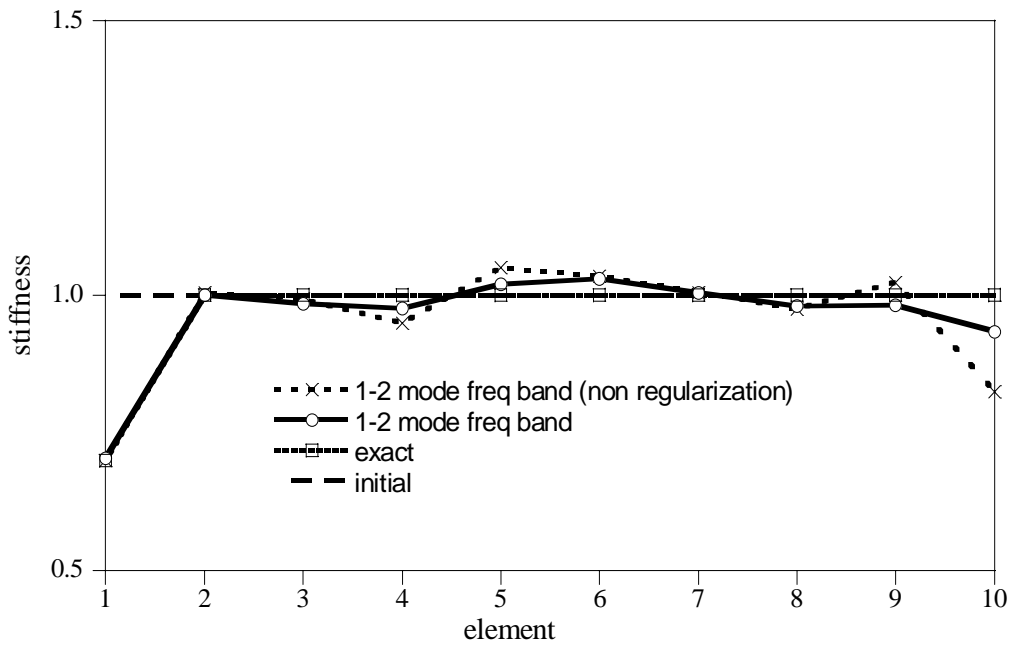


Fig. 4.38 Regularization effect for the estimated stiffness

Case 2 5% noise –40% damage at element 1 and 30% damage at element 4

Case 2 is similar to case 1 and is illustrated in Fig. 4.39 and Table 4.11, Also, it shows the exact natural frequencies and baseline data The GMS regularization factor is employed and the new regularization factor is singular value from the decomposition. The results of using each singular value as a regularization factor are better than those obtained via the method using GMS as a regularization factor for this problem (see Fig. 4.41). Measuring points are 1, 5, 10. Fig. 4.40 shows comprising of the estimated results of 5% noise and 10% noise.

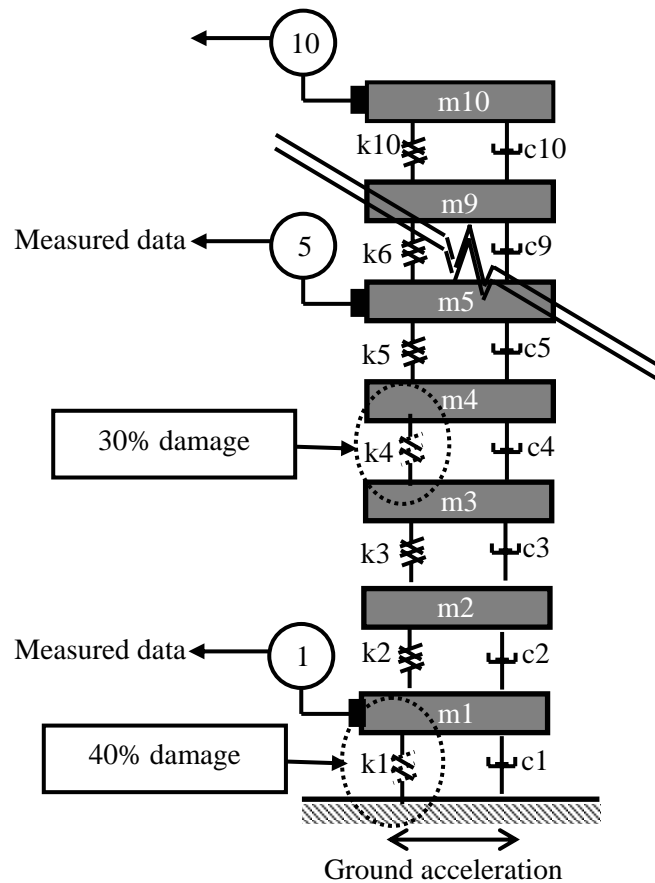


Fig. 4.39 Model for 40% and 30% reduced stiffness damage at first and fourth stories, respectively

However, a singular value cannot be decided as regularization factor in the singular numbers. In this problem, the maximum value of the singular number can converge. A singular value for regularization factor depends upon the condition of the problems. The results of estimated damping ratios are shown in Fig. 4.42.

Fig. 4.43, Fig. 4.44, Fig. 4.45 and Fig. 4.46 are FRF1, estimated stiffness for various frequency bands, estimated stiffness with regularization effect and estimated Rayleigh damping ratios, respectively and all the figures are measured at points 1, 5, 10.

Full measuring point condition is similar as pervious examples. The best result of the estimated stiffness is frequency band up to second mode see Fig.4.48a and Fig. 4.48b. FRF1 and regularization effect in estimated stiffness and estimated damping ratios are shown in Fig. 4.47, Fig. 4.49 and Fig 4.50, respectively.

Table 4.10 Comparison of the natural frequency (hz) base line data with multi-damaged data

Mode no	No damage	Damaged
1	1.2851	1.1781
2	3.8265	3.6196
3	6.2824	5.7926
4	8.5980	8.1600
5	10.7215	10.4266
6	12.6055	11.9440
7	14.2080	13.8211
8	15.4930	15.3833
9	16.4320	15.9343
10	17.0039	16.8251

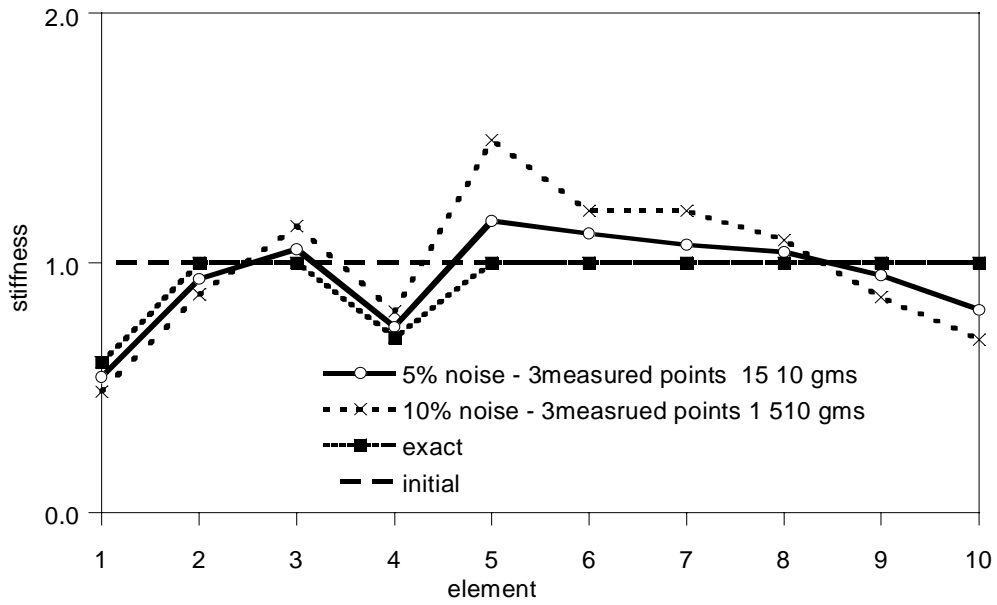


Fig. 4.40 Estimated stiffness at different noises 5% and 10%

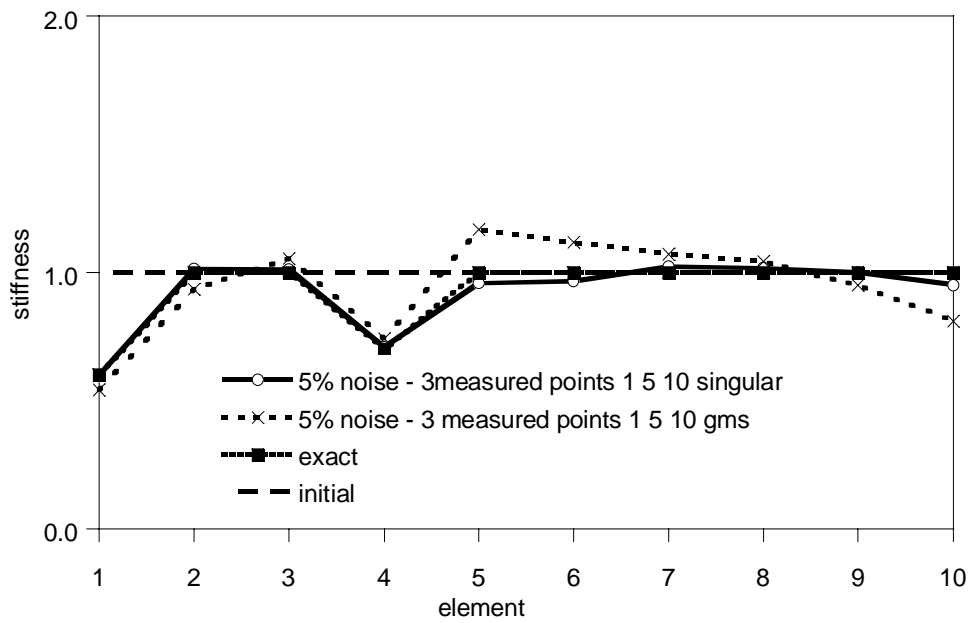


Fig. 4.41 Estimated stiffness at different regularization factors.

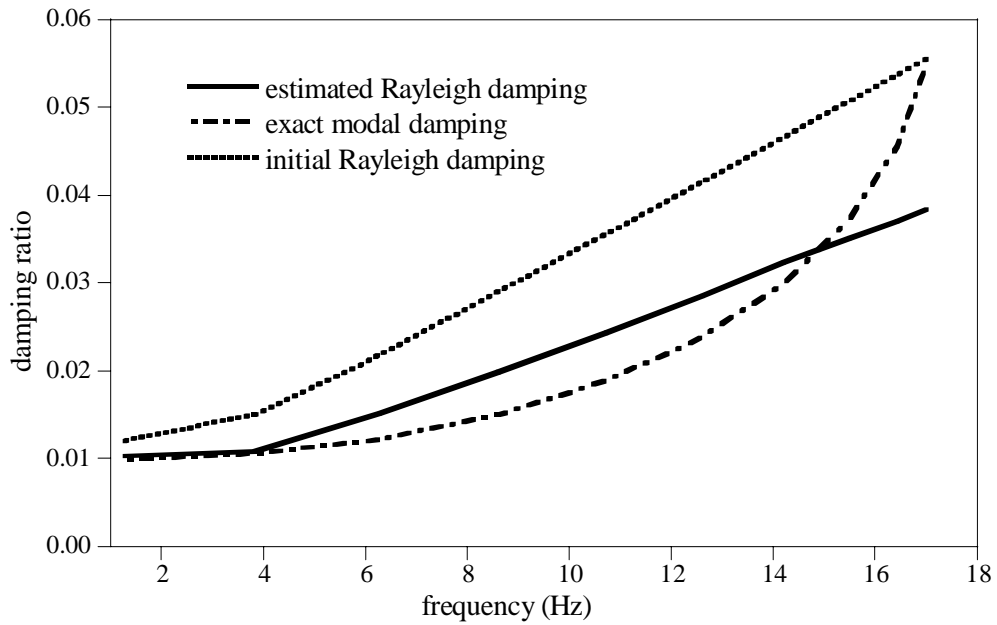


Fig. 4.42 Estimated Rayleigh damping ratios using GMS regularization factor

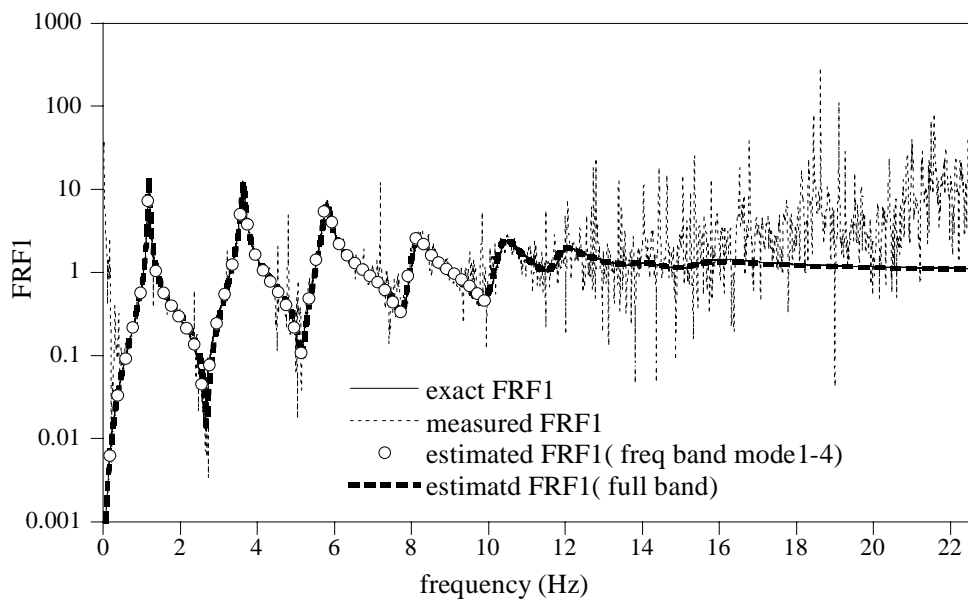


Fig. 4.43 FRF1 for 4 mode frequency band

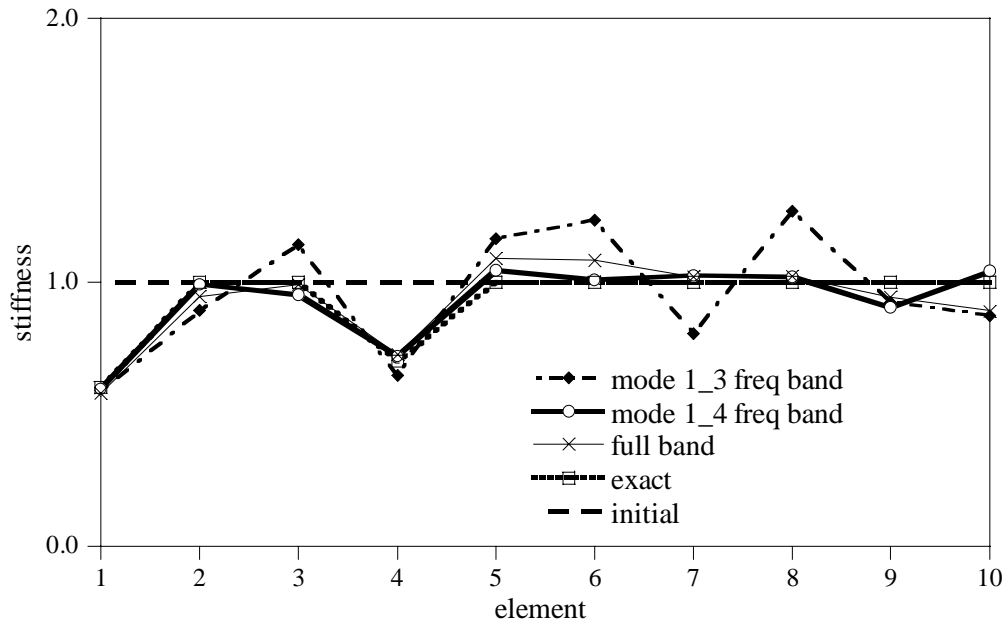


Fig. 4.44 Estimated stiffness for 4mode frequency band

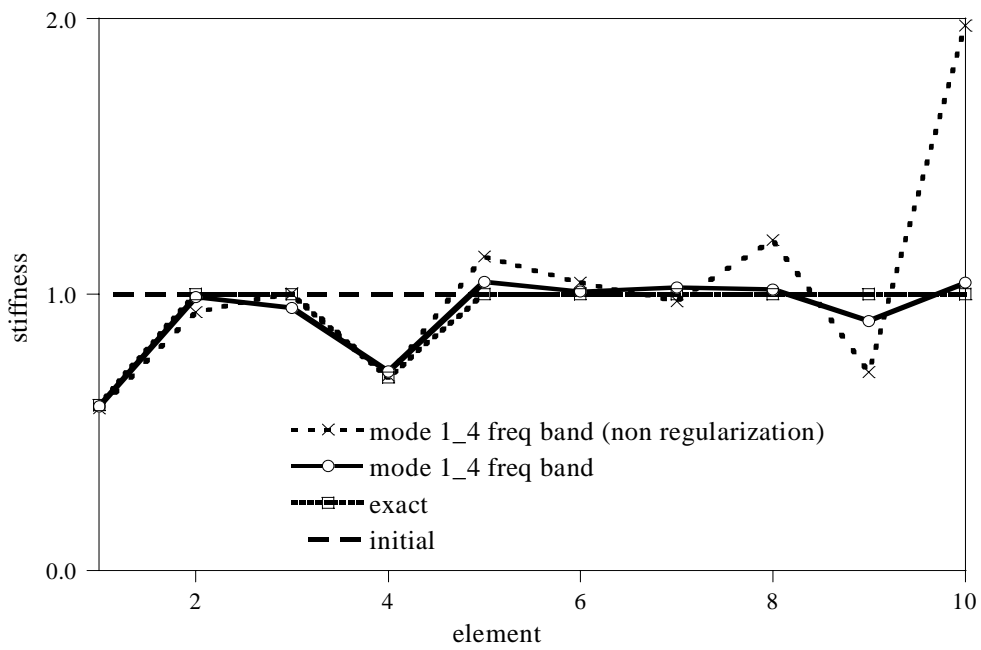


Fig. 4.45 Regularization effect of estimated stiffness at 4 mode frequency band

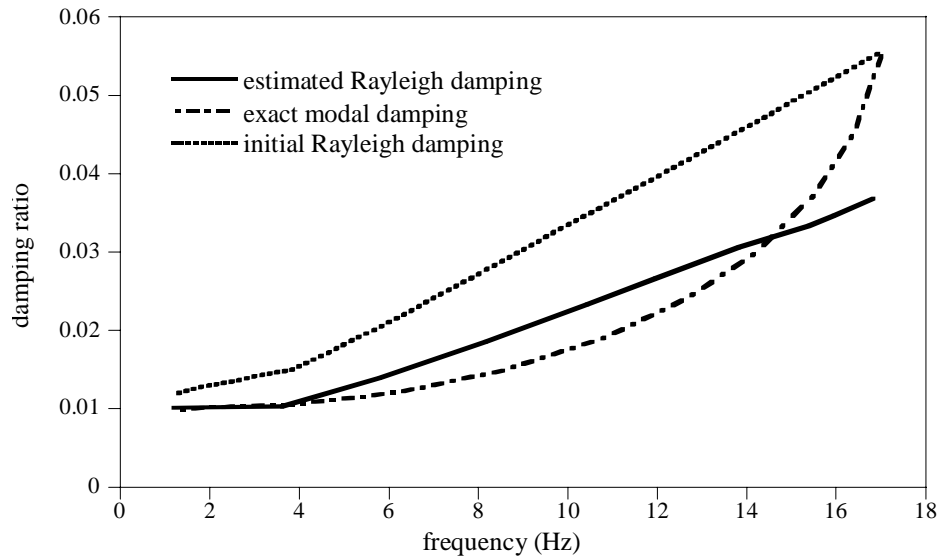


Fig. 4.46 Estimated damping ratios at 4mode frequency band

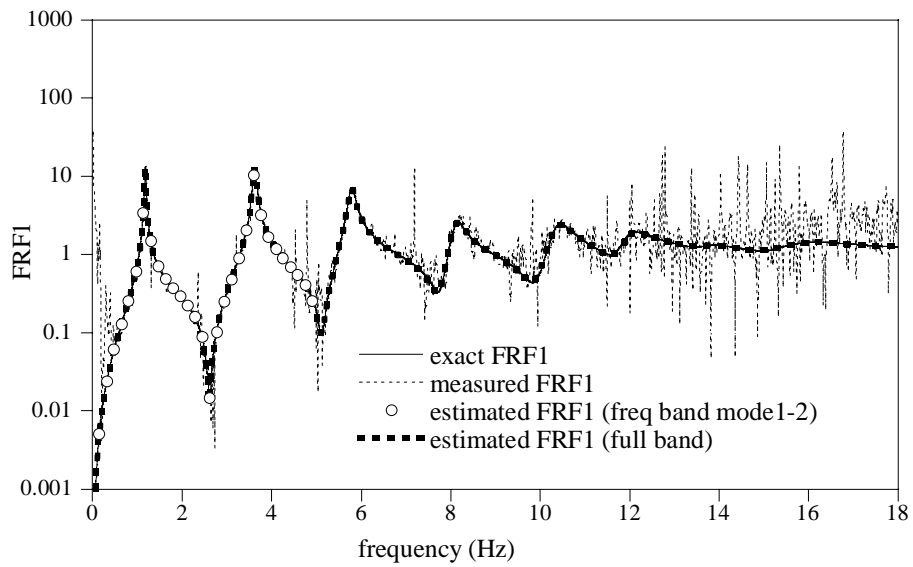
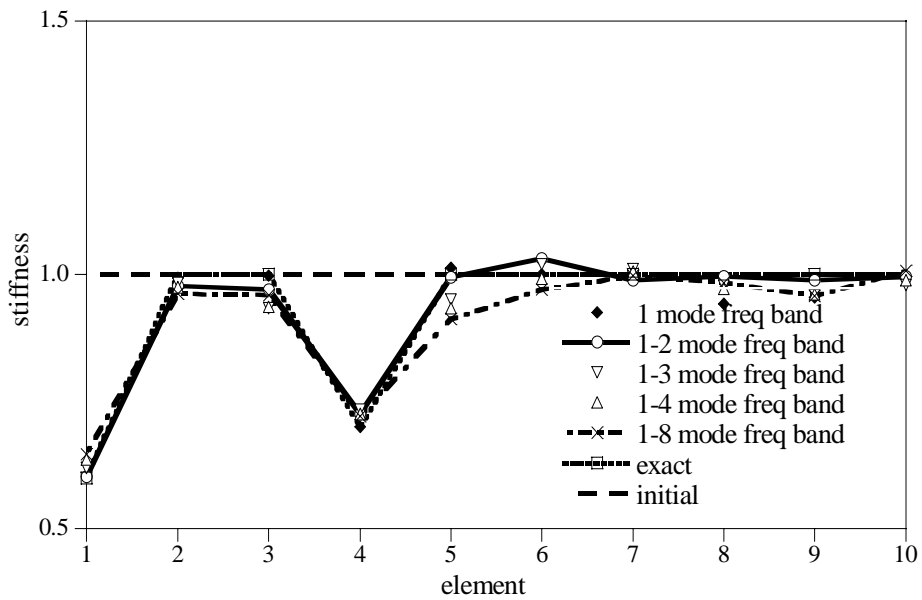
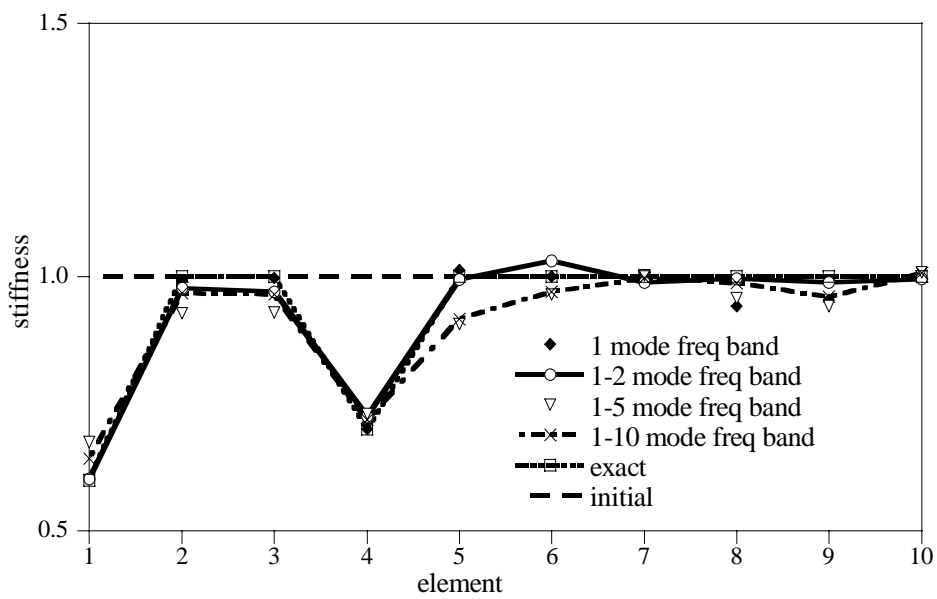


Fig. 4.47 FRF1 at full measuring point and mode2 frequency band



(a)



(b)

Fig. 4.48 Effect of the frequency range for the estimated stiffness in SI.
 (a) 1-8 mode. (b) 1-10 mode.

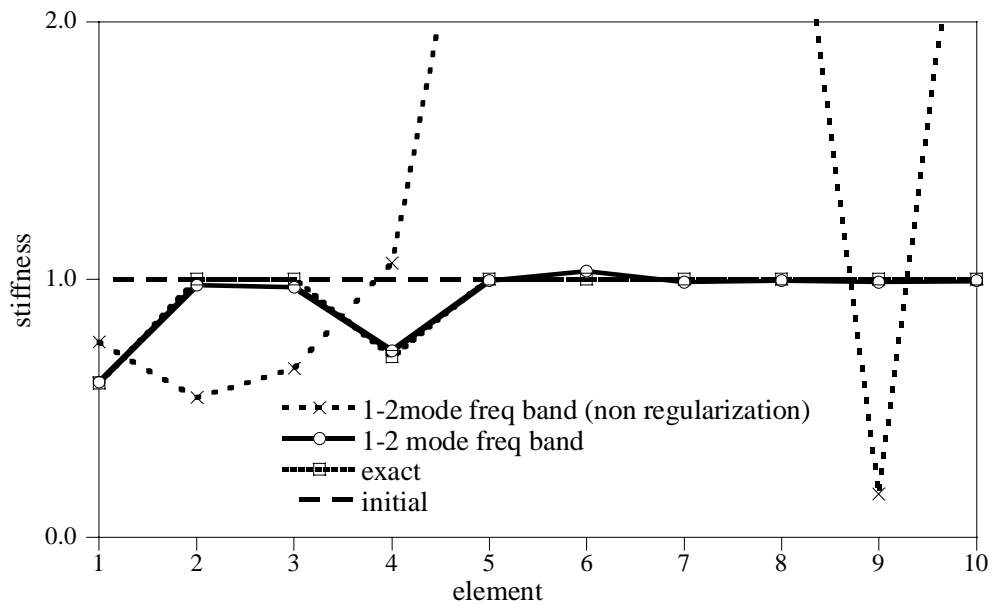


Fig. 4.49 Regularization effect of estimated stiffness at 2 mode frequency band

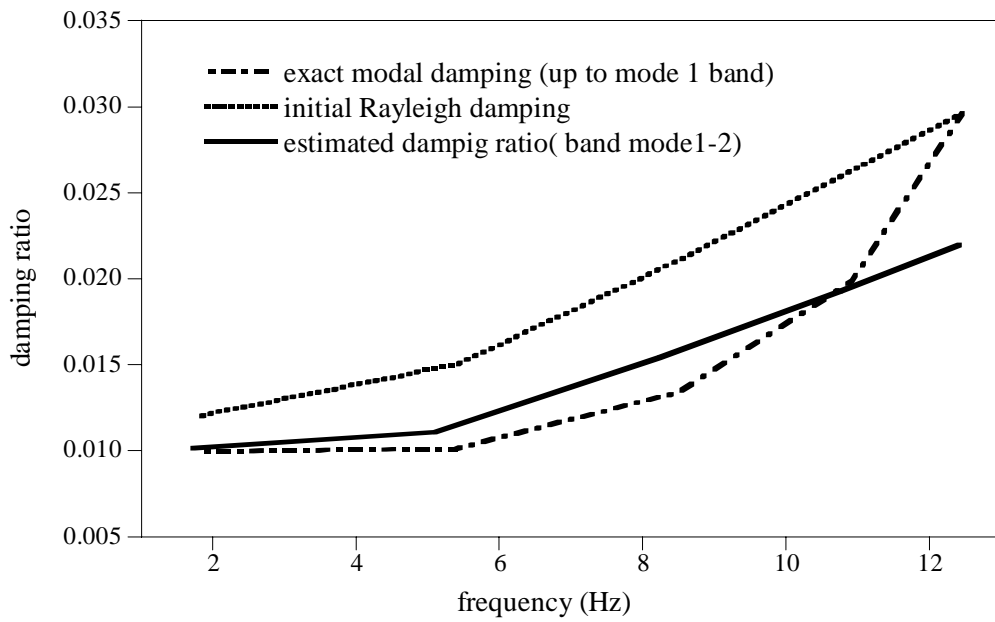


Fig. 4.50 Estimated damping ratios at 2mode frequency band and full measuring

Summary of example one and two are using full frequency band or partial frequency bands, a selected measuring points and full measuring points

There are the best estimated stiffness conditions

Table. 4.11 summary of examples one and two

Case	Damage %	Damage location (element)	Noise %	Measured points	Mode shape (up to mode)	Partial band (up to mode)	Full measuring (up to mode)
5 story (single damage)	30	1	10	3,5	3	3	2
5 story (multi damage)	60 30	1 3	10	1,2,5	2	3	2
10 story (single damage)	30	1	10	1,5,10	4	5	2
10 story (multi damage)	40 30	1 4	5	1,5,10	4	4	2

4.3 Numerical Example3 – Parameter estimation for a 5 story shear building

The idealized frame structure and model are shown in Fig. 4.51. In this example, second and third modes of the frame structure are very close position. 5% noise include error in measuring data. The measuring points are 1,3 and 5. Structural properties are in Table 4.12.

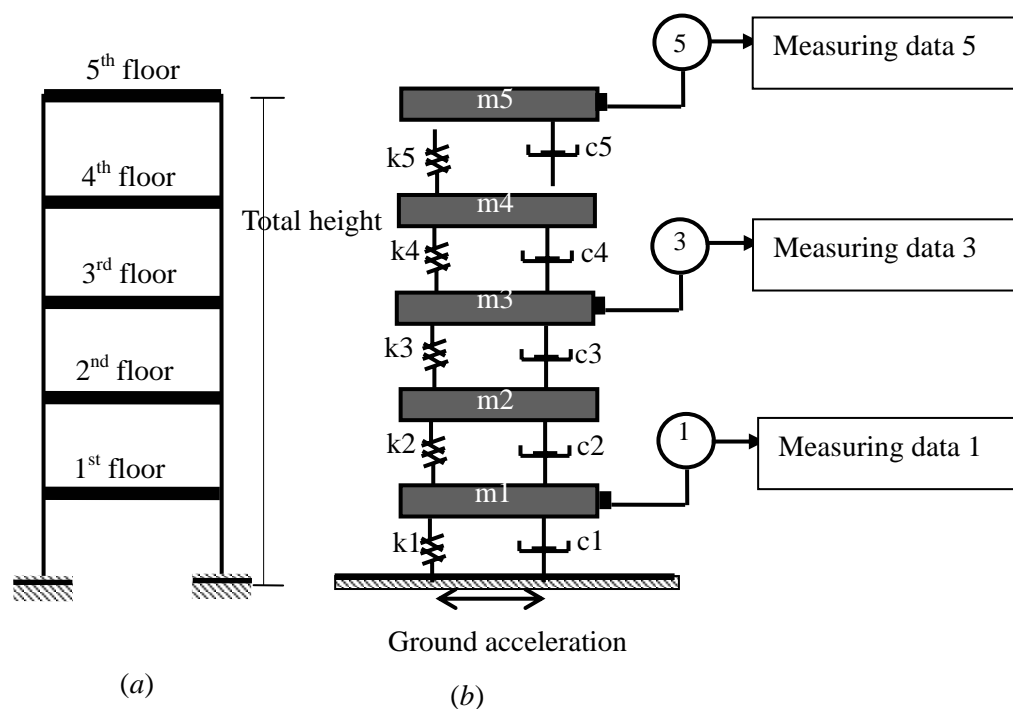


Fig. 4.51 Five story shear building (a) Frame structure. (b) Modeling.

The exact and estimated natural frequencies are shown in Table 4.13. The second mode and the third mode of the natural frequencies are very close at exact and estimated natural frequencies of the structure. Table 4.14 shows exact and estimated stiffness of the structure. In estimated stiffness are calculated by used regularization and non regularization method in SI. The modal damping ratios are used exact and Rayleigh damping is used initial

damping and estimated damping is also Rayleigh damping ratios.

Table 4.12 Structural properties

Element	Stiffness (N/m)	Mass(kg)
1	50,000.00	50,000.00
2	1,000.00	1,000.00
3	1,000.00	1,000.00
4	1,000.00	1,000.00
5	1,000.00	1,000.00

Table 4.13 Natural Frequency (Hz)

Mode	exact	estimated
1	0.0550	0.0550
2	0.1530	0.1550
3	0.1660	0.1600
4	0.2441	0.2600
5	0.2991	0.3200

Table 4.14 Stiffness (N/m)

Element	exact	Regularized	Non regularized
1	50,000.00	49,428.15	49,359.14
2	1,000.00	1,024.69	1,009.92
3	1,000.00	969.91	986.01
4	1,000.00	1,009.51	1,004.01
5	1,000.00	1,009.28	1,034.06

Table 4.15 Damping ratios

Mode	Exact modal damping	Initial Rayleigh damping	Estimated Rayleigh damping
1	0.0300	0.0500	0.0370
2	0.0310	0.0500	0.0339
3	0.0393	0.0520	0.0351
4	0.0550	0.0669	0.0441
5	0.0780	0.0786	0.0514

Second mode and third mode are very close or coincide. All of the values of mode shapes at point 2 are nearly zero. Alternatively, points of inflection are at point 2. It can be seen in Fig. 4.52. Therefore, the point 2 is unsuitable to use as a measuring point. Here, measuring points are selected 1, 3 and 5 to obtain reasonable results.

Fig.4.53 is estimated FRF1 and measured FRF1 with 5% noise at no damage. Fig 4.54 shows detail. The second and third modes are as very close between two modes at FRF1. Fig. 4.55, Fig. 4.56 and Fig. 4.57 show the exact FRFs , measured FRFs and estimated FRFs at measuring point 1, 3 and 5 respectively.

The regularized estimated stiffness and non regularized stiffness are shown in Fig. 4.58. This example is 5% noise and no damage. Therefore, the regularized and non regularized estimated stiffness are the same. It shows the verification of the system parameters estimation. Fig. 4.59 shows that estimated Rayleigh damping ratios are reasonable.

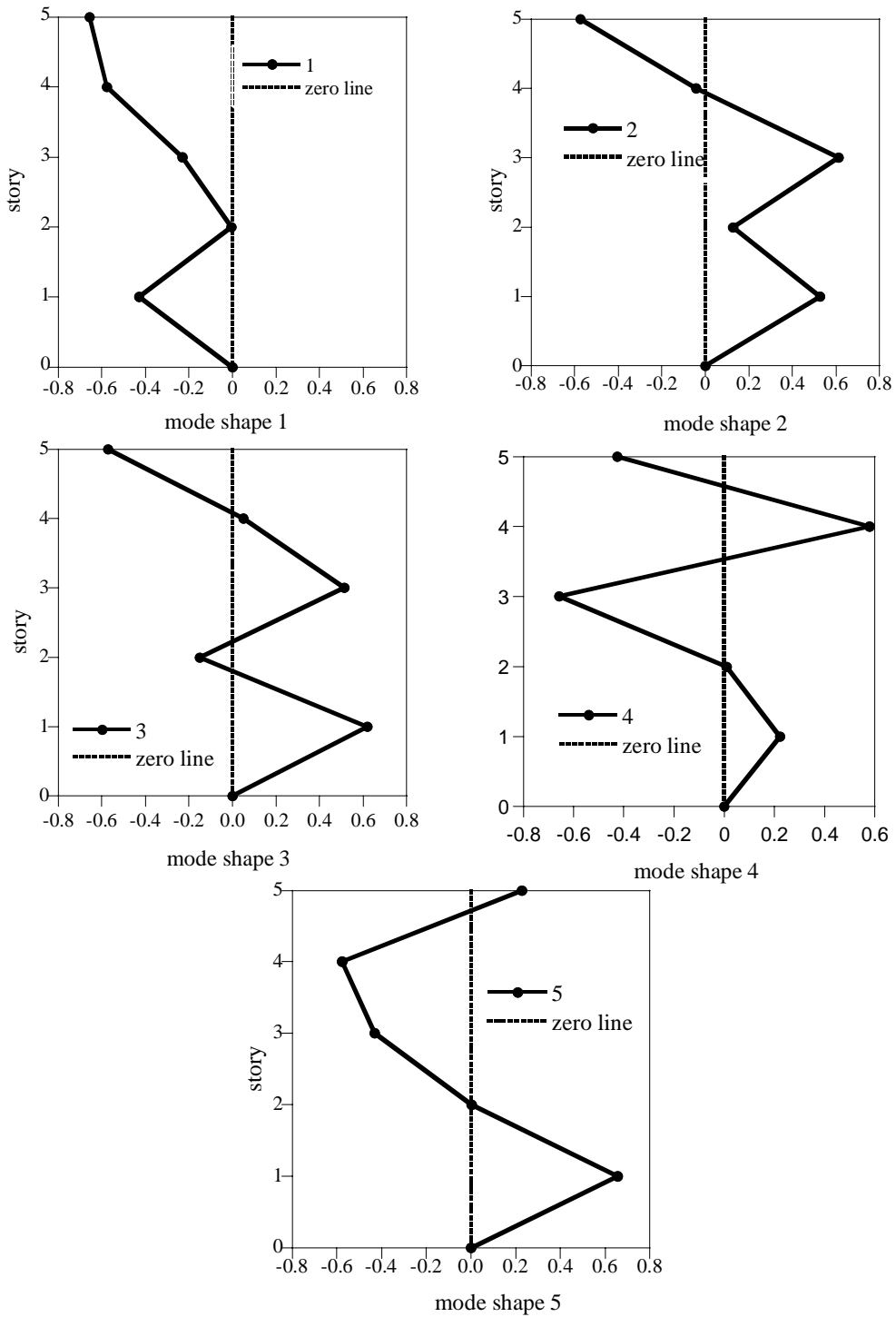


Fig. 4.52 Mode shapes of the structure

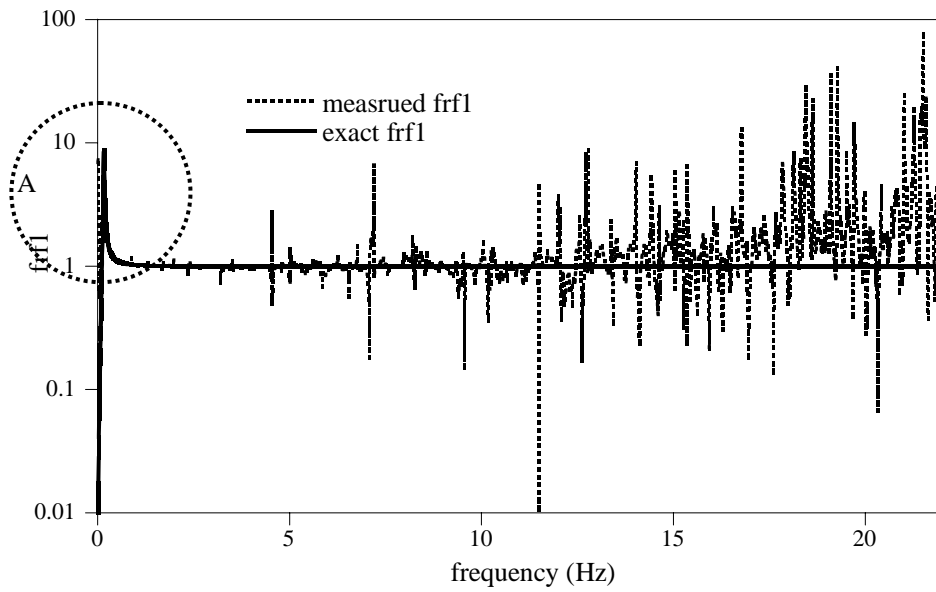


Fig. 4.53 Measured FRF1 and exact FRF1 with 5%noise and no damage case

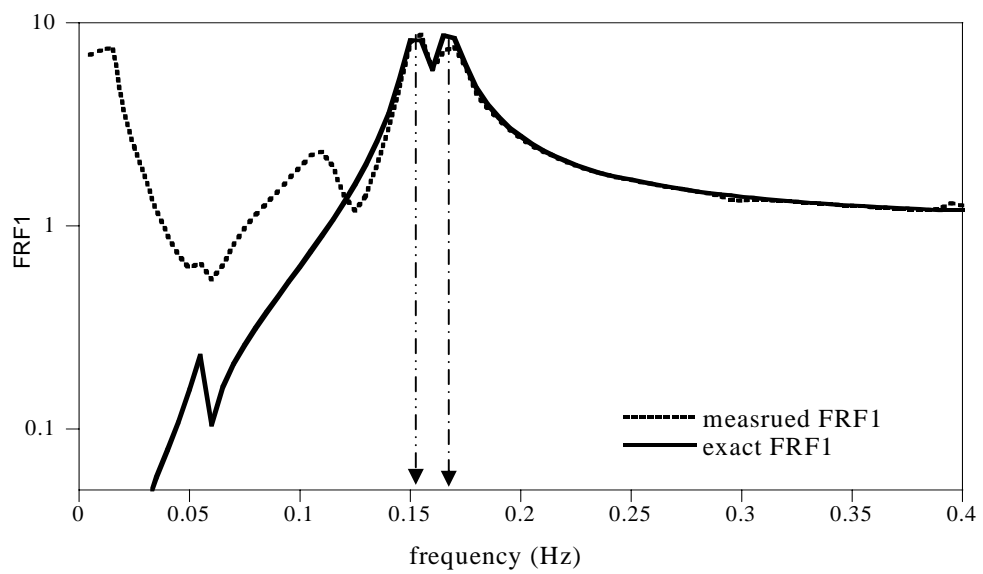


Fig. 4.54 Detail A for second and third modes which are very close between two modes

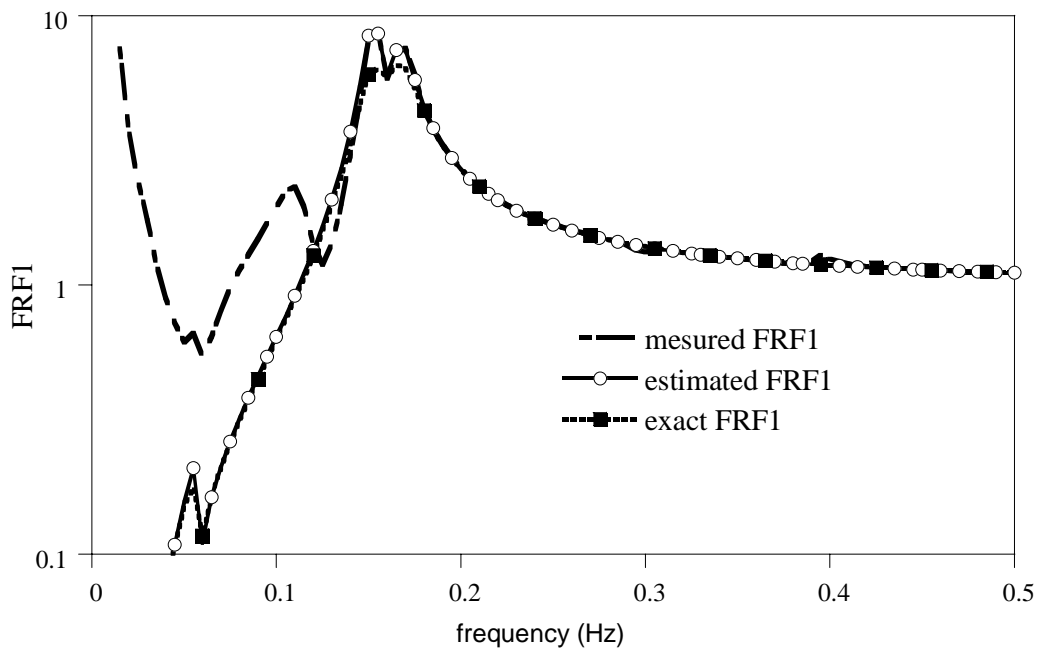


Fig. 4.55 FRF1 at measuring point at 1

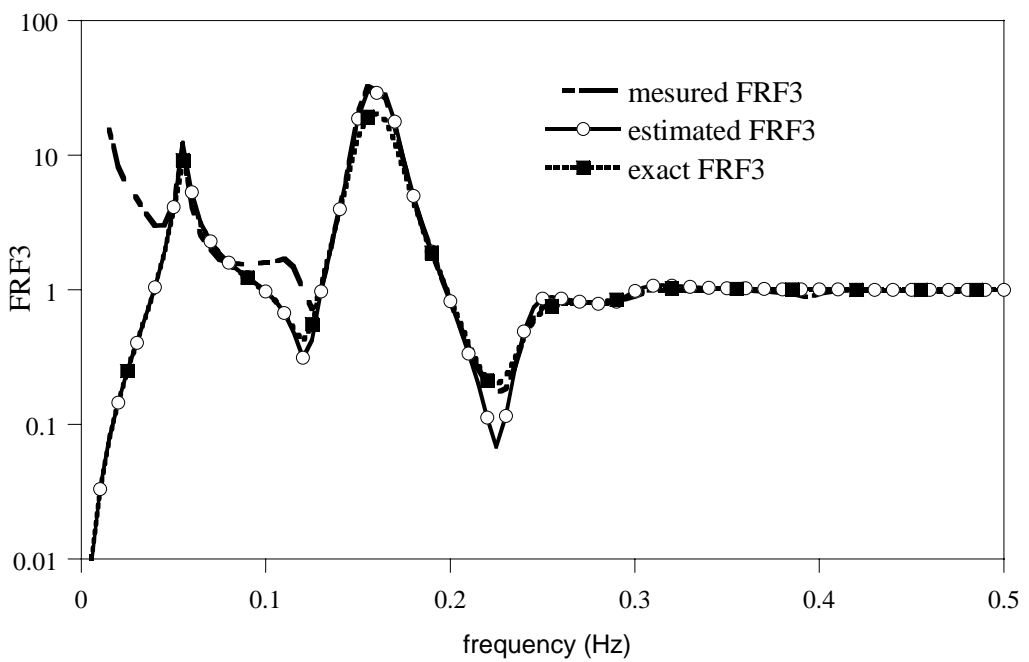


Fig. 4.56 FRF3 at frequency band in SI and measuring point at 3

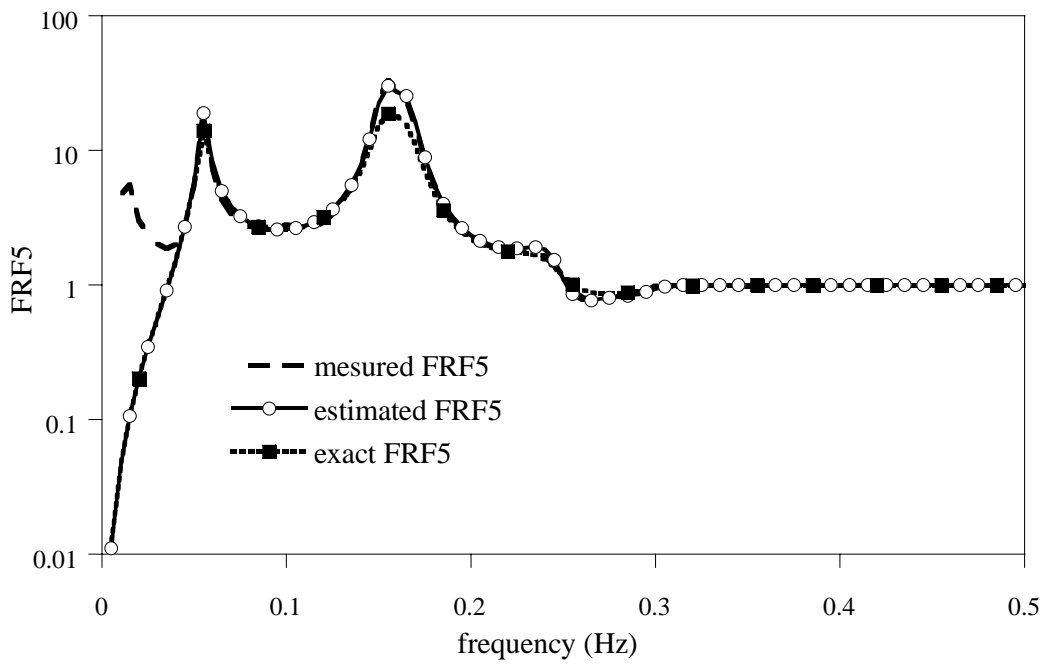


Fig. 4.57 FRF5 at frequency band in SI and measuring point at 5

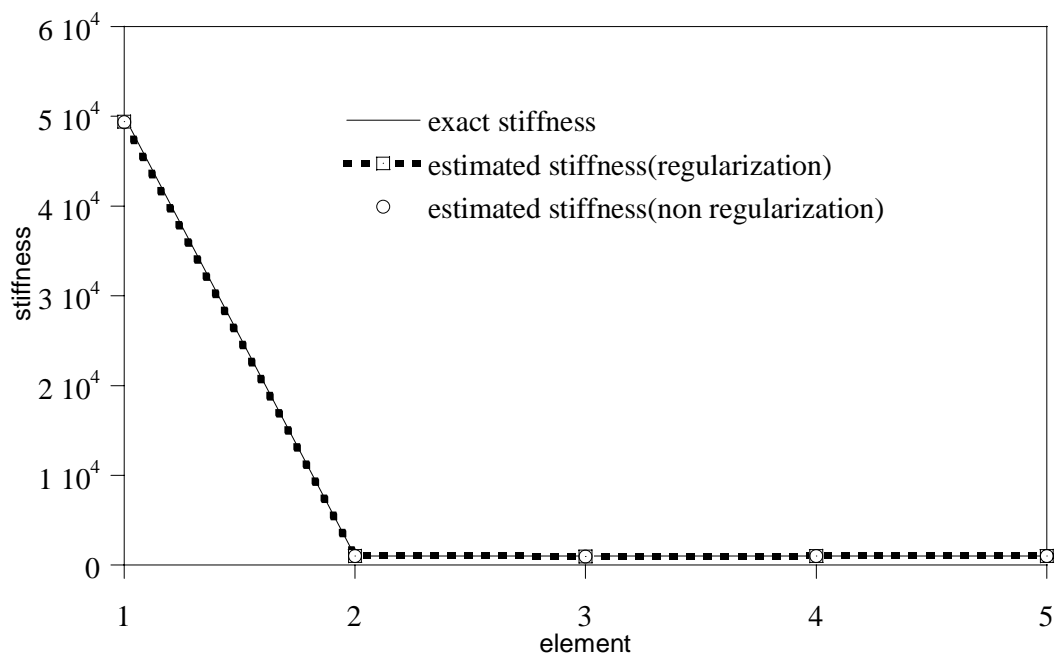


Fig. 4.58 Comparison of the regularized estimated stiffness and non regularized stiffness

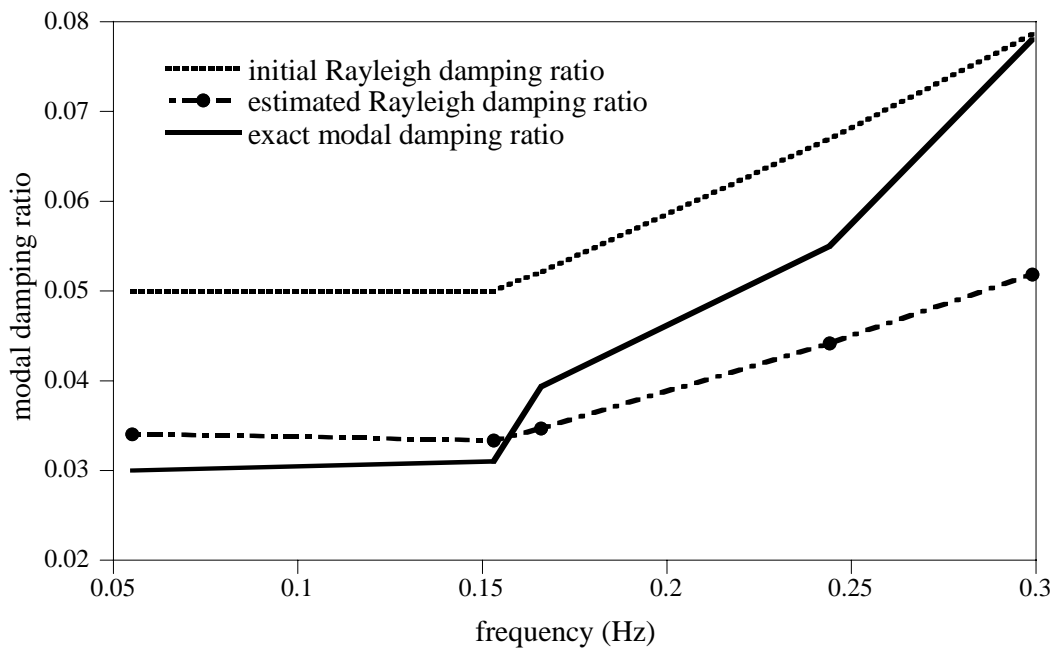


Fig. 4.59 Comparison of the regularized and non regularized estimated stiffness

4.4 Experimental study

The proposed method is applied to detect damage in a 3-story shear building using accelerations measured from experiments. The experimental model and the finite element model of the shear building are shown in Fig. 4.60 and Fig. 4.61, respectively. The floor plate consists of 45cm × 45cm rectangular steal plate welded to 5mm plate on 4 sides to increase the flexural stiffness and provide connections to columns. The 1st, 2nd and 3rd floor plate weighs 11.2 kg, 11.2 kg, 10.46 kg, respectively. The material properties of columns are given in Table 4.16. Two sets of cross bracings are installed in the perpendicular direction to the plane of vibration to prevent out-of-plane vibration in each story. Since the weights of cross bracings are very small compared with those of the floor plates and the columns, the weights of the cross bracings are neglected in SI. Stiffness of column and mass are shown in Table 4.17.

One accelerometer is placed at the center of the each floor plate, and acceleration is measured from free vibration induced by sudden release of a static loading. A steel block of 12.78 kg is used as a static loader, and is applied at the top floor in horizontal direction. Acceleration is measured in the time period from 0 sec to 200 sec with the sampling rate of 50 Hz. However, the acceleration data measured during the early 60 seconds are used in the SI process. The natural frequencies of the frame structural model are 2.5 Hz , 6.8Hz and 9.2 Hz.



Fig. 4.60 Experimental model 3-story shear building

Table 4.16 Material properties of columns

	Thickness (cm)	Area (cm ²)	Length (cm)	Mass (kg)
1 st floor	0.4	2.0	32.0	1.20
2 nd floor	0.3	1.5	31.5	0.88
3 rd floor	0.3	1.5	31.5	0.86

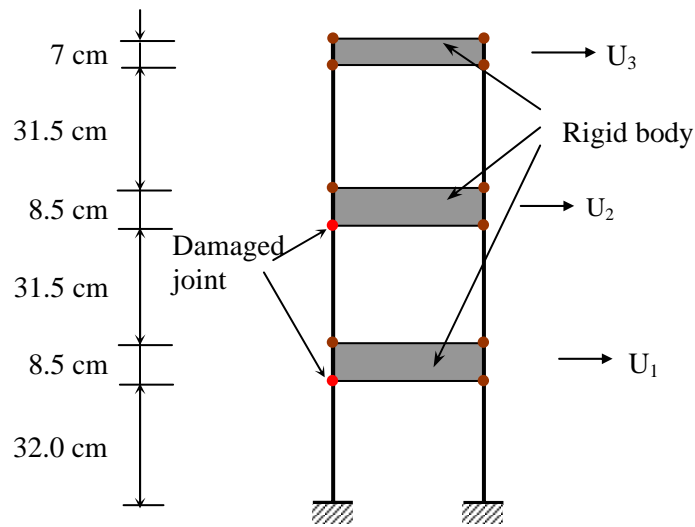


Fig. 4.61 Frame structural model

Table 4.17 stiffness and mass of frame structure

story	Stiffness (N/m)	Mass (kg)
1 st floor	21,480.10	11.20
2 nd floor	9,530.30	11.20
3 rd floor	9,530.30	10.46

Damage of the shear building is imposed by loosening two bolts at the joints between the columns and the floor plates at the 1st and 2nd floor. The damaged joints act like hinges as shown in Fig. 4.63, and thus flexural rigidities of the 1st floor and the 2nd floor are approximately reduced by 37.5%. Fig. 4.66 shows the identification results of the flexural rigidities of the damaged state. In the figures, the reductions in the flexural rigidities of the 1st and the 2nd floor are clearly seen, and the damage status of the structure is assured. Fig. 4.67 illustrates the variation of the estimated damping properties in time. Fig 4.64 and Fig. 4.63 are damaged and no damage FRFs from measured acceleration.



Fig. 4.62 Joint damage status

The estimated FRF using the converged system parameters at the final time step is compared to the measured FRF for the 1st floor in Fig. 4.65. The estimated FRF agrees very well with the measured FRF, which implies that the system parameters estimated by the proposed method represent the actual status of the structure closely.

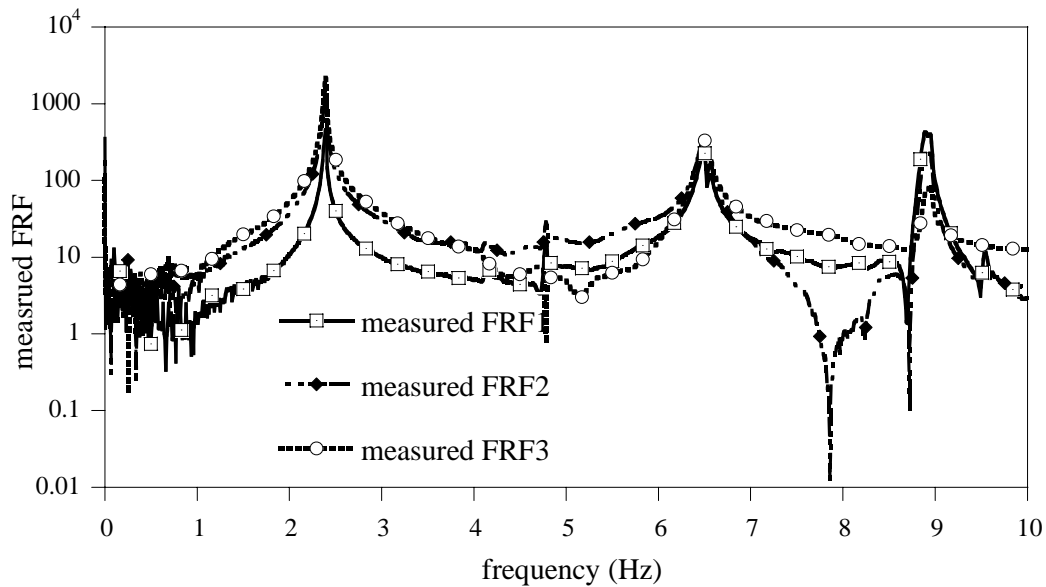


Fig. 4.63 Measured FRF at 1st, 2nd and 3rd floor (no damaged condition)

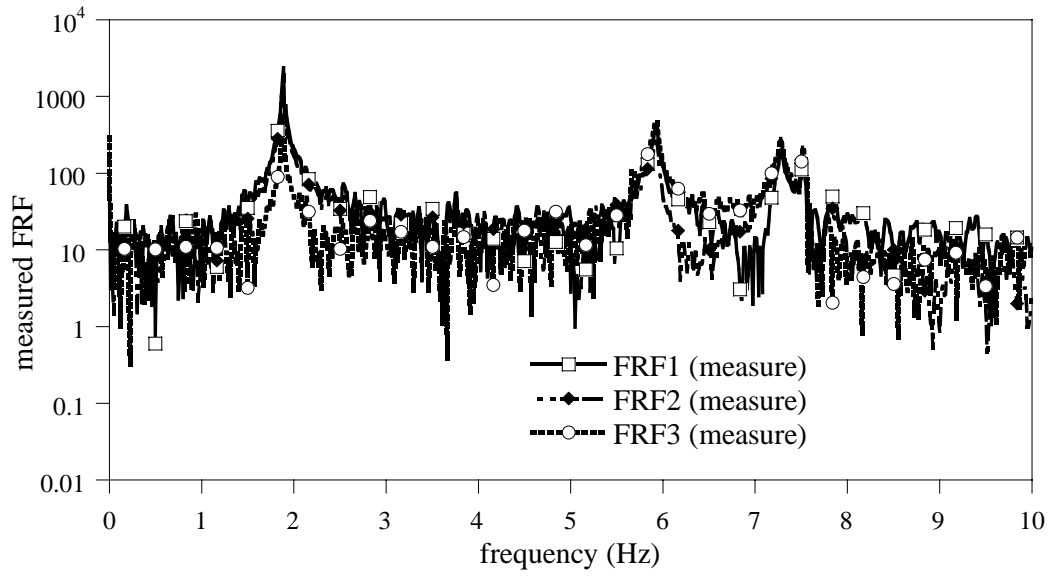


Fig. 4.64 Measured FRF at 1st, 2nd and 3rd floor (damaged condition)

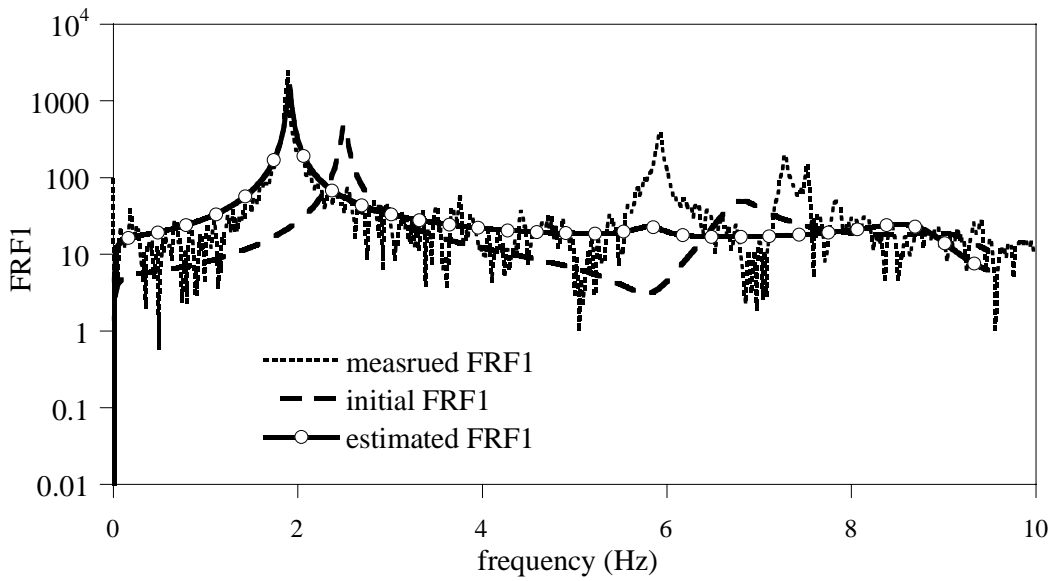


Fig. 4.65 Measured FRF1 at 1st floor and estimated FRF1

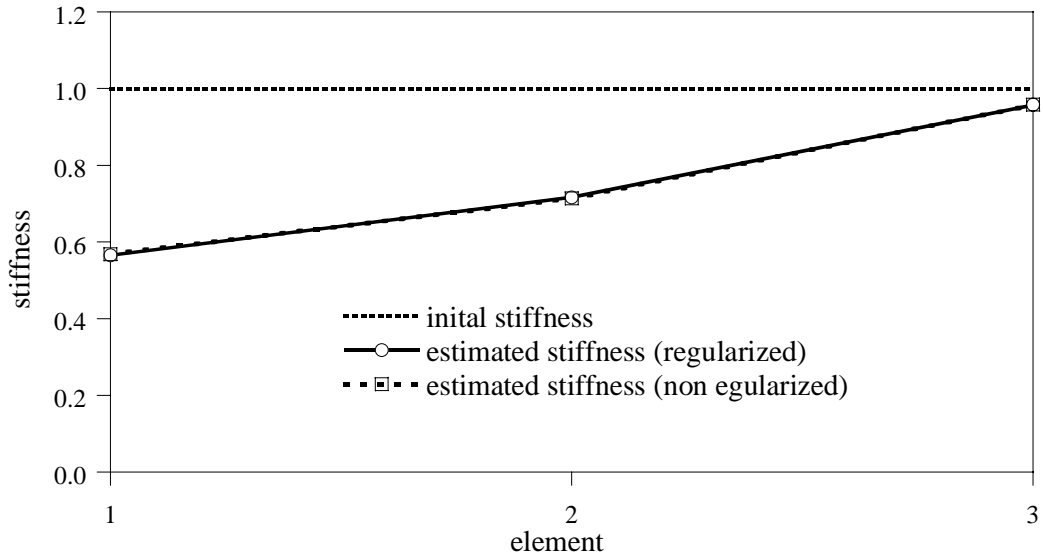


Fig. 4.66 Regularized and non regularized estimated stiffness

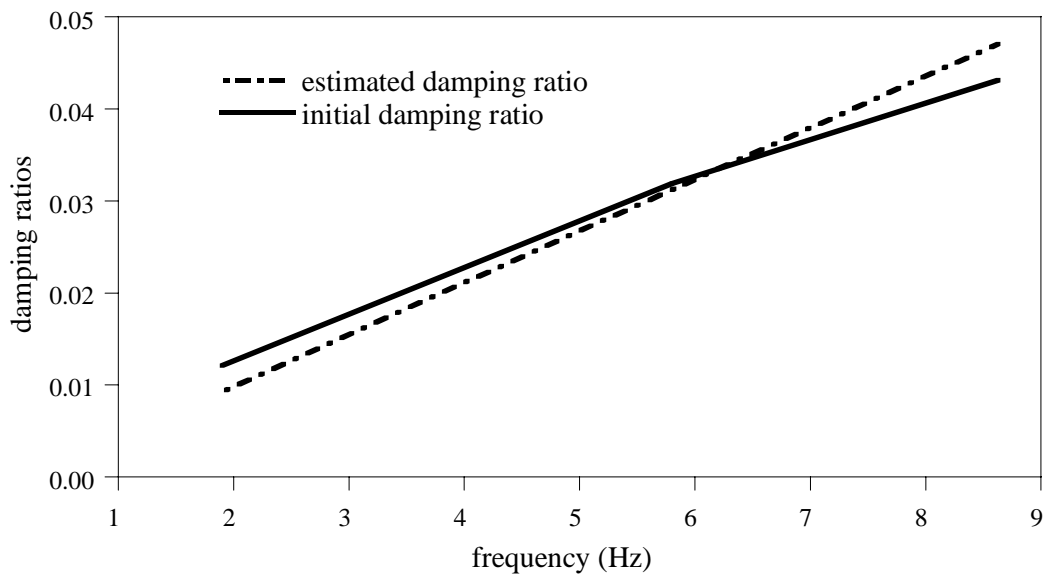


Fig. 4.67 Rayleigh estimated damping ratios

Chapter 5

Conclusions

This study presents a damage detection algorithm based on system identification with a regularization technique in the frequency domain. Previous researchers have developed static or modal measured responses and seismic time history data, which have also been used for civil structures. The current algorithm uses dynamic time history data transformed to dynamic acceleration response in the frequency domain by using FFT.

An output error estimator can give the difference between the frequency response function (FRF) from the measured acceleration response and the corresponding calculated frequency response function (FRF) to estimate the unknown structural parameters. System identification is used as a basic concept in developing this algorithm. The minimization of the least squared error nonlinear inverse problem is a direct differentiation of L_2 norm of the output error estimator.

Generally, noise is inevitable and occurs randomly in a real situation. Hence, we should include the effect of noise in measurements. If we can perfectly exclude the noise from each measured acceleration vector, we can obtain the compatible acceleration vector and the correct system parameters. However, it is not possible to obtain the compatible acceleration vector because we cannot perfectly exclude the noise. Sparseness and noise are the main problems in the damage detection algorithm. Sparseness can be resolved by increasing the number of measured degrees of freedom or mitigating the number of variables. This means that the noise in the measurements causes the ill-posed properties of

the inverse problem in the output error estimator. The ill-posedness of the inverse problem is unlike the forward problem, suffers from inherent instabilities such as non-existence, non-uniqueness and discontinuity.

There are several potential remedies for the ill-posedness. Ill-posed properties can be solved using the regularization technique. A general concept of regularity condition of system property for SI is presented. Based on the proposed regularity condition, a regularization function based on the L2 norm with respect to the system properties is proposed. A regularity condition of system properties is discretized in terms of system parameters. Two different approaches to impose the discretized regularity condition on minimization of error function are presented; a truncated singular value decomposition (TSVD) and Tikhonov regularization. In the TSVD, the truncation number determines the degree of regularity while the regularization factor does this in the Tikhonov regularization. In the Tikhonov regularization, the most important issue is to keep consistent regularization effect on the parameter estimation, which is controlled by a regularization factor. In this study, the object function is modified by the addition of a continuous regularization function to stabilize the output error estimator.

This study illustrates that the error function with the Tikhonov regularization function results in a solution of a generalized average between a priori estimates and the a posteriori solution. Here, a priori estimates represent known baseline properties of system parameters, and the a posteriori solution denotes the solution obtained by given measured data. A geometric mean scheme (GMS) is used as optimal regularization factors in

nonlinear inverse problems. In the GMS, the optimal regularization factors are defined as the geometric mean between the maximum and minimum singular value for balancing the maximum and minimum effect of the a priori estimates and a posteriori solution in a generalized average sense.

A nonlinear constrained optimization problem is used to solve the optimization problem of the least squared form in the parameter estimator. The recursive quadratic programming and the Fletcher active set strategy are used to solve the nonlinear constrained optimization problem. The structural systems are represented by a shear building model with known topology and geometry. Therefore, the constitutive parameters which parameterized in terms of the vector are the unknown to be estimated.

The proposed method can estimate the stiffness properties accurately even though the damping characteristics are approximated by the Rayleigh damping. The proposed method yields accurate solutions for numerically generated data and the experimentally measured data at full frequency band or selected frequency bands and using full measuring data or selected measuring data. It is believed the proposed method provides an engineering tool to identify dynamic characteristics of structures and to detect damage in structures using measured accelerations.

REFERENCES

Akt00

Aktan, A. E., Catbas, F. N., Grimmelsman, K. A., and Tsikos, C. J., "Issues in infrastructure health monitoring for management" *Journal of Engineering Mechanics*, ASCE, 126(7), 711-724 (2000)

Ali75

Alifanov, O. M. and Artyukhin, E. A., "Regularized numerical solution of non-linear heat conduction problems" *Journal of Engineering Physics*, 29, 934-938 (1975)

Ani95

Anil K. Chopra, "Dynamics of Structures", Theory and Applications to Earthquake Engineering, Printed in the United States of America, 1995.

Ata01

Ata Mugan, (2001) "Frequency domain analysis of time integration algorithms", *Comput. Methods Appl. Mech. Engrg.*, Vol.190, pp.5777-5793.

Bec84

Becks J. V. and Murio, D. A., "Combined function specification – regularization procedure for the solution of inverse heat conduction problem" *AIAA Journal*, 24 180-185 (1984)

Bec85

Becks, J. V., Blackwell, B., and St. Clair, C. R., *Inverse Heat Conduction : Ill-Posed Problems*, (Wiley, New York, 1985)

Bui94

Bui, H. D., *Inverse Problems in the Mechanics of Materials: An Introduction*, CRC Press, Boca Raton (1994)

Doe99

Doebing, S. W., Farrar, C. R., Prime, M. B., and Shevitz, D. W., *Damage Identification and Health Monitoring of Structural and Mechanical Systems From Changes in Their Vibration Characteristics: A Literature Review*, Los Alamos National Laboratory Report LA-13070-MS (1996)

Doe96

Doebling, S. W. and Farrar, C. R., *The State of the Art in Structural Identification of Constructed Facilities*, (A Report by the ASCE Committee on Structural Identification of Constructed Facilities, 1999)

PDF format is available in http://ext.lanl.gov/projects/damage_id

Ge98a

Ge, L. and Soong, T. T., "Damage identification through regularization method. I: Theory" *Journal of Engineering Mechanics*, ASCE, 124(1) 103-108, 1998

Go196

Golub, G. H. and Van Loan, C.F., *Matrix Computations*, 3rd ed., The Johns Hopkins University Press, London (1996)

Gra80

Graeme H. Mcverry (1980), "Structural identification in the frequency domain from earthquake records", *Earthquake engineering and structural dynamics*, Vol 8, pp.161-180.

Gro84

Groetsch, C. W., *The theory of Tikhonov Regularization for Fredholm Equations of the First Kind*, Pitman Advanced Publishing, Boston (1984)

Han92a

Hansen, P. C., "Analysis of discrete ill-posed problems by means of the L-curve" *SIAM review*, 34(4), 561-580 (1992)

Han92b

Hansen, P. C., Sekii, T., Shibahashi, H., "The modified truncated SVD method for regularization in general form" *SIAM J. Sci. Stat. Comput.*, 13, 1142-1150 (1992)

Han98

Hansen, P. C., *Rank-deficient and Discrete Ill-Posed Problems : Numerical Aspects of Linear Inversion*, (SIAM, Philadelphia, 1998)

Hje96b

Hjelmstad, K. D., "On the uniqueness of modal parameter estimation" *Journal of Sound and Vibration*, 192(2), 581-598 (1996)

Hon94

Honjo, Y., Wen-Tsung, L., and Guha, S., "Inverse analysis of an embankment on soft clay by extended Bayesian method", *International Journal for Numerical Methods in Engineering* 18, 709-734 (1994)

Hwa98

H. Y. Hwang (1998), "Identification techniques of structure connection parameters using frequency response functions", *Journal of Sound and Vibration*, Vol. 212(3), pp. 469-479.

Joh87

Johnson, C., *Numerical Solution of Partial Differential Equations by the Finite Element Methods*, (Cambridge University Press, New York, 1987)

Kal96

Kaller, F. and Bertrant, M., "Tissue elasticity reconstruction using linear perturbation method" *IEEE transaction of medical imaging*, 15(3), 299-313 (1996)

Kan99

Kan, J. S., "Structural damage assessment from modal data using a system identification algorithm with a regularization technique, Master. Thesis, Department of Civil engineering, Seoul National University, 1999.

Kim03

H.-Y. Kim (2003), "Vibration-based damage identification using reconstructed frfs in composite structures", *Journal of Sound and Vibration*, Vol. 259(5), pp. 1131-1146.

Lee99

Lee, H. S., Kim, Y. H., Park, C. J., and Park. H. W., "A new spatial regularization scheme for the identification of geometric shapes of inclusions in finite bodies" *International Journal for Numerical Methods in Engineering*, 46(7), 973-992 (1999)

Lee00

Lee, H. S., Park, C. J., and Park. H. W., "Identification of geometric shapes and material properties of inclusions in two dimensional finite bodies by boundary parameterization" *Computer Methods in Applied Mechanics and Engineering*, 181(1-3), 1-20 (2000)

Lee02

U. Lee and J. Shin (2002), "A frequency-domain method of structural damage identification formulated from the dynamic stiffness equation of motion", *Journal of Sound and Vibration*, Vol. 257(4), pp. 615-634.

Lim00

T. C. Lim and J. Li (2000), "A theoretical and computational study of the frf-based substructuring technique applying enhanced least square and tsvd approaches", *Journal of Sound and Vibration*, Vol.231(4), pp. 1135-1157.

Lue89

Luenberger, D. G., *Linear and Nonlinear Programming* 2nd edn. (Addison-Wesley, Reading, 1989)

Mah96

Mahnken, R. and Stein, E., "Parameter identification for viscoplastic models based on analytical derivatives of a least-squares functional and stability investigations" *International Journal of Plasticity*, 12(4) 451-479 (1996)

Man89

Maniatty, A., Zabarab, N., and Stelson, K., "Finite element analysis of some inverse elasticity problems", *Journal of Engineering Mechanics, ASCE* 115, 1303-1317 (1989)

Mel95

Mellings, S. C. and Aliabadi, M. H., 'Flaw identification using the boundary element method', *International Journal for Numerical Methods in Engineering*, 38, 399-419 (1995)

Mor93

Morozov, V.A., *Regularization Methods for Ill-posed Problems, English Ed.*(CRC Press, 1993)

Nor89

Norris, M. A. and Meirovitch, L., "On the problem of modeling for parameter identification in distributed structures" *International Journal for Numerical Methods in engineering*, 28, 2451-2463 (1989)

Ode79

Oden, J. T., *Applied Functional Analysis : A First Course for Students of Mechanics and Engineering Science*, (Prentice-Hall, Englewood Cliffs, NJ, 1979)

Par01

Park, H.W., Shin, S.B., and Lee, H.S., "Determination of an optimal regularization factor in system identification with Tikhonov function for linear elastic continua" *International Journal for Numerical Methods in Engineering*, 51(10), 1211-1230 (2001)

Par02

Park, H. W, "Regularization techniques in system Identification for Damage Assessment of Structures, P.hD. Thesis, Department of civil engineering, Seoul National University, 2002.

San91

Sanayei, M. and Onipede, O., "Damage assessment of structures using static test data", *AIAA Journal*, 29(7), 1174-1179 (1991)

Sch90

Schnur, D. S. and Zabarar, N., "Finite element solution of two dimensional inverse elastic problems using spatial smoothing" *International Journal for Numerical methods in Engineering*, 30, 57-75 (1990)

Sch92

Schnur, D. S. and Zabarar, N., "An inverse method for determining elastic material properties and a material interface", *International Journal for Numerical Methods in Engineering*, 33, 2039-2057, (1992)

Shi94

Shin, S., *Damage Detection and Assessment of Structural Systems from Measured Response*, Ph.D. Thesis, Department of civil engineering, University of Illinois at Urbana-Champaign, 1994

Shi99

Shin, S. and Koh, H. M., "A numerical study on detecting defects in a plane stressed body by system identification", *Nuclear Engineering and Design*, 190, 17-28 (1999)

Tan89

Tanaka, M. and Yamagiwa, K., "A boundary element method for some inverse problems in elastodynamics" *Applied Mathematical Modelling*, 13, 307-312 (1989)

Tik77

Tikhonov, A. and Arsenine, V., *Solutions to Ill-Posed Problems*, (Winston-Wiley, New York, 1977)

Vog86

Vogel, C. R., "Optimal choice of a truncation level for the truncated SVD solution of linear first kind integral equations when data are noisy," *SIAM J. of Numerical Analysis*, 23(1), 109-117 (1986)

Yeo99

Yeo, I. H., *Statistical Damage Assessment of Structures from Static Responses Using System Identification with Tikhonov Regularization*, Ph.D. Thesis, Department of civil engineering, Seoul National University, 1999

Yeo00

Yeo, I. H., Shin, S., Lee, H. S., and Chang, S. P., "Statistical Damage Assessment of Framed Structures from Static Responses" *Journal of Engineering Mechanics, ASCE*, 126 (4), 414-421 (2000)

가
가

가

Rayleigh

damping

가

가,

Tikhonov

L_2 -norm

geometric mean scheme (GMS)

response

transform

recursive quadratic

programming

, Gauss-Newton

: , , , ill-posedness, ,

, recursive quadratic programming

: 99415-817

CURRICULUM VITAE

Tin Tin Win was born on August 13, 1963 in Yangon, Myanmar. She graduated from No.3 High School at Thingangyun, Yangon, in 1980. She received a diploma from the department of Civil Engineering at the Government Technical Institute of Insein in December 1983. Then she received a Bachelor degree in Civil Engineering in 1992 and a Master's degree in Civil Engineering in 1996 from Yangon Institute of Technology, Myanmar. She serves as a lecturer at the department of Civil Engineering in Yangon Institute of Technology. She came to Korea as a state scholarship student of Myanmar and has continued her graduate studies up to now at the department of Civil Engineering in the Seoul National University. Her graduate research deals with inverse problems in the engineering mechanics and regularization techniques in system identification of structures at frequency domain.

ACKNOWLEDGEMENTS

First of all, I would like to express my deepest gratitude to Professor Hae Sung Lee of the School of Civil, Urban and Geosystem Engineering in Seoul National University for his invaluable help, understanding, patience, constant encouragement, guidance, thought-provoking advice and discussions throughout the work.

I am greatly indebted to Professor Hyun-Moo Koh, Professor Jae-Kwan Kim, Professor Soo-Bong Shin and Dr Nam-Sik Kim for their constructive comments on the dissertation manuscript. Dr Hyun Woo Park of the same lab is thanked for his kind help in academic matters.

I am deeply grateful to Professor Dr Htin Aung, Head of the department of civil engineering at Yangon Technological University in Myanmar. I also thank my colleagues of the same department from Myanmar for their patient encouragement.

I wish to express my deep appreciation to my colleagues of the same lab – Ki Seok Kim and all of the lab members who have provided assistance in various phases of the work. They have contributed their time, effort, knowledge, and patience in helping me undertake this work, and their involvement has been essential for the completion of this thesis. In particular Yang Kwang Ahn is thanked for his help in running my research program together.

I wish to express my sincere gratitude to many Korean friends from the same school of Civil, Urban and Geosystem Engineering, Seoul National University for their kind help

and amicable friendliness during my stay in Korea. I also want to thank all the staff and faculty members of the school for their help in many departmental works.

I am deeply grateful to the SEOAM Foundation, Korea for its financial support. Part of the research fund is provided by Korean Earthquake Engineering Research Center.

I thank Myanmar friends in Korea for their kind help and encouragement in various phases of the work during my stay in Korea.

Final thanks go to my family, especially my elder brother U Khin Shwe, for their understanding and patient encouragement while I have been away from them for my further studies in Korea.